

LOCAL CYTOSKELETAL AND ORGANELLE INTERACTIONS IMPACT  
MOLECULAR MOTOR-DRIVEN EARLY ENDOSOMAL TRAFFICKING

Allison Lorraine Zajac

A DISSERTATION

In

Cell and Molecular Biology

Presented to the Faculties of the University of Pennsylvania

in

Partial Fulfillment of the Requirements for the  
Degree of Doctor of Philosophy

2013

Supervisor of Dissertation

---

E. Michael Ostap  
Professor of Physiology

Co-Supervisor of Dissertation

---

Erika L.F. Holzbaur  
Professor of Physiology

Graduate Group Chairperson

---

Daniel S. Kessler  
Associate Professor of Cell and Developmental Biology

Dissertation Committee:

Roberto Dominguez, Professor of Physiology  
Michael A. Lampson, Assistant Professor of Biology  
Michael S. Marks, Professor of Pathology and Laboratory Medicine  
Tatyana Svitkina, Associate Professor of Biology

LOCAL CYTOSKELETAL AND ORGANELLE INTERACTIONS IMPACT  
MOLECULAR MOTOR-DRIVEN EARLY ENDOSOMAL TRAFFICKING.

COPYRIGHT

2013

Allison Lorraine Zajac

## Acknowledgements

I would first like to thank my advisors Drs. E. Michael Ostap and Erika L.F. Holzbaur, and our collaborator Yale E. Goldman, for their mentorship during the work leading to this dissertation. I would also like to thank everyone in the Ostap, Holzbaur, Goldman, and Discher labs for their help, advice, and support throughout graduate school. More specifically, I would like to thank the investigators listed in the materials and methods (Chapter 2) for generous sharing of plasmids and software, Drs. Martin Pring for consultation on statistics, and Jennine Dawicki McKenna, Roger E. Goldman and Adam G. Hendricks for assistance with microscopy and programming. NIH Funding: P01GM087253 (E.L.F.H., E.M.O., and Y.E.G.), T32 GM-07229 (A.L.Z.).

## ABSTRACT

### LOCAL CYTOSKELETAL AND ORGANELLE INTERACTIONS IMPACT MOLECULAR MOTOR-DRIVEN EARLY ENDOSOMAL TRAFFICKING.

Allison L. Zajac

E. Michael Ostap

Erika L.F. Holzbaur

Molecular motors generate the force needed for long-distance transport of cargos and organelles in the cell. How motor proteins attach to a diverse array of cargos and navigate to the correct location in the cell with enough fidelity to maintain organelle integrity is only starting to be understood. Studying the properties of individual motors, and their fine-tuning by regulatory molecules, is one area of active investigation in vitro. However, the organization of the cell, and the variability of the environment within a single cell, cannot be fully reconstituted in vitro. We investigated the effects of the crowded intracellular environment on early endosomal trafficking. Live-cell imaging of an endosomal cargo (endocytosed epidermal growth factor-conjugated quantum dots) combined with high-resolution tracking was used to analyze the heterogeneous motion of individual endosomes. The motile population of endosomes moved towards the perinuclear region in directed bursts of microtubule-based, dynein-dependent transport interrupted by longer periods of diffusive motion. Actin network density did not affect motile endosomes during directed runs or diffusive interruptions. Simultaneous two-

color imaging was used to correlate changes in endosomal movement with potential obstacles to directed runs. Termination of directed runs spatially correlated with microtubule-dense regions, encounters with other endosomes, and interactions with the endoplasmic reticulum, suggesting these interactions interrupt directed transport. Early endosomal and lysosomal interactions with the ER were characterized by dramatic deformation and tubulation of the ER. During a subset of run terminations, we also observed merging and splitting of endosomes, and reversals in direction at speeds up to ten-fold greater than characteristic in vitro motor velocities. These observations suggest endosomal membrane tension is high during directed run termination. Our results indicate that the crowded cellular environment significantly impacts the motor-driven motility of organelles. Rather than simply acting as impediments to movement, interactions of trafficking cargos with intracellular obstacles may facilitate communication between membrane-bound compartments or contribute to the generation of membrane tension necessary for fusion and fission of endosomal membranes or remodeling of the endoplasmic reticulum.

## Table of contents

<b>List of tables</b> .....	x
<b>List of illustrations</b> .....	xi
1 Introduction.....	1
1.1 Historical perspective: Early observations of intracellular motion and investigations of their source.....	1
1.2 Early endosomes and the endosomal pathway.....	5
1.2.1 Epidermal Growth Factor.....	7
1.3 What drives long distance transport in the cell?.....	10
1.3.1 Molecular motors.....	10
1.3.2 Organelle and cargo movement by motors.....	20
1.3.3 Cytoskeletal track preferences.....	28
1.3.4. Motor ensemble properties.....	35
1.3.5 Other sources of motion in the cell.....	38
1.3.6 Spatial variation in the cell.....	45
1.4 Current view of early endosomal motion.....	46
1.5 Thesis overview.....	47
2 Materials and Methods.....	49
2.1 Methods for Chapter 3.....	49
2.1.1 Cell culture and transfection.....	49

2.1.2 EGF dye labeling.....	50
2.1.3 Lysosomal labeling.....	50
2.1.4 Transferrin endocytosis assay.....	51
2.1.5 Cytoskeletal drug treatment.....	51
2.1.6 Microscopy.....	52
2.1.7 Tracking and data analysis.....	53
2.1.8 GFP-Rab5 and mCherry-Rab7 trajectory analysis.....	58
2.1.9 Cytoskeletal drug treatment analysis.....	59
2.1.10 Parsing of EGF-Qdot trajectories into directed runs and pauses.....	60
2.1.11 MSD analysis of concatenated track segments.....	61
2.1.12 Spatial correlation between early endosomal pause sites and the position of organelles.....	62
 3 Local cytoskeletal and organelle interactions impact molecular motor-driven early endosomal trafficking.....	 63
3.1 Abstract.....	64
3.2 Introduction.....	65
3.3 Results.....	67
3.3.1 Intracellular dynamics of early endosomes.....	67
3.3.2 The actin network regulates the confinement of early endosomes.....	69
3.3.3 The transition periods before and after directed runs are diffusive.....	71

3.3.4 Interactions with organelles spatially correlates with early endosome pause locations.....	72
3.3.5 Early endosomal membrane tension may regulate the pauses in directed motion.....	73
3.3.6 Early endosomes deform the ER during trafficking.....	74
3.3.7 Early endosomal motion is influenced by MT organization.....	75
3.4 Discussion.....	73
3.4.1 Early endosomes contain subpopulations with distinct motility characteristics, differentially regulated by the actin cytoskeleton.....	75
3.4.2 The motion during pauses is diffusive.....	77
3.4.3 High endosomal membrane tension may induce pausing and facilitate cargo sorting.....	78
3.4.4 Conclusions.....	79
3.5 Figures.....	81
3.6 Tables.....	107
4 Discussion.....	114
4.1 Heterogeneity in the movement of different early endosomes.....	115
4.1.1 Imaging time affects interpretation.....	115
4.1.2 Differences in effectors and motors exists within Rab5 compartment.....	116
4.1.3 Physically distinct areas of the cell.....	122

4.2 Heterogeneity in motion within individual tracks.....	125
4.2.1 Pausing due to engagement of an opposite polarity motors.....	126
4.2.2 Motion during pauses.....	130
4.3 What are the benefits of saltatory motion for early endosomes and other organelles?.....	138
4.3.1 Sorting.....	138
4.3.2 Facilitating membrane sculpting.....	138
4.3.3 Decreasing search time.....	140
4.4 Relevance to the transport of other cargos and organelles.....	141
4.4.1 MT intersections.....	141
4.4.2 Organelle-organelle interactions.....	142
4.5 A potential role for the ER in regulating transport? .....	143
4.5.1 Introduction to the ER.....	144
4.5.2 Future Directions.....	146
4.6 Figures.....	156
Bibliography.....	162

## List of tables

### Chapter 3

Table 1. Comparison of the motility of early endosomes and late endosomes/lysosomes .....	107
Table 2. MSD analysis of simulated trajectories after parsing the trajectories into directed runs and pauses.....	108
Table 3. Motion characteristics of EGF-Qdots.....	110
Table 4. The false-positive rate in determination of directed runs using individual parsing criteria.....	111
Table 5. Alternative MSD analysis using concatenated 0.75 s trajectory segments.....	112
Table 6. Spatial correlation between Rab5-positive endosomal pauses and organelle positions.....	91

## List of illustrations

### Chapter 3

Figure 1. Characterization of cytoskeletal and endosomal organization in Arpe-19 cells.....	81
Figure 2. Motility in the early endosomal population.....	84
Figure 3. Early endosomal tracking and motion analysis.....	86
Figure 4. The effect of cytoskeletal disruption on early endosomal motion.....	89
Figure 5. Parsing of trajectories into directed runs and pauses.....	91
Figure 6. Analysis of motile trajectories.....	94
Figure 7. The motion of individual EGF-Qdot-containing early endosomes during encounters with other Rab5-positive early endosomes.....	99
Figure 8. Early endosomal movement is affected by interactions with the ER and multiple MTs.....	101
Figure 9. Interactions between early endosomes and the ER and between early endosomes and MT-dense regions are also observed in COS-7 cells.....	103
Figure 10. Comparison of MSD and MSS analysis to classify motion and estimate the uncertainty in $\alpha$ .....	105
<b>Chapter 4</b>	
Figure 1. Rab5-positive early endosomal positioning depends on dynein/dynactin and KIF16b.....	156

Figure 2. KIF16b localizes to a subset of Rab5-positive early endosomes, often in patches.....157

Figure 3. KIF16b continuously generates tubules that pinch off Rab5-positive early endosomes and travel rapidly towards the cell periphery.....158

Figure 4. The growth of new KIF16b tubules moves the Rab5-positive endosome body with it.....159

Figure 5. Nearly all late endosomes/lysosomes associate with the ER and deform the ER during movement.....180

## Chapter 1. Introduction

### 1.1 Historical perspective: Early observations of intracellular motion and investigations of their source

This dissertation investigates the types of motion early endosomes use to achieve long-distance transport in the cell using high-resolution imaging and super-resolution tracking. The history of the investigation of intracellular motion is tightly coupled to advances in imaging technology. Robert Hooke first coined the term “cell” to describe the compartmentalization he observed in cork under the microscope in 1665 (Hooke, 1665). Although the ability to collect images did not exist during early microscopic investigations, many of these studies were of dynamic processes in live specimens. Cytoplasmic streaming in plant cells, with its accompanying flow of vesicles, was first described in 1774 by Bonaventura Corti (Corti, 1774). The observation that new cells come from the division of an existing cell was made by Dumortier and von Mohel in the 1830s, and Walther Fleming described mitosis in 1879 (Harris, 1999). The first time-lapse image series, or micro-cinematography, was published in 1909 by Julius Ries, who took time-lapse photographs of a fertilized sea urchin egg developing over 14 hours (Ries, 1909).

All of these cellular processes require motor-driven forces and only occur in live

specimens. In contrast, diffusion, or Brownian motion, as described by Robert Brown in 1827 for pollen grains diffusing in water, was a motion that did not require living material. The first record of this type of random motion in inanimate material is credited to the Roman philosopher Lucretius, who described the movement of dust particles in “On the Nature of Things” in 60 BC.

Early work in neurons suggested a system existed in cells to actively transport cargos and organelles long distances. The axons of these extended cells could be ligated, and the material that was transported, such as mitochondria, would collect at the ligation site (Zelena, 1968; Zelena et al., 1968). Direct evidence for long-distance slow transport in the axon was obtained in 1963 by Droz and Leblond by radiolabeling material only in the cell body and tracking its progress down the axon over time (Droz and Leblond, 1963). In addition to the slow axonal transport explored in this study, a more rapid form of transport was also observed in nerves. In 1969, Kreutzberg applied the new microtubule (MT) depolymerizing drug colchicine to a nerve and demonstrated that fast axonal transport required MTs (Kreutzberg, 1969). In 1982, the use of video-enhanced direct interference contrast microscopy allowed Gilbert, Allen and colleagues to visualize small vesicles in squid axons move bidirectionally, with pauses in motion, and “elastic recoils”(Allen et al., 1982). Vesicle movement persisted in extruded axoplasm, indicating soluble factors can produce motion outside the context of the cell (Brady et al., 1982).

The motor proteins responsible for generating the force to power the movements in all these cellular processes were unknown during these studies. The first studies of a protein that could generate force were on muscle myosin, proposed to be a protein that could slide actin filaments by Hugh Huxley and Andrew Huxley in 1954 (Huxley and Niedergerke, 1954; Huxley and Hanson, 1954). The first myosin motor in a non-muscle cell was identified in 1974 by Clarke and Spudich (Clarke and Spudich, 1974), demonstrating that motor proteins perform tasks other than muscle contraction. Reconstitution of the motor-driven movements of actin filaments in vitro (Sheetz and Spudich, 1983; Spudich et al., 1985) greatly advanced the ability to study how these motor proteins work. Recently, imaging of a myosin V motor walking along an actin filament was achieved with high-speed AFM (Kodera et al., 2010), allowing direct visualization of the motion of the motor previously inferred from many other biochemical and imaging approaches.

In 1985, two other classes of motors were identified in nerve axoplasm. The bidirectional movements of vesicles observed in axoplasm in 1982 were found to rely on two different motors. One, kinesin, could move vesicles towards the end of the axon where MT plus-tips are located (Vale et al., 1985a), and another molecule could move vesicles towards the minus-ends of MTs (Vale et al., 1985b). This minus-end directed motor, cytoplasmic dynein, was identified in 1987 by Paschal and Valle (Paschal et al., 1987). Comparison of cytoplasmic dynein to axonemal dyneins, which were studied for their ability to bend cilia and flagella starting in 1963 (Gibbons, 1963), using electron

microscopy confirmed that these motors have similar structures and are likely in the same family (Vallee et al., 1988). Early studies of dynein-driven motility also revealed that a cytosolic factor activated dynein activity (Schnapp and Reese, 1989; Schroer et al., 1989). This activator, the dynactin complex, was identified in mammalian systems in 1991 (Gill et al., 1991; Schroer and Sheetz, 1991), as one of the first examples of regulation of motor-driven vesicle transport.

Since these early studies identified the three families of motor proteins responsible for the intracellular movements observed under the microscope for hundreds of years, a large number of new motors and regulatory factors have been identified, the biochemical-mechanical coupling of purified motors has been investigated in detail, and imaging technology has advanced. The development of tools such as GFP (Olenych et al., 2007) to specifically label proteins and organelles in live cells has facilitated comparisons of the motion of different cargos. Observation of many cargos has shown that their transport does not occur in one, homogenous, movement from point A to point B. Most cargos exhibit saltatory motion similar to the vesicles in axoplasm, in which directed, rapid motion is interspersed with pauses in transport, random motion, and sometimes switches in direction.

This dissertation explores the motion exhibited by one organelle, the early endosome, using high temporal and spatial resolution tracking of individual early endosomes and detailed analysis of the motion. Although many of the motors and motor regulatory

molecules associated with different organelles are known, how they work together to produce the motion seen during their transport is not clear. However, in many cases, the effect of individual regulatory molecules on a motor is known. By collecting detailed information about the movement of early endosomes and comparing this to the described effects of different motor regulatory factors, this dissertation aims to identify which molecular factors are responsible for regulating the motion of early endosomes in the cell. Since this dissertation focuses on the motor-driven movement of early endosomes, the function of early endosomes in the transport of cargo and nutrients from the cell surface will be reviewed to highlight how movement and maturation are linked for this organelle. Additionally, the biochemical and biophysical properties of molecular motors that allow them to move cargo will be discussed as a necessary starting point for evaluating the expected motion of different motors and the effect of different regulatory molecules in the cell. The main emphasis will be placed on motors and regulatory factors previously implicated in the movement of early endosomes.

## **1.2 Early endosomes and the endosomal pathway**

After endocytosis of a cargo like epidermal growth factor (EGF) and its receptor, vesicles uncoat and fuse with early endosomes (Pfeffer, 2007), a tubular-vesicular compartment involved in concentrating and sorting endocytic cargo for different fates in the cell (Miller et al., 1986). Endosomes mature and sort cargo at the same time, a process involving fusion, fission, and changes in protein composition. Transferrin, for example,

enters tubules that pinch off early endosomes and get recycled back to the plasma membrane (Maxfield and McGraw, 2004). Other cargo such as cation-independent mannose-6-phosphate receptor (CI-MPR) and some pathogens exit early endosomes using retromer-based sorting and are transported to the Golgi (Cullen and Korswagen, 2012; Hao et al., 2013). Epidermal growth factor receptor (EGFR) is sorted into the intraluminal vesicles (ILVs) of multivesicular bodies (MVBs). Most MVBs mature to late endosomes and fuse with lysosomes, where the low pH and proteases degrade all contents (Miller et al., 1986).

Rab5 is required for the existence of the early endosomal compartment, and, through its many effectors, is the master regulator of early endosomal function (Gruenberg and Maxfield, 1995; Zeigerer et al., 2012; Zerial and McBride, 2001). It remains unclear whether uncoated vesicles can fuse with themselves and de novo recruit Rab5 to form early endosomes or must fuse with a pre-existing Rab5 compartment (Gruenberg and Maxfield, 1995; Zeigerer et al., 2012). Rab5 cycles between a GDP state and an active, membrane-associated GTP state. Once Rab5 is on early endosomes it can recruit its guanine nucleotide exchange factor (GEF), Rabex-5, to create a positive feedback loop for its recruitment. Rab5 also recruits the kinase Vps34, which creates a high concentration of the phospholipid, phosphatidylinositol 3-phosphate (PI(3)P) on early endosomes relative to other membranes in the cell (Christoforidis et al., 1999). Many of Rab5's effectors, such as EEA1, bind both Rab5 and PI(3)P weakly, acting as coincidence

detectors to enhance recruitment specifically on early endosomes (Simonsen et al., 1998; Stenmark and Aasland, 1999).

Two models have been proposed for the transfer of cargo from early endosomes to late endosomes. In the Rab conversion model, the Rab5 positive early endosomes mature into late endosomes by decreasing their Rab5 level while increasing their Rab7 level, resulting in a switch to Rab7 effectors and conversion to late endosomes (Rink et al., 2005). Most studies currently point towards Rab conversion. In support of the conversion model, one of Rab5's effectors, SAND-1/Mons, was recently demonstrated to inhibit Rab5 recruitment, while simultaneously promoting the recruitment of Rab7 (Poteryaev et al., 2010). However, transfer of Semliki Forest virus from early to late endosomes occurs via budding of Rab7 positive domains away from the early endosome (Vonderheit and Helenius, 2005). It is not clear if this is a pathway induced only by the virus or a pathway used by endogenous cargo as well. After late endosomes acquire Rab7 they continue to mature and eventually fuse with lysosomes, leading to degradation of their contents (Sorkin and Goh, 2008).

### **1.2.1 Epidermal Growth Factor**

Rita Levi-Montalcini and Stanley Cohen received the Nobel Prize in Physiology or Medicine in 1986 for their discovery of the first two growth factors, neuronal growth factor (NGF) and epidermal growth factor (EGF).

Cohen injected salivary gland extract into newborn mouse pups and found a component in this extract, EGF, accelerated the development of epidermal lineages, resulting in precocious eyelid opening and tooth eruption (Cohen, 1962). Human EGF was subsequently purified from the urine of pregnant women in large enough quantities to demonstrate this growth factor was a conserved non-cell autonomous regulator of development across species (Cohen and Carpenter, 1975). EGF is now known to affect many cell types, not just epidermal cells, and to regulate diverse processes such as proliferation, differentiation, and migration (Dhomen et al., 2012; Sorkin and Goh, 2008). EGF signaling is often perturbed in cancer cells and many cancer therapeutics target EGF signaling and trafficking (Dhomen et al., 2012).

EGF binding to the EGF receptor induces activation of EGFR's tyrosine kinase activity, and auto-transphosphorylation of the EGFR dimer (Cohen et al., 1980). EGFR can interact with different adaptor molecules to activate many different signaling pathways, including PI3K, mTOR, and ERK (as reviewed in (Pawson and Scott, 1997)). However, there are more biological outcomes from EGF stimulation than known signaling pathways, indicating that other factors influence cellular responses to EGF (Citri and Yarden, 2006).

One such factor is endosomal trafficking. While in endosomes, the tyrosine kinase domains of EGFR are still exposed in the cytoplasm and capable of recruiting signaling molecules. These "signaling endosomes" (Grimes et al., 1996) can recruit different

effectors to the receptor than those at the plasma membrane. However, some conflicting evidence indicates EGFR signaling is restricted to the plasma membrane (Sousa et al., 2012).

Phosphorylation and ubiquitination of EGFR are important factors involved in triggering both endocytosis and sorting in the endosomal system (Sorkin and Goh, 2008). EGFR trans-phosphorylates its cytoplasmic tails on tyrosine residues. These p-Tyr residues are recognized by GRB2, a SH2/SH3 domain protein (Jiang et al., 2003; Johannessen et al., 2006). GRB2 recruits CBL leading to ubiquitination of EGFR (Joazeiro et al., 1999; Levkowitz et al., 1999), recruitment of clathrin machinery, endocytosis of EGF/EGFR, and trafficking through the endosomal system to lysosomes for degradation (Haglund et al., 2003; Jiang et al., 2003). However, internalization of EGFR is robust, and EGFR mutants that cannot be ubiquitinated are still endocytosed using a different route (Huang et al., 2007).

EGFR signaling is regulated by controlling the levels of phosphorylated and ubiquitinated EGFR. Phosphorylation of EGFR can be reversed by phosphatases such as PTP1B (Haj et al., 2002), TCPTP (Mattila et al., 2005), and RPTP $\kappa$  (Xu et al., 2005). Dephosphorylation of EGFR by PTP1B arrests signaling and allows EGFR sequestration into MVBs (Eden et al., 2010). Ubiquitination can be reversed by DUBs such as AMSH (McCullough et al., 2004) and UBPY (Mizuno et al., 2005). Ubiquitination of EGFR is necessary for its internalization into the ILVs of MVBs and eventual degradation in lysosomes. In the

absence of EGFR ubiquitination, EGFR is sorted to recycling endosomes and ultimately back to the plasma membrane (Eden et al., 2012).

The transport of EGF in the early endosome is a critical step in regulating EGF signaling, a pathway involved in many developmental processes and disease states like cancer.

Early endosomes transport EGFR a significant distance in the cell, from the cell surface to the perinuclear region, and are associated with many different motors and motor regulatory molecules. However, which motors drive endosomal motion at different stages of maturation, help navigate different regions of the cell, or are regulated to alter EGFR signaling is unknown.

### **1.3 What drives long distance transport in the cell?**

#### **1.3.1 Molecular motors**

Directed transport is powered by molecular motors. These motors convert the chemical energy produced by ATP hydrolysis into mechanical energy, allowing them to step along polarized cytoskeletal filaments. There are two polarized cytoskeletal networks in the cell, the actin and MT cytoskeletons. In most cell types, microtubules are nucleated from the centrosome in the perinuclear region and their minus-ends remain anchored near the centrosome (Brinkley, 1985). The plus-ends of microtubules grow towards the edges of cells, creating a polarized array of microtubules used by motors for long distance transport. Actin filaments have a plus- and a minus-end, also referred to as the

barbed (+) and pointed (-) ends. Actin filaments nucleated near the plasma membrane grow with their plus-ends towards the cell edge (Borisov and Svitkina, 2000). However, actin filaments can be nucleated throughout the cell and can be arranged into structures of mixed polarity filaments (Dominguez and Holmes, 2011). Actin filaments are generally thought to be used for local transport.

Several actin filament- and MT-based motors (myosin Vb (Provance et al., 2008), myosin VI (Aschenbrenner et al., 2003), myosin 1b (Raposo et al., 1999), kinesin-1 (Loubery et al., 2008), kinesin-2 (Loubery et al., 2008), KIF16b (Hoepfner et al., 2005), and dynein (Aniento et al., 1993; Flores-Rodriguez et al., 2011)), as well as MT (Pierre et al., 1992) and actin (Taunton et al., 2000) dynamics, have been implicated in early endosomal trafficking. Purification and *in vitro* characterization of the intrinsic properties of different motors have given us insight into how each one is adapted for its role in the cell. Special emphasis will be placed on reviewing research on the properties of motors implicated in early endosomal transport. Understanding the details of the mechanism by which different motors attach to cargo and generate force is necessary to interpret how different regulators would influence the motion of a given motor, leading to changes in the motion of early endosomes.

#### **1.3.1.1 Myosin motors**

There is a large family of myosin motors conserved throughout many species (Berg et al., 2001; Odrionitz and Kollmar, 2007). Myosins share three structural features, a globular motor domain that binds to actin filaments and ATP (Ruppel and Spudich, 1996), a lever arm that binds to light chains such as calmodulin (Howard and Spudich, 1996; Warshaw et al., 2000), and a tail domain that diverges the most in sequence and is involved in cargo binding (Krendel and Mooseker, 2005).

Myosins move along actin filaments by undergoing a conformational change in response to binding and hydrolyzing ATP, reviewed in a simplified scheme here. When no ATP is bound, the motor domain is strongly bound to actin filaments. ATP binding induces a conformational change in the motor domain leading to its release from actin. ATP is hydrolyzed to ADP-Pi and leads to another conformational change, the reverse power stroke, which is when the myosin lever arm is “cocked”. This is followed by myosin rebinding to actin. Pi release from the motor domain accompanies the power stroke and is followed by another strong binding state. Finally ADP is released and ATP can rebind and begin the cycle again. The relationship between the chemical and mechanical cycles of myosin was first proposed by Lymn and Taylor in 1971 to describe muscle contraction (Lymn and Taylor, 1971).

In vitro characterization of the ATPase cycle, force production, and response to force of many different myosins has provided insight into the role they are capable of playing inside the cell. Four functional groupings of myosins based on these properties were

proposed by Bloemink and Geeves: (1) fast movers (2) slow/effective force holders (3) strain sensors and (4) gates (Bloemink and Geeves, 2011).

Myosin V is a dimeric motor that spends the majority of its ATPase cycle strongly bound to actin (ADP release is rate limiting) (De La Cruz et al., 1999). This means that myosin V can undergo many ATPase cycles and walk processively along the actin filament because the chance that both motor domains are detached from actin is low. This property is called a high duty ratio (Howard, 2001). Myosin V was the first myosin shown to be processive (Mehta et al., 1999), and also the first to be directly visualized walking using high-speed atomic force microscopy (AFM) imaging (Kodera et al., 2010). For comparison, myosin II family motors, which form bipolar filaments in muscle sarcomeres and stress fibers, have a low duty ratio (Kovacs et al., 2003) which results in myosin heads detaching from actin after a single power stroke (Finer et al., 1994).

In addition to a high duty ratio, myosin V has several other properties that make it a good transport motor. Myosin V takes 36 nm steps, which allows it to step in the same place along the long pitch of the actin helix and move in a straight path (Walker et al., 2000), there is strain-based gating between the two motor domains to couple their ATPase cycles for better processivity (Purcell et al., 2005; Veigel et al., 2002), and the elasticity of its tail domain has been proposed to allow it to pull cargo through the viscous intracellular environment without the motor domain experiencing a resistive load (Hammer and Sellers, 2012; Schilstra and Martin, 2006). In vitro, single molecules

of myosin V move at  $\sim 0.5 \mu\text{m/s}$  towards the barbed end of actin filaments with a run length of  $\sim 400\text{-}800 \text{ nm}$  and a stall force of  $3 \text{ pN}$  (Baker et al., 2004; Clemen et al., 2005; Mehta et al., 1999).

Myosin VI is also a processive motor (Rock et al., 2001) with a high duty ratio (De La Cruz et al., 2001) that gates its two motor domains. However, it has an extra sequence prior to its lever arm that leads the power stroke to move in the opposite direction to other myosins. Therefore, myosin VI walks towards the minus, or pointed end, of the actin filament (Wells et al., 1999). Artificially dimerized myosin VI motors have a variable step size (Rock et al., 2001) and take a “wobbly” path along actin filaments (Sun et al., 2007). Myosin VI motors move at  $\sim 0.2 \mu\text{m/s}$  in vitro with a run length of  $\sim 230 \text{ nm}$  and stall force of  $3 \text{ pN}$  (Rock et al., 2001).

Class I myosins motors, such as myosin 1b, are single-headed motors. Myosin 1s are not thought to be cargo transporting motors in vivo, but instead to be involved in force sensing or tension maintenance (Pollard and Ostap, 1996). In addition to generating force, myosin motors are also sensitive to loads applied to them. One example of this is the strain based gating that couples the ATPase cycles of the motors in myosin V and myosin VI. Applying a small load ( $\sim 1 \text{ pN}$ ) to myosin 1b traps it in a strongly bound state for several seconds (Laakso et al., 2008), suggesting it is involved in tension sensing and/or maintenance. However, other class I motors, such as myosin 1c, are much less force sensitive despite similar sequence and structure, highlighting the importance of

characterizing each myosin (Greenberg et al., 2012). Myosin Ib has a step size of ~8 nm (Laakso et al., 2008) and a speed of ~150 nm/s in an ensemble (Lin et al., 2005).

In conclusion, early endosomes have been associated with myosins that can move processively towards both the plus and minus ends of actin filaments, and myosins that are thought to function as tethers and tension sensors.

### **1.3.1.2 Kinesin motors**

There are 14 classes of kinesin motors (Lawrence et al., 2004) with three general domain architectures (Verhey and Hammond, 2009). The majority of kinesins are plus-end directed transport motors that contain an NT globular motor domain that binds MTs and ATP, a neck linker that coordinates the two motor heads, and a stalk/tail region that binds to light chains and cargo or adaptor molecules (Hirokawa, 1998; Hirokawa et al., 1989). When the motor domain is in the center of the protein, the motors are generally involved in MT destabilization like MCAK. When the motor domain is in the CT, as for the kinesin-14 family, the motor moves towards the MT minus-end. The plus-end directed kinesin motors kinesin-1 (Loubery et al., 2008), kinesin-2 (Loubery et al., 2008), and KIF16b (Hoepfner et al., 2005) have been implicated in moving early endosomes.

The motor domain of kinesins has a similar fold to myosin motors (Kull et al., 1996). However, the kinesin chemical-mechanical cycle differs. Instead of ATP binding leading

to a weak binding state like it does in myosins, binding of ATP to the lead head in a kinesin dimer leads to docking of the neck linker on the motor domain, which causes the rear motor domain to move forward and eventually bind the next tubulin dimer (Case et al., 2000; Rice et al., 1999). Strain between the two motors in a kinesin dimer leads to a coupling of their ATPase cycles, and processive motility (Yildiz et al., 2008).

Kinesin-1 is involved in the rapid, long-distance transport of many different cargos in all cells, and 2 specialized isoforms are expressed in the brain. Kinesin-1 is a tetramer containing two motors and 2 light chains. Kinesin-1 walks using a hand over hand mechanism, taking 8 nm steps (Svoboda et al., 1993) between tubulin dimers along a single protofilament in a microtubule (Wang et al., 1995). Single kinesin-1 motors generate ~5-7 pN of force in vitro (Visscher et al., 1999) and have a run length of ~1  $\mu\text{m}$ , making them very good long distance transport motors. Cargo binding can be done through both the kinesin globular tail regions and the kinesin light chains (Verhey and Hammond, 2009).

Kinesin-2 is a heterotrimer made of two motor domains, KIF3A and KIF3B, and an essential light chain, KAP3 (Cole et al., 1993). *Xenopus* kinesin-2 produces ~5 pN of force (Schroeder et al., 2012), so its force production is similar to kinesin-1, but it has a shorter run length (Muthukrishnan et al., 2009; Shastry and Hancock, 2010) and is more likely to detach under load (Schroeder et al., 2012).

KIF16b is a kinesin-3 family member. This family is thought to be monomeric or weakly dimerized in the cytosol, and dimerized when bound to cargo (Hoepfner et al., 2005; Verhey and Hammond, 2009). Few studies of KIF16b have been performed in vitro, but preliminary work demonstrated it can processively move cargo as an ensemble at a speed of ~200 nm/s towards the plus-end of MTs (Hoepfner et al., 2005).

In conclusion, early endosomes contain plus-end directed kinesin motors that are efficient long-distance transporters in vitro but vary in their gating, speed, and run length.

### **1.3.1.3 Cytoplasmic dynein**

Dynein is the major minus-end directed MT motor. In contrast to the myosin and kinesin families, there is only 1 cytoplasmic dynein motor, although other axonemal isoforms exist that are important for transport and movement in cilia. However, dynein is a 1.6 MDa complex with many interacting partners that may help adapt it for different tasks. The dynein motor consists of 2 heavy chains (DHC; MT binding domain, AAA ATPase motor domain, and tail), 2 intermediate chains (DIC) that bind DHC, 3 light chains that bind DIC (TcTex1, LC8, LC7/roadblock), and 2 light intermediate chains (LIC) that bind DHC (Kardon and Vale, 2009).

The dynein motor is a member of the AAA ATPase family which are large, ring-like hexamers of ATPase domains (Neuwald et al., 1999). Dynein is unusual among AAA

proteins in that all 6 repeats of the ATP binding domain are encoded on a single transcript and are slightly different from each other. Only AAA 1-4 bind ATP; AAA 1 and AAA 3 are thought to be involved in motility but ATP binding to AAA 2 and AAA 4 has an unknown function proposed to be regulatory (Kon et al., 2004; Reck-Peterson and Vale, 2004).

The MT binding domain is at the end of 10 nm antiparallel coiled-coil stalk domain that emerges from AAA 4 (Gee et al., 1997), separating the MT binding site and the ATP binding sites by a large distance. Recent structural studies of the yeast dynein motor domain suggest that a buttress across the AAA ring transmits the conformational changes during the ATPase cycle to the stalk domain (Carter et al., 2011). FRET measurements indicate that sliding within the stalk, leading to a change in register of the coiled-coil, couples ATP-induced conformational changes to changes in MT binding affinity (Kon et al., 2009).

Dynein is a high duty ratio motor, and its strongly bound states are nucleotide-free and ADP bound. Binding to ATP releases dynein from MTs (Vale, 2003). Purified dynein is processive (Wang et al., 1995) and only the motor and MT binding domains are required for motility (Reck-Peterson et al., 2006). It takes variable steps from 8-24 nm (Mallik et al., 2004; Reck-Peterson et al., 2006), and can move towards both the minus-end, plus-end (Ross et al., 2006), and sideways to adjacent protofilaments (Reck-Peterson et al.,

2006). However, in an ensemble, dynein movement is minus-end directed (Mallik et al., 2005).

Although yeast dynein differs from mammalian dynein in that it is slower and produces more force (Gennerich et al., 2007), it has been studied at the single molecule level in more detail. Although all biophysical and biochemical properties of yeast dynein may not be conserved, studies on the mechanism of yeast dynein motility should inform our thinking of how mammalian dynein walks. Unlike myosin and kinesins, which coordinate the ATP cycles of the two motor domains to walk in a gated fashion, dynein's two motor domains are not tightly coupled (DeWitt et al., 2012; Qiu et al., 2012). Studies in vitro of yeast dynein indicate that the direction and stepping of the two dynein heads are largely uncoordinated until a large separation between them occurs, which may lead to strain-induced gating similar to myosin and kinesin motors (Qiu et al., 2012). Thus dynein is unique in its flexible step size and direction.

Mammalian dynein is a weak motor, stalling at only  $\sim 1$  pN of force (Mallik et al., 2004; Schroeder et al., 2010), although one study measured a stall force closer to 7 pN (Toba et al., 2006). Dynein moves at  $\sim 300$ - $800$  nm/s and has a run length of about  $1 \mu\text{m}$  (Mallik et al., 2005; Ori-McKenney et al., 2010; Ross et al., 2006). However, in the cell dynein is usually associated with a large modulating complex, dynactin (11 subunits, 1 MDa) (Gill et al., 1991; Schroer and Sheetz, 1991) and a variety of other interaction partners. Although dynactin is required for most dynein functions in the cell (Schroer,

2004), the mechanism by which is promotes dynein activity is poorly understood since purified yeast and mammalian dynein are motile in the absence of dynactin in vitro.

### **1.3.2 Organelle and cargo movement by motors**

Most organelles and cargo in the cell contain multiple motors, often different types of motors, and exhibit different types of motion over time. There are several levels of regulation of motor activity at the level of an individual cargo that will be discussed here: (1) the recruitment of motors to the cargo (2) cargo loading onto the cytoskeletal track (3) competition between different types of motors (4) regulatory proteins that alter motor activity through interaction with the motor (5) or through motor interaction with the cytoskeletal track.

Although many types of regulation are known to be possible, and in some instances can be reconstituted in vitro, there is still little known about how or why an individual cargo changes movement at a given time considering the multitude of potential regulatory molecules and motors associated at once. This dissertation approaches the problem of the coordination and regulation of motors on a cargo by focusing on the motion the cargo exhibits and comparing that to potential types of motor regulation which will be reviewed in detail here.

#### **1.3.2.1 Cargo-specific recruitment of motors**

The number and type of motors attached to an individual transport cargo plays an important role in how that cargo moves. Motors can attach directly to cargo proteins, lipids on the cargo, or be recruited via adaptor/scaffolding proteins (Verhey and Hammond, 2009). Recruitment of motors to cargo is also an important method of regulating motor activation via relieving autoinhibitory interactions within the motor (kinesin-1, kinesin-2, myosin V) or promoting dimerization by creating a locally high concentration of a motor (myosin VI, KIF16b).

The Rab family of GTPases play an important role in defining endosomal compartments (Zerial and McBride, 2001). Rab5 effectors are responsible for the recruitment of several endosomal motors, although many questions remain about the timing and spatial organization of those recruitments.

KIF16b contains a PX domain specific for PI(3)P lipids in its tail (Hoepfner et al., 2005).

Mutagenesis of this PX domain to disrupt PI(3)P binding or depletion of PI(3)P on early endosomes inhibits KIF16b recruitment to early endosomes (Blatner et al., 2007).

Although these studies suggest PI(3)P binding is required for KIF16b recruitment to early endosomes, it is not known if KIF16b has other early endosomal binding partners. One study identified an interaction between Rab14 and KIF16b that indicated another role for this motor on the Golgi (Ueno et al., 2011). Few studies have been done on KIF16b so its binding partners and roles in the cell are still poorly described. Other kinesin-3 family members are thought to exist as monomers in the cytoplasm and undergo cargo-

mediated dimerization (Verhey and Hammond, 2009) . KIF16b may use a similar mechanism. In vitro however, purified KIF16b can move PI(3)P-enriched cargos as an ensemble (Hoepfner et al., 2005).

Myosin I family members are monomeric motors that interact with membranes via their cargo binding tail domains and link them to actin via their motor domains. All myosin I family members contain a putative PH domain in their tail (Hokanson et al., 2006), which has been confirmed to mediate myosin 1b membrane binding to phosphatidylinositol 4,5-bisphosphate (PIP<sub>2</sub>) and phosphatidylinositol 3,4,5-triphosphate (PIP<sub>3</sub>) (Komaba and Coluccio, 2010). PIP<sub>2</sub> is highly enriched on the plasma membrane, but it is also involved in early endosomal functions and is thought to coordinate with PI(3)P for regulation of some protein interactions (Gallop et al., 2013). Therefore, PIP<sub>2</sub> is one candidate for myosin 1b recruitment to early endosomes.

Myosin VI dimerization is induced by binding to endosomal cargo (Altman et al., 2007; Yu et al., 2009). Myosin VI is associated with many different cargos including autophagosomes, secretory vesicles, and endosomes. Several interaction partners have been found for endocytic clathrin structures (Dab2, PIP<sub>2</sub>), uncoated vesicles (GIPC, Tom1, Toml1), and early endosomes (LMTK2) (Buss and Kendrick-Jones, 2011).

Class V myosins are autoinhibited by an interaction between their tail and motor domains (Liu et al., 2006; Thirumurugan et al., 2006). This interaction reduces

processivity by converting myosin V into a low duty-ratio motor (Sato et al., 2007). The attachment between myosin Vb and early endosomes is unknown. As an example of a cargo attachment of a different class V myosin, myosin Va's attachment to melanosomes will be discussed. Myosin Va is recruited to melanosomes through an interaction with the Rab27a effector melanophilin (Wu et al., 2002). A Rab5 effector has not been found to interact with myosin Vb, but Rab-mediated attachment is a common theme in motor recruitment and a likely future area of exploration.

Kinesin-1 and kinesin-2 family members are autoinhibited via a folded conformation in which the tail interacts with the motor domains in the absence of cargo (Coy et al., 1999; Friedman and Vale, 1999; Hammond et al., 2010a). Binding of these motors to cargo relieves autoinhibition. The means of attachment of these motors to early endosomes is unknown. Two kinesin-1 interaction partners are associated with early endosomes, the scaffold huntingtin (McGuire et al., 2006) and dynein intermediate chain (Ligon et al., 2004), although a role for them in recruiting kinesin-1 to early endosomes has not been shown.

Dynein and dynactin are required for the minus-end directed transport of early endosomes to the perinuclear region as well as the morphological changes associated with MVB formation (Driskell et al., 2007). The mechanism of dynein association with early endosomes is not fully understood but recent studies in the fungus *Aspergillus nidulans* suggest that the p25 subunit of dynactin is required for dynein activity

specifically on early endosomes (Zhang et al., 2011). In COS-7 cells, both the p25 and p27 subunits of dynactin, which are in the pointed end complex, were found to be required for normal positioning and motility of early endosomes but not for several other dynein functions (Yeh et al., 2012). The binding partners of p25 and p27 on early endosomes are unknown.

### **1.3.2.2 Transport initiation factors**

A cargo with attached, active motors still needs the motors to bind to the appropriate cytoskeletal track for directed transport to occur. In vitro, active motors bind actin filaments and microtubules and begin transport without additional factors, but there is evidence that dynein in particular uses loading factors in the cell.

In neurons from both mice and drosophila, the p150 subunit of dynactin was shown to facilitate loading of cargo at the distal ends of axons where there is an enrichment of MT plus-ends (Lloyd et al., 2012; Moughamian and Holzbaur, 2012). CLIP-170, a plus-tip tracking protein, was suggested to load endocytic vesicles onto MTs in mammalian cells (Pierre et al., 1992). More recent studies of melanosome trafficking in *Xenopus* melanophores found that CLIP-170 was required for normal rates of melanosome loading onto MTs as well. Additionally, the melanosomes bound to MTs preferentially near the plus-tips where CLIP-170 is concentrated (Lomakin et al., 2009), and increasing the total number of dynamic MTs enhanced transport initiation rates (Lomakin et al.,

2011). In *Aspergillus*, which forms a long hyphal extension with a concentration of MT plus-ends reminiscent of the distal end of an axon, the dynein-binding protein Lis1 is an initiation factor for dynein-mediated transport of endosomes (Egan et al., 2012). These studies suggest dynein-mediated cargo transport in particular may require a loading phase near the plus-ends of MTs. Whether this is true in all cells, especially cells without the highly polarized clustering of plus-tips like neurons and the hyphal tips of fungus, is unresolved.

Other examples of non-motor mediated linkages of cargos to MTs include vesicle-associated MAP2 (Severin et al., 1991) and homotypic tethering between Rab proteins that leads to vesicle clustering near the cytoskeleton (Lo et al., 2012). These types of cargo-MT tethers could assist in both cargo transport initiation and also enhance processivity by maintaining cargo attachment to the MT when motors detach from the MT.

### **1.3.2.3 Coordination of multiple motors**

Most cargoes and organelles contain several motors of multiple types. How is transport achieved with these competing motors? One proposed mechanism is a coordinated regulation of which motor is “on” at different times via recruitment of regulatory proteins to switch between types of motor activity (Gross, 2004). Other mechanisms include a force-dependent tug-of-war between motors (Muller et al., 2008), and

preference for different modifications on the cytoskeletal tracks (Hammond et al., 2010b; Jacobson et al., 2006).

#### **1.3.2.4 Regulatory proteins**

As already discussed, dynactin is necessary for most dynein functions in vivo and increases dynein processivity in vitro (King and Schroer, 2000). Other proteins alter dynein activity, including Lis1, Nde1, and Ndel1 (Lam et al., 2010). Lis1 is unique in that it binds to the dynein motor domain. For mammalian and yeast dynein, Lis1 stabilizes a persistent MT binding state in dynein (Huang et al., 2012; McKenney et al., 2010). Mutations in Lis1 are associated with defects in nuclear migration in neurons (Vallee and Tsai, 2006), and Lis1 is required for specifically moving large endosomes in cultured neurons (Yi et al., 2011), which has led to the model that Lis1 binding to dynein adapts it to move large cargos.

Kinesin-1 is constitutively active as a truncated motor in vitro, and exhibits similar speeds and run lengths in live cells (Courty et al., 2006). However, since the full-length protein exists in an autoinhibited state, its activity can be regulated in the cell. Studies in drosophila suggest that similar to dynactin for dynein, the microtubule associated protein (MAP) MAP7/ensconsin is necessary for all kinesin-1 mediated transport activity in vivo (Barlan et al., 2013; Sung et al., 2008). MAP7 binds directly to kinesin-1 and MTs. In vitro, binding of full-length kinesin to MTs is enhanced by MAP7 (Sung et al., 2008). In

mammalian systems, it is not clear if MAP7 is crucial for all kinesin-1 functions. MAP7 null mice are viable, but do exhibit defects in spermatogenesis due to disorganization of a bundled MT structure called the spermatid machete (Komada et al., 2000).

Some scaffolds, such as huntingtin (Htt), bind to several motors, possibly allowing them to coordinate motor activity (Caviston and Holzbaur, 2009). Notably Htt binds to the DIC subunit of dynein (Caviston et al., 2007; Sahlender et al., 2005), through HAP1 to kinesin-1 (Caviston et al., 2007; McGuire et al., 2006; Twelvetrees et al., 2010), and through optineurin to myosin VI (Sahlender et al., 2005). Htt depletion leads to dispersal of early endosomes, similar to the effect of DHC knock-down (Caviston et al., 2011), suggesting the Htt scaffold may be one way of regulating which motors are active or associated with early endosomes.

#### **1.3.2.5 Signaling based coordination of motor activity**

Melanosome transport in melanophores is one of the best characterized examples of a signaling pathway regulating the direction of transport. In response to melanocyte-stimulating hormone (MSH), the granules are transported outwards and distributed evenly throughout the cell using transport on MTs and actin filaments. In response to melatonin, the melanosomes are transported back to the perinuclear region. Purified melanosomes contain kinesin-2, dynein, and myosin V (Rogers et al., 1997). When cell extract from and MSH-treated cells is added to purified melanosomes, it biases their

movement towards the MT plus-end and when extract from melatonin-treated cells is added, melanosomes movement is biased towards the MT minus-end (Rogers et al., 1997). Further study of this system demonstrated that at least two signaling pathways are involved in regulating motor activity, ERK and PKA. In response to MSH, cAMP levels rise, stimulating PKA activity and somehow biasing motor activity in favor of kinesin-2 (Park et al., 2007). Melatonin has the opposite effects. MEK and ERK are both bound to melanosomes (Deacon et al., 2005). In response to melatonin, ERK signaling is activated and there is an increase in transport in both directions (Deacon et al., 2005).

In addition to phosphorylation-based changes in motor activity via kinase cascades, signaling pathways that increase intracellular calcium can regulate motor activity. High calcium concentrations release calmodulins from the IQ motifs in the lever arms of myosins, making the lever arms floppy and unable to transduce force (Lewis et al., 2012). This has been demonstrated to change the step size and force production of myosin Ib (Lewis et al., 2012).

### **1.3.3 Cytoskeletal track preferences**

Once a cargo has commenced movement, proteins associated with the cytoskeletal track have the ability to act as obstacles to transport or to enhance motor activity.

Tubulin contains several post-translational modifications (PTMs) that are associated with recruitment of specific motors, and MT binding proteins such as MAPs are known

to be important regulators of motility. Similarly, actin-binding proteins can affect actin filament structure, actin network organization, and motor interactions with actin.

### **1.3.3.1 Microtubules**

MTs polymerize from GTP-tubulin dimers. Over time, the GTP is hydrolyzed to GDP within the MT lattice. GTP hydrolysis is thought to alter the structure of the tubulin dimer, leading GDP tubulin to form curved peels during depolymerization (Hyman et al., 1995). The polymerizing plus-tips of MTs are enriched in GTP tubulin. A cryo-electron microscopy reconstruction of the interaction between the yeast homolog of the plus-tip tracking protein EB1 (Mal3) and MTs showed that Mal3 sits between MT protofilaments near the GTP site, suggesting it is well-placed to sense the nucleotide state (Maurer et al., 2012). In addition to the growing plus-tips of MTs, some islands of GTP tubulin were found scattered in the MT lattice using an antibody specific for GTP tubulin (Dimitrov et al., 2008). GTP islands in neuronal cells lead to preferential enhancement of kinesin-1 based transport (Nakata et al., 2011).

Tubulin can also be modified by several post-translational modifications which each have been reported to affect MAP and motor binding, and MT stability.

Detryrosinated MTs are produced when the c-terminal (CT) tyrosine of  $\alpha$ -tubulin is removed. This modification is associated with poor interaction of kinesins that depolymerize MTs such as MCAK (Peris et al., 2009) but enhanced kinesin-1 association

in cells (Dunn et al., 2008), suggesting that detyrosination is a modification that favors the production of stable MTs used for long distance trafficking.

The glutamate residues on the CT tails of  $\alpha$  and  $\beta$  tubulin can be glutamylated (Glu-MTs). Decreasing this modification in mice lead to specific defects in KIF1A-mediated transport, indicating that glutamylation regulates motor-specific trafficking (Ikegami et al., 2007).

MTs can also be acetylated on lysine residues. The major lysine residue modified by acetylation is found on the inner wall of the MT, making it unclear how the acetylase could access this site, and how this would influence binding of MAPs and motors. In vivo, kinesin-1 movement occurs preferentially on acetylated MTs (Cai et al., 2009; Reed et al., 2006). In neurons, increasing MT acetylation enhanced BDNF motility in both the retrograde and anterograde directions suggesting dynein is also affected (Dompierre et al., 2007). However, since the identification of the major tubulin acetylase,  $\alpha$ -TAT (Akella et al., 2010; Shida et al., 2010), the role of acetylation in directly affecting motors has been called into question in mammalian systems. In vitro, acetylated MTs do not affect kinesin-1 motility, suggesting differential binding of a MAP or other intermediary affects kinesin-1 in cells (Walter et al., 2012). Additionally, KO of  $\alpha$ -TAT1 produces viable mice that lack detectable acetylation and have only mild defects, indicating acetylation may be a marker of a specially modified subset of MTs but not the cause (Kalebic et al., 2013).

MAPs can either inhibit transport via acting as roadblocks or MAPs can enhance motor activity. For example, the MAP tau is a largely unstructured protein that binds along the MT with its CT tail extending away from the lattice. Tau binding to MTs inhibits kinesin-1 transport in vitro at the single molecule level (Dixit et al., 2008; Vershinin et al., 2007) or in an ensemble (Vershinin et al., 2007). In contrast, dynein, which has the ability to back and side step, can pass tau patches on the MT in vitro (Dixit et al., 2008; Vershinin et al., 2008). Tau thus allows dynein transport to dominate.

Another MAP, doublecortin, binds in between the protofilaments of 13 protofilament MTs, keeping it away from the ridge of the MT where motors bind (Fourniol et al., 2010). Doublecortin increases the run lengths of KIF1A-driven vesicles in neurons by stabilizing the weak ADP binding state of KIF1A to the MT (Liu et al., 2012).

One very striking visual example of the effect of these MT modifications on kinesin-1 transport was shown during the process of axon initiation (Jacobson et al., 2006). When newly plated axon cell bodies are imaged during dendrite and axon growth, the motor domain of kinesin-1 accumulates in different neurites over the course of many hours. When the axon is specified and begins to outgrow the other neuritis, kinesin-1 stays in this axon. Since this experiment was performed with a truncated kinesin-1 construct that cannot bind cargo, the switching between axons is likely driven by MT modifications that switch between neurites during early stages of growth (Jacobson et al., 2006; Nakata and Hirokawa, 2003).

### 1.3.3.2 Actin filaments

Actin is modified by a large number of post-translational modifications (PTMs), including: acetylation, ADP-ribosylation, arginylation, O-linked N-acetylglucosaminolyation, methylation, phosphorylation, ubiquitination, and redox-dependent modifications (Terman and Kashina, 2013). Amino-terminal (NT) acetylation of actin increases myosin-actin interactions in muscle (Abe et al., 2000), but other PTMs are largely unexplored for their role in regulating motor binding or activity. Since actin filament binding stimulates myosin's ATPase activity, changes in actin structure could be hypothesized to lead to downstream changes in motor ATPase activity. However, many PTMs lead to drastic changes in actin, such as the inability to polymerize (Terman and Kashina, 2013), and so many PTMs of actin may affect myosin motor activity indirectly by decreasing the available actin filament tracks.

Actin filaments are more flexible than MTs and sample a spectrum of different double helical twists even as pure filaments in vitro (Galkin et al., 2010). These structural changes can favor the binding of different actin binding proteins. The actin filament severing protein cofilin (Prochniewicz et al., 2005) for example prefers unstrained actin filaments (Hayakawa et al., 2011).

Actin-binding proteins can also stabilize different actin conformations, and these structural changes can be propagated along the filament. Binding of formins (Papp et al., 2006) or gelsolin to the barbed ends of actin filaments (Prochniewicz et al., 1996)

leads to changes in the twist of the whole filament. Binding of myosin motors to actin also leads to changes in actin filament twist which can propagate (Prochniewicz et al., 2010). Myosin V has a more dramatic effect on actin structure in comparison to muscle myosin II motor domains, suggesting myosin V may modify its own track as it walks (Prochniewicz et al., 2010).

Actin polymerization in the cell requires actin nucleators. Different nucleators generate different actin architectures. Arp2/3 mediated actin polymerization generates a branched network (Mullins et al., 1998), while formin-nucleated actin forms linear filaments (Pruyne et al., 2002; Sagot et al., 2002). These different structures, and their respective actin-binding protein complements, recruit purified myosin motors differently. In an elegant, semi-in vitro experiment, different classes of fluorescently-labeled myosin motors were added to extracted cytoskeletons from different cell types and their preferential binding to different actin structures interrogated (Brawley and Rock, 2009). One structure that favors a specific myosin is the branched lamellopodial network at the leading edge of a cell. Another group demonstrated that myosin VI can match its step size to the mesh size of the branched actin network and undergo processive runs stepping between filaments (Sivaramakrishnan and Spudich, 2009). A very different structure is formed from linear actin filaments nucleated by formins and bundled by the protein fascin in filopodia. This bundled structure is preferred by myosin X, which has a step size that allows it to stagger back and forth between adjacent actin filaments in the bundle (Nagy and Rock, 2010; Ricca and Rock, 2010).

The dynamics of actin filaments also affects myosin transport. Stabilization of actin filaments by jasplakinolide in *Xenopus* melanophores impaired myosin V-based transport of melanosomes (Semenova et al., 2008). The distance myosin can transport a cargo is increased by switching actin filaments in transport simulations (Snider et al., 2004). In the cell studies, myosin V is thought to walk towards the quickly growing barbed end of the actin filament and continue along the new growth, increasing its run length and chances of switching filaments (Semenova et al., 2008).

Actin binding proteins influence which types of myosin motors bind to the actin filaments. Tropomyosin is an extended molecule that binds along actin filaments. In muscle it decorates the thin filaments and can regulate muscle myosin II binding (Gunning et al., 2008). In mammalian cells there are several different isoforms of tropomyosin, which play different roles. Tm4, for example, binds to naïve stress fibers and is necessary for the recruitment of non-muscle myosin II (Tojkander et al., 2011). Class I myosins are in contrast excluded from regions of the cell containing tropomyosin-decorated actin (Tang and Ostap, 2001). The differential recruitment of myosin II and myosin I to tropomyosin-decorated actin was also demonstrated in yeast (Clayton et al., 2010). Additionally another actin binding protein, fimbrin, has been shown to compete with tropomyosin for binding to actin (Skau and Kovar, 2010). Targeting fimbrin to tropomyosin-containing structures can displace tropomyosin and lead to myosin I recruitment, highlighting the way several types of actin binding proteins can work together to switch motor recruitment dynamically in the cell (Clayton et al., 2010).

#### 1.3.4 Motor ensemble properties

Motors generate and respond to force. In general, having multiple motors on a cargo leads to longer run lengths (Beeg et al., 2008; Mallik et al., 2005; Vershinin et al., 2007) and higher forces but not usually an increase in velocity. However, the effects of having multiple motors of the same motor type on a cargo vary by motor. For example multiple kinesin-1 motors can interfere with each other, leading to a decreased velocity (Kunwar et al., 2008; Shubeita et al., 2008). When only two kinesin-1 motors are attached to a scaffold, only one engages at a given time (Jamison et al., 2010) suggesting kinesin-1 motors do not work well together. However, this interference could also depend on the way the motors are linked together. For example when kinesin motors are attached to a lipid bilayer they cluster at the tip of the moving lipid tubule and recycle back to the body of the vesicle (Koster et al., 2003). Motor mobility is prevented in most experiments using artificial scaffolds to cluster motors.

One example of the effect of resistive force on a motor is the strain-based gating used to coordinate the two heads of dimeric motors to increase processivity (DeWitt et al., 2012; Purcell et al., 2005; Qiu et al., 2012; Veigel et al., 2005; Yildiz et al., 2008). Loads can also be applied to motors in the cell from cargo and from opposite polarity motors engaging in a tug of war. In general, when a resistive force is applied to motors, a decrease in velocity is observed. The difference in the force-velocity relationship between kinesin-1 and dynein has recently been proposed to address why dynein seems

to function well in a group while kinesin-1, as described above, does not (Rai et al., 2013). Dynein slows under small loads, potentially allowing other motors in the back of the cargo not bearing the load to catch up and share the load. Kinesin-1 does not slow down until several pNs of force are applied, suggesting this may be one reason only a single kinesin seems to engage in vitro (Rai et al., 2013).

When multiple motors moving in different directions are engaged, they pull against each other resulting in a tug-of-war. Both the amount of force a motor can produce, how it responds to force, and its kinetics affect which motor will win. In silico, simulations of groups of opposite polarity motors demonstrated that taking into account only the properties of the motors, switches in direction and pauses in transport could be generated that are very similar to the saltatory movements of cellular cargos such as lysosomes (Hendricks et al., 2010; Muller et al., 2008). However, application of a tug-of-war model does not fully explain all cargo movements, indicating that direct coordination of motor activity also occurs (Kunwar et al., 2011).

Creating filament intersections in vitro induces the engagement of a different motor at a known time. When only kinesin-1 or only dynein are used, the artificial cargo pauses at MT intersections and sometimes deform the MTs during the tug-of-war (Ross et al., 2008). When artificial cargo containing both dynein and myosin V reach an actin-MT intersection, the total amount of force each motor can produce determines the filament chosen (Schroeder et al., 2010). However, total force cannot describe all tug-of-wars.

When kinesin-2 is used, the kinetics also play a role in determining the outcome of the tug-of-war (Schroeder et al., 2012).

Instead of competing with each other, motors can assist each other to increase processivity. For example, myosin V can diffuse along MTs and can increase kinesin-1's run length (Ali et al., 2007; Ali et al., 2008). In yeast the opposite scenario can be observed. A myosin V mutant that is not processive can be rescued by over expression of a kinesin that can bind F-actin and act as a tether for the low-duty myosin mutant (Hodges et al., 2009).

#### **1.3.4.1 Investigating motor coordination in the cell**

Tracking cargo in live cells results in clear steps of displacement similar to those seen for single motors in vitro. Peroxisomes (Kural et al., 2005), melanosomes (Kural et al., 2007), and endosomes (Nan et al., 2005) have been tracked with nm resolution and stepping matching the step size of the proposed motors in vitro. In the cell, optical trap based measurements of the force exerted by motors on an endogenous cargo also show displacements and forces in both directions in steps of matching stall forces of different motors, which suggests that one motor is engaged at a time or there is cooperative stepping of several motors (Hendricks et al., 2012a; Rai et al., 2013; Shubeita et al., 2008). Interestingly, many cargos stall for seconds at low forces of  $\sim 1$  pN (Hendricks et al., 2012a), indicating that small resistive forces may be important in the cell.

### **1.3.5 Other sources of motion in the cell**

Although molecular motors are known to be required for the rapid, directed transport of cargo like early endosomes, they are not the only source of motion inside the cell. The polymerization of cytoskeletal filaments can generate forces and flows that move cargo, and non-energy consuming processes like diffusion can lead to random motion of a cargo as well. The type of motion (random or biased in direction) and the speed of the motion expected from these different sources will be discussed to put into context which types of cargo movements in the cells could be attributed to non-motor sources.

#### **1.3.5.1 Cytoskeletal dynamics**

There are three classes of cytoskeletal filaments: actin filaments, microtubules, and intermediate filaments. In addition to the polarized filaments, actin and MTs, serving as tracks for motors, the cytoskeleton can move objects in the cell due to its dynamic polymerization and depolymerization and through bulk flows of its network coupling to other structures.

##### **1.3.5.1.1 Actin dynamics**

Actin filaments form a flexible double helical coil that is  $\sim 7$  nm in diameter. Although single filaments generate only  $\sim 1$  pN of force during polymerization (Footer et al., 2007), a large family of actin-binding proteins exist that can generate diverse actin-based

structures capable of generating enough force to deform membranes and move vesicles.

One actin nucleation factor, the Arp2/3 complex, binds to a mother filament and nucleates a new filaments from its side at  $\sim 70^\circ$  angle (Mullins et al., 1998). The Arp2/3 complex becomes the cross-link between the mother and daughter filaments, leading to a branched actin network. Depending on the levels of proteins, such as capping protein, that can regulate actin polymerization, these networks can contain a densely branched network of short actin filaments or a looser network with longer filaments (Akin and Mullins, 2008). Networks of short filaments with many branches are rigid and can generate sufficient force to drive plasma membrane protrusion during cell migration, potentially through a Brownian ratchet-like mechanism (Peskin et al., 1993).

In addition to moving the plasma membrane forward, branched networks can be used to move intracellular membranes. The pathogen *Listeria* hijacks this type of nucleation to generate a network of branched actin that pushes it through the cell (Theriot et al., 1992). Reconstitution of actin comet tail polymerization on beads with purified components demonstrated that actin polymerization is sufficient to generate propulsive movement (Loisel et al., 1999). This type of actin comet tail was observed on endosomes in *Xenopus* oocytes and HeLa cells (Taunton et al., 2000), on endosomes in lanthanum and zinc ion-treated macrophages (Southwick et al., 2003), on secretory lysosomes (Vincent et al., 2007), and on pinocytosed vesicles in macrophages (Merrifield

et al., 1999). Additionally, branched actin networks oriented with plus ends against the plasma membrane associate with clathrin-coated pits in mammalian cells where they are thought to contribute to membrane invagination (Collins et al., 2011).

Another class of actin nucleation factors, formins, generates linear actin filaments.

Formin-based actin nucleation can move vesicles using a different mechanism.

Recycling endosomes in mouse oocytes recruit formin-2, spire1, and spire2 to nucleate actin filaments from their surface. This allows them to form a polarized network with each other and the plasma membrane used for long-range directed movement of recycling endosomes to the plasma membrane (Schuh, 2011).

#### **1.3.5.1.2 Microtubule dynamics**

MTs are hollow rods about 24 nm in diameter that contain 13 protofilaments in most cells. They are more rigid than actin filaments, with a persistence length of mms (Egelman, 2012).

In vitro MTs generate several pNs of force. MTs respond to force applied to their plus-ends by slowing their polymerization rates, resulting in stalled MT growth at ~4 pN (Dogterom and Yurke, 1997). MT growth rates are also regulated by microtubule binding proteins, in particular proteins that specifically bind the plus-tips of growing MTs such as the EB family. In vivo MT growth rates are higher than those seen in vitro (Komarova et al., 2009; Zanic et al., 2013). The combination of the plus-tip tracking protein EB1,

which increases the “dynamicity” of plus-tips (i.e. both growth and catastrophe increase), and XMAP215, an elongation factor, are sufficient to produce in vivo growth rates of 0.4  $\mu\text{m/s}$  (Georgatos et al., 1997; Zanic et al., 2013).

The growth at the plus-ends of MTs can contribute to the movement of membranous organelles via directly coupling to the organelle, or by creating new MT tracks for motors that are preferentially directed towards sites of cargo delivery.

The ER resident transmembrane protein STIM1 is a binding partner of the plus-tip tracking protein EB1 (Grigoriev et al., 2008). Although the binding of EB proteins to MTs is transient, the interaction between STIM1 and EB1 is able to provide a linkage through which the growing MT pulls a new tubule out of the ER (Grigoriev et al., 2008). This type of ER extension was first demonstrated in *Xenopus* extracts and the linkage termed the tip attachment complex (Waterman-Storer et al., 1995; Waterman-Storer and Salmon, 1998). The mobility of STIM1 in the ER membrane is key for allowing this diffusional coupling to occur. When calcium is depleted in the ER, STIM1 forms less mobile oligomers and coupling between the ER and MTs is lost (Grigoriev et al., 2008).

Phosphorylation of STIM1 during mitosis also disrupts ER-MT coupling and prevents ER tubules from accumulating on the mitotic spindle (Smyth et al., 2012). These two regulatory mechanisms highlight the importance of taking into account local changes in the cell environment when considering sources of organelle movement.

Since MTs are dynamically growing and shrinking, regulation of polymerization rates or stabilization of MT plus-ends against catastrophe in specific locations in the cell allows cells to preferentially direct MT motor-based traffic. In epithelial cells, cell-cell communication is facilitated by connexin-based gap junctions. Kinesin-1 mediated transport of vesicles containing connexins to cell-cell contact sites is facilitated by preferential MT stabilization at cell junctions (Shaw et al., 2007). In vitro dynein is sufficient to capture and stabilize MT plus ends (Hendricks et al., 2012b; Laan et al., 2012). “Subtly biased” MT nucleation and density have also been shown to contribute to asymmetric cargo trafficking and polarization in drosophila oocytes (Parton et al., 2011).

Translocation of MTs is another mechanism of moving cargo in the cell. MTs have many MAPs, some of which can cross-link MTs. The very rapid movements of peroxisomes in S2 cells, at rates too high to be associated with molecular motors, were associated with MT buckling events that rapidly moved both the MT and the attached peroxisome (Kulic et al., 2008). Similarly, in mammalian LLC-PK1 epithelial cells, kinesin-1, which can interact with MTs via both its motor domain and its tail domain, is responsible for buckling and sliding of MTs relative to each other (Bicek et al., 2009).

MT depolymerization also generates forces used to move cargo in cells. As MTs depolymerize, peels of curved protofilaments form (Kirschner et al., 1975; Mandelkow et al., 1991). At the kinetochore, proteins such as Dam1 and Ndc80 attach MT plus-ends

to the centromeres of chromosomes (Alushin and Nogales, 2011). The force generated by depolymerizing MTs is several pNs, and can be harnessed by these adapter proteins to move chromosomes with the shortening MTs (Volkov et al., 2013). The use of MT depolymerizing forces to move other cargo in the cell has not been described. Bacteria contain a tubulin homolog, FtsZ, which also forms curved protofilaments and can deform membranes during depolymerization. This has led to the hypothesis that MT depolymerization is a conserved source of motion (McIntosh et al., 2010).

#### **1.3.5.1.3 Intermediate filament dynamics**

Intermediate filaments, such as keratin, septins, and vimentin, are a large family of non-polar filaments that play structural roles in the cell (Goldman et al., 2012). Although these non-polarized filaments are not thought to be used by motors for transport, they are abundant and can affect organelle trafficking. In *Xenopus* melanophores, melanosomes are surrounded by cages of vimentin filaments that dampen their motion (Chang et al., 2009). Similarly, in mouse fibroblasts mitochondria associate with vimentin filaments, and depletion of those vimentin filaments increases the motility of mitochondria (Nekrasova et al., 2011). Vimentin also dampens the actin comet tail-driven movement of *Listeria*, suggesting that the vimentin network dampens the motion of any cargo and does not specifically block motor-driven transport (Giardini and Theriot, 2001).

### 1.3.5.2 Diffusion and cytoplasmic flow

Diffusion of molecules and organelles in the cytoplasm leads to random movement. The rate of diffusion depends on temperature ( $T$ ), the radius of the particle ( $r$ ) and the viscosity of the cytoplasm ( $\eta$ ), as described by the Stokes-Einstein equation (Eq 1.1):

$$D = \frac{K_B T}{6\pi\eta r}$$

However, the cytoplasm is not a uniform, dilute solution. The protein concentration is 50-400 mg/ml in the cytoplasm, the viscosity is 4-8 times that of water, and filamentous networks like the cytoskeleton lead to elastic effects (Luby-Phelps, 2000). The crowding is significant enough that reaction rates in the cell will differ significantly from the same reaction in buffer (Zhou et al., 2008). Since crowding and filamentous structures are slowing diffusion, the size of the particle determines the types of structures that impede its movement. Studies of particles of different sizes injected into the cytoplasm or nucleus demonstrated experimentally that the diffusion coefficient scales with the size of the particle (Luby-Phelps, 2000).

In addition to diffusion, cytoplasmic flows have been observed that move proteins and larger structures (Ganguly et al., 2012; Shimmen and Yokota, 2004). One very striking example of this is the cytoplasmic streaming that occurs in plants and *Drosophila* oocytes, in which molecular motor driven cycling of cytoskeletal filaments creates a

cyclone that churns the whole cytoplasm. In mammalian cells, migration creates flows from the rear to the front of the cell driven by acto-myosin contraction. These cytoplasmic flows have been seen in migrating mouse fibroblasts (Iwasaki and Wang, 2008), fish keratocytes (Keren et al., 2009), and during the ameboid migration of leukocytes and cancer cells (Friedl and Wolf, 2010).

### **1.3.6 Spatial variation in the cell**

The development of tools to visually measure the concentration of biochemical and physical factors has revealed spatial variation of many of these factors within single cells. Many of these factors are known to have an effect on motor activity in vitro and could influence cargo entering different regions of the cell. ATP concentrations can vary across the cell, and have been proposed to regulate cell motility via affecting acto-myosin contraction (van Horsen et al., 2009). The pH of the cytoplasm and different organelles, even the nucleus which contains large pores, varies (Seksek and Bolard, 1996). Local calcium concentrations vary and often need to be spatially controlled for effective signaling (Morgan et al., 2013). The temperature of the cell varies spatially, and is higher for example near the centrosome and in the nucleus than in bulk cytoplasm (Okabe et al., 2012). And the viscoelastic properties arising from the cytoskeleton vary spatially and create different mechanical properties in the cell (Wirtz, 2009). These factors may fine-tune motor activity or other adaptor protein affinities, as the cargo moves through different regions of the cell.

#### **1.4 Current view of early endosomal motion**

Live-cell imaging of early endosomal motion has suggested that early endosomes move slowly (Hoepfner et al., 2005; Rink et al., 2005) and bidirectionally (Loubery et al., 2008; Nielsen et al., 1999) until recently. Most previous work imaged endosomal dynamics at a rate of 1 frame every few seconds. A recent study, published while this work was in progress, examined GFP-Rab5 positive endosome dynamics at 30 frames per second and observed that the endosomes were actually undergoing short (~1 s) rapid movements towards the perinuclear region (Flores-Rodriguez et al., 2011). However, in between these short periods of rapid motion, little movement occurs, leading to the previous observations of slow and random-looking movement over longer time-scales. Allan and colleagues' study of the dynein-driven directed portions of early endosomes demonstrated that dynein and dynactin are responsible for the perinuclear-directed transport. However, the bulk of the endosomal lifetime, the pauses, as well as the reason for the changes in motion remain unexplored for early endosomes, and most organelles in live cells.

The huge spectrum of potential interactions between the different motors and regulatory molecules on early endosomes makes it currently unclear how these proteins and motors are contributing to early endosomal transport. Since early endosomes exchange material with the rest of endosomal system, long-term perturbations like siRNA may lead to indirect disruption of early endosomal motion due to effects on

upstream or downstream disruption of the endosomal system. Additionally, early endosomes are maturing and altering their associated motors and regulators over time. Inhibition of motors with siRNA cannot be used to determine which phases of transport depend on specific motors or regulators if dynamic switching between types of movement occurs as observed in Flores-Rodriguez et al., 2011. Therefore, analyzing the type of motion that individual early endosomal cargos exhibit at high temporal and spatial resolution is critical to determine which motors and regulators are capable of producing the endosomal motion observed. This motion analysis can be used to form a framework to evaluate models of how motors and regulatory molecules work together to achieve long-distance transport of early endosomes in the cell.

### **1.5 Thesis overview**

This study focuses on (1) characterizing the whole spectrum of early endosomal motion, how the motion changes temporally, and (2) what cellular features correlate with different types of motion. These results are used to propose a framework to evaluate which of the many regulatory interactions reviewed in the introduction might coordinate early endosomal long-distance navigation from the plasma membrane to the perinuclear region.

This work is described in Chapter 3 and the methods in Chapter 2. As a final synthesis of this work, I have also begun to investigate the cellular role of KIF16b and to determine the role of lysosomal-ER connections in ER movement (Chapter 4).

## Chapter 2. Materials and Methods

### 2.1 Methods for Chapter 3

#### 2.1.1 Cell culture and transfection

Arpe-19 cells (ATCC CRL-2303) were cultured in DMEM/F-12 (Life Technologies) supplemented with 10% fetal bovine serum (Sigma) and antibiotics/antimycotics (Life Technologies). For live-cell imaging, Arpe-19 cells were serum-starved in DMEM/F12 containing 0.5% RIA-grade bovine serum albumin (BSA, EMD Chemicals) for 4 hours and imaged in phenol-red free DMEM/F12 containing 15 mM HEPES (Life Technologies) and 0.5% BSA.

COS-7 cells (ATCC) were cultured in DMEM (Life Technologies) supplemented with 10% fetal bovine serum (Sigma) and antibiotics/antimycotics (Life Technologies). For live-cell imaging, cells were cultured in phenol-red free DMEM containing 15 mM HEPES (Life Technologies) and 0.5% BSA (EMD Chemicals).

Cells were transiently transfected with Fugene 6 (Roche) according to manufacturer's instructions and imaged 16-24 hrs after transfection. The mCherry-CC1 construct contains amino acid residues 216-550 of human p150<sup>Glued</sup> attached to mCherry. The sources of other plasmids used in this study are: GFP-Rab5a (Marino Zerial, Max Planck Institute), mCherryC1-Rab5a (Christien Merrifield, MRC Laboratory of Molecular Biology,

Addgene Plasmid: 27679), mCherryC1-Rab7 (Alexander Sorkin, University of Pittsburgh), DsRed-mito (mitochondrial marker, Thomas L. Schwarz, Children's Hospital Boston), DsRed2-ER (Clontech, Anna Akhmanova, Utrecht University), mCherry-GPP1 (Golgi marker, Adam Linstedt, Carnegie Mellon University), 3xGFP-EMTB and 2xmCherry-EMTB (Chloe Bulinski, Columbia University), mCherry-Actin (Tatyana Svitkina, University of Pennsylvania), GFP-MyosinVI FL (Folma Buss, Cambridge Institute for Medical Research), mCitrine-KIF16b (Kristen Verhey, University of Michigan), Lamp1-RFP (Walther Mothes, Yale University, Addgene Plasmid: 1817).

### **2.1.2 EGF dye labeling**

Biotin-XX EGF (Life Technologies) was diluted to 1.3 µg/ml in 50 mM Borate Buffer, pH 8.3 (Life Technologies), mixed with 20 nM Quantum Dots 655-Streptavidin (SA) (Life Technologies) and incubated on ice for 30 min prior to its addition to cells at a concentration of 1.5 ng/ml EGF. For Alexa488 and Alexa532 labeled EGF, 2 µg/ml Biotin-XX EGF (Life Technologies) in 50 mM Borate Buffer, pH 8.3 was mixed with 50 µg/ml SA-Alexa488 or SA-Alexa532 (Life Technologies) and incubated on ice for 30 min prior to its addition to cells at 100 ng/ml.

### **2.1.3 Lysosomal labeling**

To label the lysosomes with dextran, cells were incubated with 100 mg/ml Dextran-TMR (Life Technologies) for 4 hours and then chased in dextran-free media for 24 hours to

allow the dextran to accumulate specifically in the lysosomal compartment. LysoTracker Red (Life Technologies) was added to cell culture media at 1:1000 for 5 min. Cells were washed several times in warm media and imaged immediately.

#### **2.1.4 Transferrin endocytosis assay**

Cells were serum-starved for 4 hours in media containing 0.5% BSA. A pulse of 20 µg/ml Transferrin-Alexa488 or Transferrin-Alexa594 (Life Technologies) was added to the cells for 5 min at 37°C. Cells were washed 3 times in warm PBS and either fixed immediately in 4% paraformaldehyde or incubated for 35 min in the absence of labeled transferrin prior to fixation. Epifluorescent images of fixed cells were acquired and scored for perinuclear accumulation after 40 min.

#### **2.1.5 Cytoskeletal drug treatment**

Drug doses were chosen that lead to disruption of the cytoskeleton without gross morphological changes in the cells, such as retraction and rounding up, that would compromise our ability to track EGF-Qdots in a single plane (Figure 3E): latrunculin B 1 µM (EMD Chemicals), jasplakinolide 100 nM (Life Technologies), nocodazole 10 µg/ml (Sigma). For jasplakinolide dosing, the fluorescence recovery after photobleaching (FRAP) of mCherry-Actin was compared before and after a 5 min treatment with jasplakinolide to pick a dose that resulted in stabilized actin.

### 2.1.6 Microscopy

Live-cell imaging was conducted on two microscopes using oblique angle illumination fluorescence microscopy (excitation light entered the sample above the critical total internal reflection angle).

Imaging for experiments in Figures 3A, 5, 6 7, 8A-C, Table 2, and Table 5 were obtained on Microscope #1, an inverted Nikon TE-2000U microscope equipped with a Photometrics Cascade-512B camera. Solid state 488 nm (Sapphire 488 LP, Coherent) and 561 nm (Crystalaser) lasers were used for excitation through a Nikon 100x, Plan-achromat 1.49 NA oil immersion objective. A Dual-View (Photometrics) system with an insert containing a 565 dichroic, 580 LP filter, and 515/30 BP filter (Chroma Technology) was used to separate emission channels. Cells were maintained at 37°C in a FCS2 (Bioptechs) chamber. All images were acquired at 20 fps (50 ms frames) for 50 s.

Imaging for experiments in Figures 1C,E,F, 2, 4, 8D-E, 9, and Tables 1 and 3 were performed on a Nikon Eclipse Ti microscope equipped with a Hamamatsu EMCCD camera (Model # C9100-13) and a Nikon 100x, 1.49 NA, Plan-achromat oil immersion objective. Solid state 488 nm and 561 nm lasers (Perkin-Elmer) were used for excitation. Spectral separation of the emission light was performed with a QuadView (Photometrics) system using an insert containing a 540 dchr, 515/30 BP filter, and a 615/30 BP filter (Chroma).

Cells were maintained at 37°C using a custom heated microscope enclosure (Solent Scientific). All images were collected at 20 fps (50 ms frames) for 30-60 s.

Images of TetraSpek beads (100 nm, Life Technologies) were used for alignment of Dual-View and QuadView images with custom MATLAB code. Briefly, the pairs of bead positions in the two channels were used to calculate the best translational and rotational offset for the whole image. Images of EGF-Qdots were not altered prior to tracking.

Images for figures 1A, 1C, 3E were taken with a Perkin Elmer spinning disc confocal system on a Nikon Eclipse Ti microscope body.

### **2.1.7 Tracking and data analysis**

GFP-Rab5, mCherry-Rab7, and EGF-Qdots were tracked using the MATLAB-based automated tracking algorithm u-track (Jaqaman et al., 2008), provided by Gaudenz Danuser (Harvard Medical School). An alternative in-house tracking algorithm, also based on 2D Gaussian fitting, using ImageJ (Schneider et al., 2012) was applied to several movies for comparison and yielded similar tracking results and spatial resolution.

Estimation of the spatial resolution of the system (~20 nm) was performed by tracking EGF-Qdots adsorbed to glass under normal live-cell imaging conditions (Figure 3A). Additionally, cells expressing GFP-Rab5 that had internalized GFP-Qdots into early

endosomes were fixed in 4% formaldehyde for 20 min and then imaged under live-cell imaging conditions and tracked as usual. The standard deviation of the position of the stationary Qdots over 10 s was used to estimate the spatial resolution.

Trajectories were analyzed using custom MATLAB (Mathworks) code with the exception of simulations and SCI calculations which were done with custom MathCAD (PTC, Inc.) code.

MSD analysis of trajectories was done using a sliding window of 45 frames (2.25 s). The mean squared displacement was calculated (Eq. 1) using all pairs and fit to the first 5 time lags (0.25 s). For example MSD fitting of data see Figure 3B. Thresholds to define the motion as directed ( $\alpha > 1.45$ ), diffusive ( $1.45 > \alpha > 0.4$ ), or confined ( $\alpha < 0.4$ ), were chosen based on the distribution of  $\alpha$  values present in the motile set of GFP-Rab5-positive EGF-Qdot trajectories (Figure 5C). The effective 2 dimensional radius of gyration ( $Rg^{2D}$ , Figure 3C) was calculated using the relationship in Eq. 2.

To confidently use the EGF-Qdot motion as a reporter for the motion of the early endosome, we first considered factors that could lead to motion of the EGF-Qdot cargo independent of early endosome motility. MT buckling, which has been shown to affect peroxisome movement (Kulic et al., 2008), is rare in our cells (data not shown).

Movement of EGF-Qdots within the interior of the endosome is unlikely because EGF does not dissociate from its receptor until endosomes mature and acidify (Sorkin and

Goh, 2009), and beads of similar diameter to EGF-Qdots inside early endosomes (Yoshida et al., 2001) had diffusion coefficients 100 fold higher than those of our EGF-Qdots. Although we cannot rule out these and other motion sources in every case, our MSD analysis led to consistent  $\alpha$  and D values for many different EGF-Qdots, in different cells, across different time scales of analysis, which suggests the EGF-Qdots are reporting the motion of early endosomes.

To ensure our MSD measurements were reliable, we (1) based the selection of the time window size on simulations using motion parameters similar to our data; (2) calculated an independent parameter, the 2-dimensional radius of gyration, to show that increases in  $\alpha$  and D were also detected in this alternative measure; and (3) performed an additional approach, moment scaling spectrum (MSS) analysis, which also enables classification of motion into confined, diffusive and directed categories. These other analytical approaches confirmed the conclusions originally made based on MSD  $\alpha$  values. These points are explained in more detail below.

(1) Analysis of simulated trajectories that matched the experimental imaging rate, spatial resolution, and diffusion coefficient was performed to determine the smallest time-window for calculating MSD that allowed recovery of the simulated D and  $\alpha$  values (Table 2). Since diffusion is a random process, using a short-time window will produce values of  $\alpha$  and D that fluctuate from those obtained from the entire trajectory over long time-scales. This source of variability increases the width of the  $\alpha$  and D

distributions measured using the short time period on simulated diffusion (Table 2— standard deviation in  $\alpha$  is 0.14 and the standard deviation in  $D$  is  $0.014 \mu\text{m}^2/\text{s}$ ). This variability is not large enough to perturb the classification of trajectories into 3 categories based on  $\alpha$ .

(2) The 2-dimensional gyration ( $Rg^{2D}$ ) offers an independent method to assess the area range that early endosomes explore during different phases of movement and just before and after actin disruption. It is not used to classify motion, but  $Rg^{2D}$  for simulated diffusive trajectories is not statistically different from the  $Rg^{2D}$  measured for our paused data (data not shown).

(3) To further examine how reliable each  $\alpha$  value is, we compared the  $\alpha$  value for each 2.25 s track segment to another measurement, the motion scaling spectrum (MSS) slope. In MSD analysis,  $r^2$  is mean squared displacement,  $n$  is time lag,  $N$  is length of trajectory,  $p$  is position.

$$r^2(\Delta n) = \frac{1}{N - \Delta n} \sum_{n=0}^{N-\Delta n-1} |p(n + \Delta n) - p(n)|^2$$

In motion scaling spectrum (MSS) analysis, the MSD concept is generalized for analysis over many different moments ( $\nu$ ) relative to different time lags.

$$r^v(\Delta n) = \frac{1}{N - \Delta n} \sum_{n=0}^{N-\Delta n-1} |p(n + \Delta n) - p(n)|^v$$

MSD analysis is the second moment of MSS. Moments 1-6 were analyzed for our data. A plot of scaling exponents vs moments gives a linear relationship whose slope can be used to define motion as confined, diffusive, or directed (slope = 0-no motion, 0.5-diffusive, 1-directed, thresholds ½ those used for MSD analysis). MSS analysis is associated with less error than MSD analysis (Ferrari et al., 2001) and has previously been applied to classify the motion of CD36 receptors (Jaqaman et al., 2011) and viruses (Ewers et al., 2005) in live cells. We would expect MSD and MSS analysis to be highly correlated if they are accurately reflecting the motion of the particle and to vary from each other if there is large measurement error associated with either.

We performed MSS analysis on our largest dataset, all of the trajectories in Table 3 (1.9 x 10<sup>6</sup> 2.25 s trajectory segments), and compared those results to the MSD  $\alpha$  values. Importantly, MSS slope is highly correlated with  $\alpha/2$ , as expected, across the entire range of  $\alpha$  values (Figure 10). Using the MSS slope to classify the trajectories (with thresholds at ½ those used for  $\alpha$ ) resulted in very similar proportions of motion types present in the early endosomal population (MSS: 61% of time is confined, 38% is diffusive, and 1% is directed. For comparison, in Table 3 of the paper, the classifications based on MSD  $\alpha$  values were: 59% of time confined, 39% diffusive, and 2% directed).

As an additional estimate of the error on each  $\alpha$  measurement, we measured the differences between  $\alpha$  and  $2 \times \text{MSS}$  slopes for each 2.25 s track segment and plotted this distribution (Figure 10B). The 95% confidence interval for the difference distribution is 0.32, indicating that if the MSS slope were completely accurate, the  $\alpha$  values would have a 95% confidence interval of 0.32. If errors are equally shared between the two parameters, the 95% confidence interval for each measurement would be  $0.32/\sqrt{2}$ , or 0.23 (in units of  $\alpha$ ). Thus, the error on each  $\alpha$  measurement is between 0.32 and 0.23, which is low enough to enable breaking endosomal motions into three categories based on  $\alpha$ .

#### **2.1.8 GFP-Rab5 and mCherry-Rab7 trajectory analysis**

45 s movies collected at 20 fps of GFP-Rab5 and mCherry-Rab7 were tracked with u-track (Jaqaman et al., 2008). Trajectories containing at least 100 frames (5 s) were used for further analysis. The  $x,y$  position was smoothed over 6 frames and the resulting trajectory was used to calculate the net displacement and the instantaneous speed. The net displacement of each trajectory was used to define the trajectory as immotile (moving  $< 0.5 \mu\text{m}$ ) or motile (moving  $> 0.5 \mu\text{m}$ ), see Figure 3D. Directed segments were identified using a speed threshold of  $1 \mu\text{m/s}$  and scored for their direction: towards the cell edge or towards the perinuclear region (majority of MT minus-ends are located there). The number of tracks containing directed segments in both directions (% bidirectional) was also scored. To quantify the amount of very rapid movement, the

number of motile trajectories containing speeds  $> 2 \mu\text{m/s}$  was measured. The data is presented at the mean  $\pm$  SEM for 10 cells (Table 1).

### **2.1.9 Cytoskeletal drug treatment analysis**

Cells expressing GFP-Rab5 were incubated with 1.5 ng/ml EGF-Qdots for  $\sim 10$  min prior to imaging in order to preferentially label the early endosomes over more mature compartments. Cells with active minus-end directed transport of GFP-Rab5 were selected for experiments. EGF-Qdots were imaged at 20 fps for 30 s. Cytoskeletal drugs were added for 5 min at the indicated concentrations (Figure 3E) and the same cell was imaged again at 20 fps for 30 s. All EGF-Qdots within the cell border were tracked using u-track (Jaqaman et al., 2008). MSD and  $R_g^{2D}$  analysis (Figure 3B,C) was performed using a 2.25 s sliding analysis window as described above for all trajectories lasting longer than 100 frames (5 s). The median value for these measurements in each cell was compared before and after drug treatment. The percent change in the median value per cell was calculated as  $(\text{median value after drug} - \text{median value before drug}) / (\text{median value before drug}) * 100\%$ . These percentages from 10 cells were compared to the expected binomial probability for an increased or decreased median value to determine statistically significant changes in motion induced by drug treatment. To measure the shifts in the distribution of  $\alpha$  values, thresholds of 0.4 for confined and 1.45 for directed were set based on the analysis of all 2.25 s track segments done in Figure 5C. The changes in these percentages after drug treatment were analyzed using a binomial test

as well. To analyze only tracks containing directed motion and pausing, two criteria were used to select tracks: net displacement  $> 1 \mu\text{m}$  and  $\alpha > 1.5$  for 20 track segments of 2.25 s each. This subset of tracks was analyzed as described for the whole data set.

#### **2.1.10 Parsing of EGF-Qdot trajectories into directed runs and pauses**

EGF-Qdot tracks were selected that met the following criteria: net displacement  $> 2 \mu\text{m}$ , trajectory  $> 50$  frames (2.5 s), visually colocalized and exhibited correlated movement with GFP-Rab5, contained at least one directed run based on the parsing criteria described below (Figure 6A,B).

Parsing trajectories into directed runs and pauses: Track segments appearing to exhibit directed transport or diffusion were selected manually and used for initial estimations of the directed movement speed and the diffusion coefficient of the paused periods. These values as well as the tracking error, pixel size, and frame rate in our experimental data were used to simulate trajectories containing diffusion with known periods of directed runs (Figure 6C). Analysis of simulations to set 5 % false-positive thresholds for identification of directed runs was performed (Figure 6C-E, Table 4). Different time windows were tested to find the minimal time window that allowed recovery of the simulated diffusion coefficient within 15% in regions immediately before or after the directed run (Table 2, using positions identified from parsing analysis, not known positions from simulation). After applying these parameters to experimental data,

simulations were repeated with a range of diffusion coefficients to match the measured values. The thresholds for obtaining < 5% false-positives did not change. Two criteria to identify a directed run were: speed and Speed Correlation Index (SCI) (Bouzigues and Dahan, 2007), which quantifies directional stability. SCI code was provided by Drs. Cedric Bouzigues (Ecole Polytechnique), Maxime Dahan (Janelia Farms and Ecole Normale Supérieure). SCI was calculated over a 4 frame (200 ms) sliding window. The resulting SCI vs time curve was additionally smoothed over 24 frames (1.2 s). A threshold of SCI > 0.65 was found to produce less than 5% false positive directed runs using simulations (Figure 6D, Table 4). Before calculating the instantaneous speed, the position was smoothed over 24 frames (1.2 s). A threshold of 1  $\mu\text{m/s}$  was used based on simulations and resulted in < 5% false-positive selection of directed runs when the diffusion coefficient was similar that measured for early endosomes (Figure 6E, Table 4).

#### **2.1.11 MSD analysis of concatenated track segments**

In order to use a smaller time window for analysis and increase the statistical power of the MSD fitting, we also used 15 frame (0.75 s) track segments before a run, after a run, or in the middle of a run. These shorter time windows were concatenated into one large track per condition. MSD and  $R_g^{2D}$  analysis was performed on the resulting large tracks. Bootstrapping (100 randomly selected sets of track segments were generated) was performed to calculate the SEM.

### **2.1.12 Spatial correlation between early endosomal pause sites and the position of organelles**

GFP-Rab5 was imaged relative to markers for other organelles at 20 fps for 50 s. 10 GFP-Rab5 particles that visually appeared to contain directed movements and pauses were selected per cell (5 cells). Kymographs of the Rab5 trajectories were made using the Multiple Kymograph plugin in ImageJ ((Schneider et al., 2012); plugin authors J. Rietdorf and A. Seitz, European Molecular Biology Laboratory), and pauses in the movement, defined as regions where the speed dropped below  $0.4 \mu\text{m/s}$ , were scored. The locations of the pauses were scored for the presence of one of the other organelles within 1 pixel (135.5 nm) of the pause site. As a control for random overlap that varies with the different organelle densities, we selected random points in the kymographs and scored those for overlap with the other organelles. Statistical significance was determined by performing a t-test on the % of pause locations that overlapped with organelles in comparison to the % of random locations that overlapped with organelles.

## CHAPTER 3.

Local cytoskeletal and organelle interactions impact molecular  
motor-driven early endosomal trafficking.

This work was originally published as:

Zajac, A. L., et al. (2013). "Local Cytoskeletal and Organelle Interactions Impact  
Molecular-Motor- Driven Early Endosomal Trafficking." *Curr Biol.* 23(13):1173-80.

Allison L. Zajac, Yale E. Goldman, Erika L.F. Holzbaur\*, and E. Michael Ostap\*

\*corresponding authors

### 3.1 Abstract

**Background.** In the intracellular environment, motor-driven cargo must navigate a dense cytoskeletal network among abundant organelles.

**Results.** We investigated the effects of the crowded intracellular environment on early endosomal trafficking. Live-cell imaging of an endosomal cargo (endocytosed epidermal growth factor-conjugated quantum dots) combined with high-resolution tracking was used to analyze the heterogeneous motion of individual endosomes. The motile population of endosomes moved towards the perinuclear region in directed bursts of microtubule-based, dynein-dependent transport interrupted by longer periods of diffusive motion. Actin network density did not affect motile endosomes during directed runs or diffusive interruptions. Simultaneous two-color imaging was used to correlate changes in endosomal movement with potential obstacles to directed runs. Termination of directed runs spatially correlated with microtubule-dense regions, encounters with other endosomes, and interactions with the endoplasmic reticulum. During a subset of run terminations, we also observed merging and splitting of endosomes, deformation of the endoplasmic reticulum, and directional reversals at speeds up to ten-fold greater than characteristic *in vitro* motor velocities. These observations suggest endosomal membrane tension is high during directed run termination.

**Conclusions.** Our results indicate that the crowded cellular environment significantly impacts the motor-driven motility of organelles. Rather than simply acting as impediments to movement, interactions of trafficking cargos with intracellular obstacles may facilitate communication between membrane-bound compartments or contribute to the generation of membrane tension necessary for fusion and fission of endosomal membranes or remodeling of the endoplasmic reticulum.

### 3.2 Introduction

Molecular-motor driven intracellular trafficking of cargos is essential for maintaining cellular homeostasis (Lippincott-Schwartz et al., 2000). *In vitro* analyses of molecular motors have provided insight into intrinsic movement characteristics such as directionality, run length, speed, and force sensitivity (Mallik and Gross, 2004). However, motility in the cell is strongly affected by the organization and dynamics of cytoskeletal tracks (Parton et al., 2011; Schuh, 2011; Semenova et al., 2008), interactions with other organelles (Elbaz and Schuldiner, 2011), and crowding in the cytoplasm (Zhou et al., 2008). Thus, characterization of the full range of motion of individual cargo is needed to understand how intracellular obstacles and organelle interactions impact directed transport.

To investigate the movement of single cargos in live cells, we focused on the trafficking of epidermal growth factor (EGF) in early endosomes. After EGF activates its receptor

(EGFR), the two are endocytosed, transported through the endosomal system from early to late endosomes, and ultimately degraded in lysosomes (Sorkin and Goh, 2009). Both actin- and microtubule (MT)-based motors are associated with early endosomes, including: myosin Vb (Provance et al., 2008), myosin VI (Aschenbrenner et al., 2003), myosin Ib (Raposo et al., 1999), kinesin-1 (Loubery et al., 2008), kinesin-2 (Loubery et al., 2008), KIF16b (Hoepfner et al., 2005), and dynein (Aniento et al., 1993; Driskell et al., 2007; Loubery et al., 2008). Early endosomes exhibit a complex mixture of dynein-driven directed runs toward the perinuclear region interrupted by intervals of little net transport (Flores-Rodriguez et al., 2011). The goal of the present study is to characterize the full spectrum of motions exhibited by individual early endosomes to provide insight into (i) why directed motion is interrupted, (ii) what types of residual movement are occurring during the interruptions, and (iii) what functional roles the combination of directed runs and interruptions play in endosomal trafficking and maturation.

We measured early endosomal trajectories using high temporal and spatial resolution imaging and developed objective methods to analyze distinct phases of motion within single trajectories. We found that a subpopulation of early endosomes exhibited mostly confined motion, regulated by the density of the actin network. In contrast, the motile population of early endosomes exhibited a combination of directed, dynein-dependent movement interspersed with longer diffusive pauses. We observed spatial overlap between sites of pausing and regions of dense MTs, other early endosomes, and the endoplasmic reticulum (ER), suggesting these cellular factors may interrupt directed

runs. Further, these interactions and the associated pauses in directed motion may play functional roles in endosomal maturation and sorting.

### **3.3 Results**

#### **3.3.1 Intracellular dynamics of early endosomes**

We surveyed the dynamics within the early endosomal population using high speed (20 frames per second (fps)) imaging in Arpe-19 cells, a human epithelial cell-line with an actin-rich cortex and a polarized MT array (Figure 1A). Several fluorescent markers (Rab5 and endocytosed EGF) were compared to ensure that our labeling strategy did not introduce artifactual movements or perturb the trafficking kinetics of endocytosed transferrin (Figure 1B). Early endosomes could be divided into two groups based on their movement. An immotile subpopulation covered little distance over the period of observation ( $< 0.5 \mu\text{m}$  over 45 s). A motile subpopulation moved in short, perinuclear-directed bursts interrupted by periods of little net displacement, which we will refer to as pauses (Figure 2A). Analysis of 2,839 trajectories from GFP-Rab5-positive early endosomes in 10 cells (Figure 2B) showed that  $62 \pm 2\%$  (mean  $\pm$  SEM) are immotile (Table 1). In the motile population,  $78 \pm 4\%$  of rapid movements were directed towards the perinuclear region, where the majority of MT minus-ends are located (Table 1). The dependence of this rapid transport on dynein/dynactin (Flores-Rodriguez et al., 2011) was confirmed by expression of the dominant-negative construct CC1 (the coiled-coiled-

1 domain of p150<sup>Glued</sup>) to disrupt dynein/dynactin function, although other motors such as myosin VI and KIF16b are also present (Figure 1C,D). For comparison, late endosomes/lysosomes labeled with several markers, including the GTPase Rab7, underwent significantly more bidirectional movement than early endosomes (Figure 1E,F, Figure 2C, Table 1).

To allow tracking at higher resolution, early endosomes were labeled with endocytosed EGF-conjugated quantum dots (EGF-Qdots, Figure 2A). Interpreting complex motion inside cells is complicated by limitations on spatial and temporal resolution (~20 nm at 20 fps, Figure 3A). Changes in motion more rapid than the frame-rate will be missed, and confinement cannot be observed if the object doesn't encounter the barrier during the imaging time. Finally, the cytoplasm is a heterogeneous viscoelastic environment so care must be taken when interpreting the source of motions. We have tried to address these caveats by controlling our imaging and analysis conditions as detailed below.

Motion was characterized using mean-squared displacement (MSD) analysis:  $MSD = \langle r^2 \rangle = 4Dt^\alpha + 2\sigma^2$  (Eq. 1), where  $D$  is the diffusion coefficient,  $t$  is the time lag,  $\alpha$  is the scaling exponent, and  $\sigma$  is the measurement error which was fixed at 20 nm (Figure 3A,B). The  $\alpha$  scaling exponent was used to classify motion as directed ( $\alpha > 1.45$ ), diffusive ( $0.4 < \alpha < 1.45$ ), or confined ( $\alpha < 0.4$ ) (Figure 3B, see M&M) (Berg, 1993). We also used an independent method to characterize the area explored by an endosome, the 2-dimensional radius of gyration ( $R_g^{2D}$ ) (Figure 3C, Eq. 2). All motion analysis was

performed using a short sliding time window (2.25 s) to capture the heterogeneity within individual trajectories. This time window allowed recovery of  $\alpha$  and  $D$  to within 15% in simulated trajectories (Table 2).

We characterized the motion parameters  $\alpha$ ,  $D$ , and  $Rg^{2D}$  for all EGF-Qdots,  $\sim 10$  min after their addition to cells, to ensure they were internalized into early endosomes. Analysis of EGF-Qdot trajectories indicated that the majority ( $59 \pm 9\%$ ) of the EGF-Qdot lifetime was confined (median  $\alpha = 0.32 \pm 0.09$ , Table 3). To investigate the motion specifically for the motile population of EGF-Qdots, we selected only the subset of trajectories containing directed movement (net displacement  $> 1 \mu\text{m}$  and  $\alpha > 1.5$  for 1 s) for analysis (Figure 3D). Even in this set of motile trajectories, only  $23 \pm 8\%$  of the endosomal lifetime was directed (Table 3). The majority of the time ( $52 \pm 12\%$ ) the motion in these motile trajectories was diffusive (median  $\alpha = 0.84 \pm 0.24$ , Table 3), suggesting pauses are diffusive and distinct from the confined, immotile population.

### **3.3.2 The actin network regulates the confinement of early endosomes.**

To obtain insight into the regulation of different types of endosomal motion, we investigated the effects of one potential modulator, the actin cytoskeleton. Previous studies suggested actin could play several roles, including: forming a restrictive cage (Aschenbrenner et al., 2003) that may be used by myosins to tether endosomes (Provance et al., 2008), serving as tracks for myosin-driven transport (Aschenbrenner et al., 2003),

or polymerization of *Listeria*-like actin comet tails to generate propulsive forces (Taunton et al., 2000) (Figure 4A). These roles predict that actin disruption would either increase endosomal motion (caging, tethering) or decrease endosomal motion (myosin transport, propulsion).

We tested these models by measuring changes in motility parameters for all EGF-Qdots in the same cell before and after a 5 min drug perturbation of the actin cytoskeleton. Cells were treated with latrunculin B to depolymerize actin filaments, jasplakinolide to stabilize and increase the density of the actin network, or nocodazole to disrupt directed motion by depolymerizing the majority of MT tracks (Figure 3E). As expected, nocodazole treatment significantly lowered the median  $\alpha$ , D, and  $Rg^{2D}$  and the amount of directed motion (Figure 4B,C). In contrast, treatment of cells with latrunculin B significantly increased the median  $\alpha$ , D, and  $Rg^{2D}$  (Figure 4B). These endosomes exhibited less confinement and more diffusive motion, but directed motion was unchanged (Figure 4C). Stabilization of actin filaments with jasplakinolide significantly decreased directed movement (Figure 4C). These effects suggest that the dominant role played by actin is restriction of early endosomal motion (caging, tethering).

To address the role of actin in regulating early endosomal motion specifically during directed trafficking, we selectively analyzed motile tracks (Figure 4D). Analysis of this subset of tracks showed no significant effect of latrunculin B or jasplakinolide (Figure 4E,

F), suggesting that actin density does not affect the motion of early endosomes once directed transport has commenced.

### **3.3.3 The transition periods before and after directed runs are diffusive.**

We objectively parsed Rab5-positive, motile EGF-Qdot trajectories into directed runs and pauses to allow analysis of the motion in these two phases separately and to investigate the temporal relationship between changes in motion (Figure 5A, Figure 6A,B). Two criteria were used to determine the position of directed runs: a directional correlation algorithm, termed Speed Correlation Index (SCI) (Bouzigues and Dahan, 2007), and the instantaneous speed (Figure 5B, Figure 6C,D, Table 4).

The directed runs exhibited  $\alpha$  exponents from MSD fits  $>1.45$  (Figure 5B,C), independently supporting our parsing criteria. The lifetime ( $T_{av} = 1.2$  s, Figure 6F) of the directed runs was longer than that of individual dynein runs *in vitro* (Ross et al., 2006), suggesting multiple dynein motors are present. Consistent with previous work (Flores-Rodriguez et al., 2011; Lakadamyali et al., 2006), early endosomes achieved very high instantaneous speeds (2- 4  $\mu\text{m/s}$ , Figure 6G). Since increasing the number of dyneins *in vitro* does not enhance minus-end directed speeds (Mallik et al., 2005), additional factors in the cell likely promote faster dynein motility. We found that pauses had a longer average lifetime than directed runs ( $T_{av} = 4.7$  s, Figure 6H), and a broader range of  $\alpha$  values, although the majority (65%) were diffusive (Figure 5C). MSD analysis of the

longest pauses observed, without using a sliding time window, yielded similar results (Figure 6I-K), indicating pauses are diffusive over longer time-scales.

Isolating the periods immediately before and after a directed run provides insight into the initiation and termination of directed trafficking in the cell since it is during these transition periods when motors are either engaged or halted. The motions immediately before and after directed runs were diffusive (Figure 5A,D, Table 5). The diffusion coefficients for these periods were similar to each other (before  $D = 0.024 \pm 0.030 \mu\text{m}^2/\text{s}$ , after  $D = 0.028 \pm 0.018 \mu\text{m}^2/\text{s}$ ), to  $D$  values for entire pauses (Figure 6K), and to measurements of  $D$  for other organelles (Luby-Phelps, 2000). The motion occurring after a directed run, although diffusive, had a significant (~2 fold) enrichment of motion aligned with the MT axis (Figure 6L, Figure 5D). This suggests that after the end of a directed run endosomes maintain a transient connection to the MT.

### **3.3.4 Interactions with organelles spatially correlates with early endosome pause locations.**

We investigated factors that may trigger pauses in directed transport by spatially correlating the sites of pausing with two aspects of cellular architecture likely to affect cargo trafficking: (i) the presence of other organelles and (ii) the local organization of the MT network.

To determine if organelle-early endosome interactions contribute to pauses, we compared the location of GFP-Rab5-positive endosomal pauses with the position of other organelles. The Golgi, mitochondria, and late endosomes/lysosomes showed no significant spatial correlation (Table 6). In contrast, a significant percentage of pauses spatially correlated with the location of both other Rab5-positive endosomes ( $25 \pm 2\%$ ;  $p < 0.05$ ) and ER tubules ( $39 \pm 13\%$ ;  $p < 0.05$ , Table 6), relative to randomly chosen locations. We further investigated these two organelle interactions in the following sections.

### **3.3.5 Early endosomal membrane tension may regulate the pauses in directed motion.**

Sparse labeling of early endosomes with EGF-Qdots allowed us to track individual early endosomes relative to the dense total GFP-Rab5 population. EGF-Qdots underwent multiple rounds of merging and splitting from other GFP-Rab5 punctae during trafficking (Figure 7A). The motions during pauses when two early endosomes merged were diffusive (Figure 7B), suggesting that the two endosomes either moved diffusively together or that confinement induced by their interaction was brief.

Some interruptions in minus-end directed transport were associated with rapid reversals in direction (Figure 7C(i)), with speeds exceeding that of molecular motors ( $>30 \mu\text{m/s}$ , Figure 7C(ii)). Even following this very abrupt change in motion, the pauses were diffusive ( $\alpha \sim 0.6-0.8$ , Figure 7C(i-ii)). These rapid reversals suggest that some

pauses in directed motion correlate with tension on the endosomal membrane, an elastic structure that can recoil rapidly. Figure 7C(iii) highlights one reversal where fission appears to occur when the GFP-Rab5 signal splits into two dimmer particles. During sorting of endosomal cargo, transferrin-positive tubules extend from EGF punctae and eventually undergo fission to enter the recycling pathway (Mesaki et al., 2011). We observed transferrin-positive tubules extending towards the cell periphery and undergoing fission as the attached EGF punctae moved rapidly ( $\sim 2\mu\text{m/s}$ ) toward the perinuclear region (Figure 7D). This suggests that the directed movement of early endosomes must be coordinated with membrane tension in the larger tubular network, which sometimes results in fission and membrane recoil events.

### **3.3.6 Early endosomes deform the ER during trafficking.**

To investigate the effect of interactions between early endosomes and the ER, we looked for correlated movement of these two organelles before or during pauses. We observed long-lived interactions that resulted in dramatic and rapid ER deformation in both Arpe-19 and COS-7 cells (Figure 8A-C, Figure 9A). We also saw instances of Rab5 punctae at the front of newly extending ER tubules (Figure 8B,C). The long lifetimes of these attachments and the requirement for endosome-generated force to deform the ER for continued directed movement suggest this type of membrane contact site is a previously unappreciated regulator of early endosomal motility.

### **3.3.7 Early endosomal motion is influenced by MT organization.**

To investigate how MT track organization affects early endosomal movement, we imaged GFP-Rab5 simultaneously with 2xmCherry-EMTB, the microtubule binding domain of the microtubule associated protein (MAP) ensconsin (Faire et al., 1999). Pausing of GFP-Rab5-positive endosomes runs occurred at regions of dense, apparently intersecting MTs (10/10 cells, Figure 8D). In 8/10 cells, we observed a few elongated early endosomes that were large enough to enable visualization of rotations, deformations, and sometimes fissions during pauses in MT dense regions (8/8 cells, Figure 8D). However, we also observed sharp changes in direction without measurable pausing, which we interpret as MT track switching (10/10 cells, Figure 8E). Although the high MT density in Arpe-19 cells prevented us from quantifying the contribution of MT intersections to pausing, frequent MT track switching and pauses at MT-enriched regions were also observed in parallel studies in COS-7 cells (Figure 9B). These observations suggest that MT track organization impacts early endosomal movement, potentially through multiple motors on the endosome engaging different MTs.

## **3.4 Discussion**

**3.4.1 Early endosomes contain subpopulations with distinct motility characteristics, differentially regulated by the actin cytoskeleton.**

Our high resolution imaging of early endosomal dynamics and motion classification suggests there are two subpopulations of early endosomes that differ in both their motility characteristics and regulation by the actin cytoskeleton. Immotile (moving < 0.5  $\mu$ m over 45 s) endosomes were confined by the actin network (Table 3, Figure 4B,C). Motile early endosomes contained directed runs and diffusive pauses unaffected by perturbation of the actin cytoskeleton (Table 3, Figure 4E,F, Figure 5, Figure 6I-K, Table 5). Stabilization of the actin network decreased the amount of directed movement in the whole population (Figure 4C), supporting a model where confinement of peripheral early endosomes by actin regulates the initiation of directed transport. MyosinVI is required for endosomes to navigate the actin-rich cell periphery in some cell types (Aschenbrenner et al., 2003). The reduced localization of myosin VI-GFP to motile early endosomes (Figure 1C) and the decreased density of the actin filaments in the cell interior near MTs (Figure 1A) suggests that both changes in endosomal actin-interacting proteins and local changes in the actin cytoskeleton may contribute to the lack of an effect of actin disruption on motile early endosomes.

The directed runs are MT and dynein/dynactin dependent (Flores-Rodriguez et al., 2011) and 89% are directed towards MT minus-ends in the perinuclear region. Some pauses in directed transport appear to be initiated by a tug-of-war between motors engaging different MTs (Figure 8D), suggesting that dynein may be engaging in a tug-of-war with itself. However, early endosomes also associate with MT plus-end-directed kinesins despite their lack of bidirectional movement (Figure 1D) (Driskell et al., 2007; Hoepfner

et al., 2005; Loubery et al., 2008). One possibility is that a low ratio of kinesins to dyneins creates a tug-of-war that manifests as a pause, but dynein ultimately wins.

### **3.4.2 The motion during pauses is diffusive.**

The diffusive nature ( $\alpha$  scaling exponent of MSD plots  $\sim 1$ ) of endosomal motion during pauses in directed transport (Table 3, Figure 5, Figure 6I-K, Table 5) indicates that the endosomal motion is randomly directed, but does not restrict that motion to free diffusion. Types of movement suggested to result in diffusive scaling in 2 dimensions include: free diffusion in the cytoplasm (Wirtz, 2009), the movement of motors on mixed polarity filaments (Nelson et al., 2009), or tethering through a long and/or flexible linkage (Gu et al., 2012). Diffusive scaling in 1 dimension can result from a tug-of-war between mixed polarity motors (Muller et al., 2010) or diffusion of a MAP or motor along the MT lattice (Ross et al., 2006). Movement of myosins along mixed polarity actin filaments is unlikely since actin perturbations did not affect endosomal motion during pauses (Figure 4E,F), and movement along mixed polarity MTs is also unlikely because the MTs are radially arrayed (Figure 1A). Since the periods immediately after a directed run had alignment with the MT track (Figure 6L), interactions requiring continued interactions between the early endosome and MT, such as a bidirectional tug-of-war between MT motors, or diffusion of a MAP or motor, could occur. However, since the distance a diffusing endosome ( $D \sim 0.026 \mu\text{m}^2/\text{s}$ ) is expected to move during the average pause lifetime ( $T_{\text{av}} = 4.7 \text{ s}$ ) is  $\sim 700 \text{ nm}$ , about 10-fold greater than dynein's

length (Vale, 2003), and the movement was randomly directed before a directed run commenced (Figure 6L), the endosome likely detaches from the MT at some point during pauses (Figure 5D).

### **3.4.3 High endosomal membrane tension may induce pausing and facilitate cargo sorting.**

The location of endosomal pauses overlapped with MT intersections (Figure 8D, Figure 5B), other early endosomes (Table 6, Figure 7B), and ER tubules (Table 6, Figure 8A-C, Figure 9A). Rather than acting as random obstacles to directed movement, we hypothesize that interactions with these structures, and the consequent pauses, contribute functionally to cargo sorting.

Rab5 forms microdomains on larger tubular endosomal structures involved in cargo sorting (Sonnichsen et al., 2000). Instead of a motor-motor tug-of-war, a tug-of-war may occur between the dynein-driven movement of Rab5 microdomains and the tension in the attached tubular-vesicular endosome. The extremely rapid reversals in direction ( $> 30 \mu\text{m/s}$ , Figure 7C(ii)) and deformation and fission of early endosomes (Figure 7C(iii), Figure 8D) indicate membrane tension is high during pauses.

*In vitro* studies have demonstrated that teams of kinesin-1s can tubulate a model vesicle (Koster et al., 2003). However, the stall force of dynein is lower than kinesin-1((Mallik et al., 2004)), and studies estimating the number of motors on other endosomal

populations suggested only a few motors are present (Hendricks et al., 2010). A small team of dynein motors could thus be stalled by tension in the membranes during sorting. Since dynein is a flexible motor, capable of back-stepping to avoid obstacles (Dixit et al., 2008; Ross et al., 2006) and acting as a gear under load (Mallik et al., 2004), it may be well adapted to handle this backward pulling force and maintain contact with the MT for continued tubule extension and efficient sorting.

Early endosomal connections result in dramatic deformation and tubulation of the ER (Figure 8A-C, Figure 9A). Contacts between early endosomes and the ER facilitate dephosphorylation of active receptor tyrosine kinases like EGFR by the ER resident phosphatase PTP1b (Haj et al., 2002). At the ultrastructural level, the ER and endosomal membranes are closely approximated (< 30nm) and bridged by unidentified protein fibrils (Eden et al., 2010). The force required to maintain an extended tubule from the ER *in vitro* is ~20 pN, even in the presence of cytosol (Upadhyaya and Sheetz, 2004). Since many organelles contact the ER (Elbaz and Schuldiner, 2011), understanding how the force required to deform the ER affects motility is relevant to many trafficking pathways. Conversely, the ability of motile organelles to deform and tubulate the ER may contribute to the maintenance of ER structure and distribution.

#### **3.4.4 Conclusions**

Our high-resolution tracking and motion analysis demonstrated that there is a population of immotile, confined early endosomes that are regulated by actin network density, and motile early endosomes undergoing a combination of directed, dynein-driven movement and diffusive pauses. Early endosomal interactions with MT intersections, other early endosomes, and the ER likely contribute to pausing in directed movements. These interruptions in dynein-driven transport may play functional roles such as facilitating early endosomal cargo sorting and maintenance of ER structure.

### 3.5 Figures

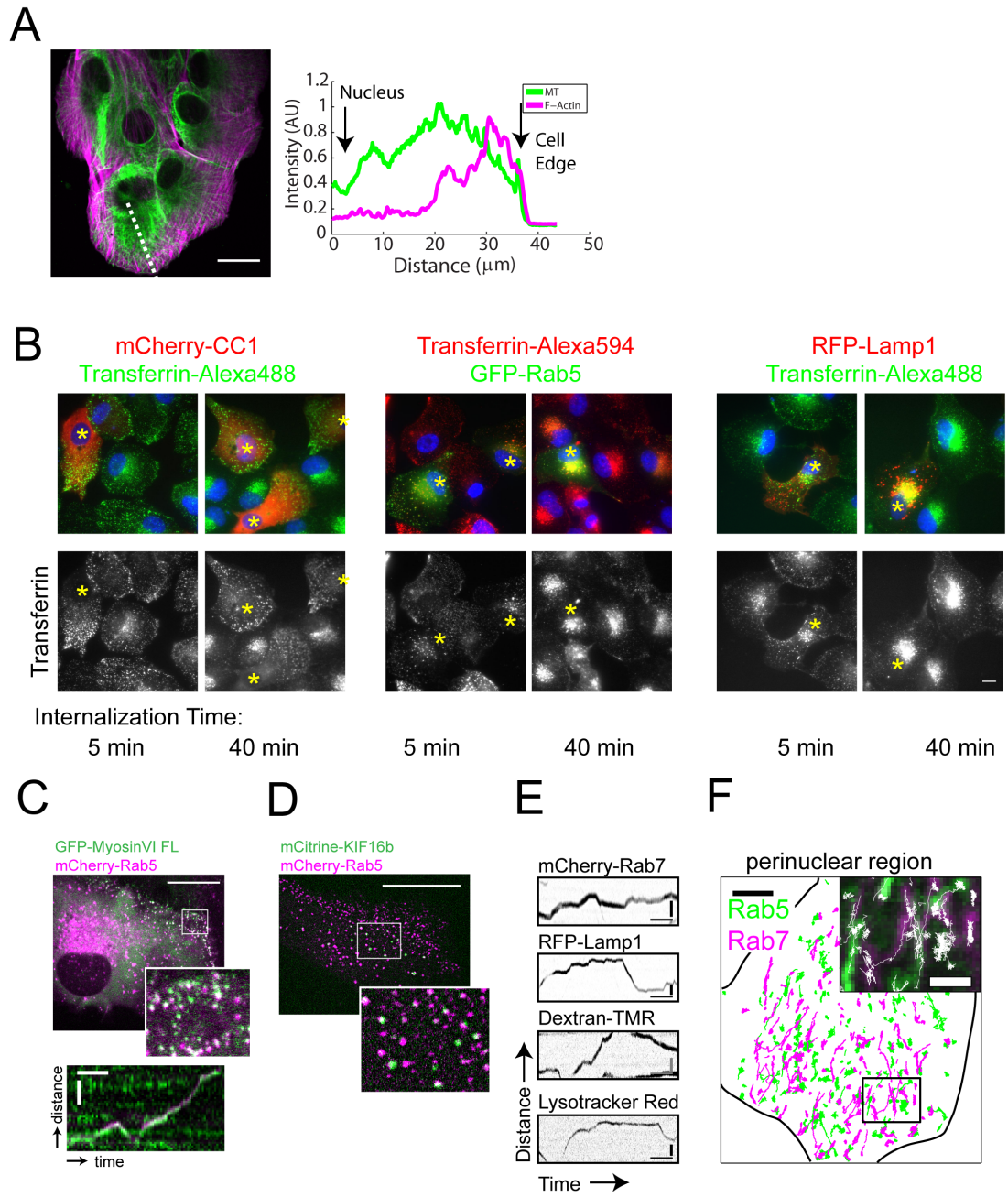


Figure 1. Characterization of cytoskeletal and endosomal organization in Arpe-19 cells.

- A. Actin filament density is high in the periphery of Arpe-19 cells and MT density is high in the cell interior. Arpe-19 cells were fixed and stained for endogenous MTs (green) and F-actin (phalloidin, magenta). The dotted line indicates the position of the line scan of intensity. The linescan (width 11 pixels) shows the fluorescence intensity of the MT and F-actin channels from the cell edge to the nucleus. Scale bar: 20  $\mu\text{m}$ .
- B. Expression of early or late endosome/lysosome markers does not affect transferrin trafficking to the perinuclear region. Arpe-19 cells were transiently transfected with mCherry-CC1 to disrupt dynein/dynactin as a positive control to inhibit trafficking to the perinuclear region, the early endosomal marker GFP-Rab5, or the late endosomal/lysosomal marker RFP-Lamp1. Cells were serum-starved for 4 hours prior to addition of 20  $\mu\text{g}/\text{ml}$  transferrin for 5 min. Cells were washed in 37°C PBS and fixed (5 min time point) or incubated in transferrin-free media for 35 min prior to fixation (40 min time point). Nuclei are stained with Hoechst dye. Epifluorescent microscopy was used to image cells. The \*s indicate transfected cells. Scale bar: 10  $\mu\text{m}$ .
- C. Myosin VI localizes preferentially to peripheral, immotile early endosomes. Top: Arpe-19 cells expressing GFP-Myosin VI (full-length human) and mCherry-Rab5 were imaged using a spinning disc confocal microscope. The colocalization (white) is highest in the periphery of the cell. Scale bar: 20  $\mu\text{m}$ . Bottom: Arpe-19 cells co-expressing GFP-Myosin VI (green) and mCherry-Rab5 (magenta) were imaged at 7

- fps. A kymograph of a motile early endosome shows that there is some localization of myosin VI to motile early endosomes. Scale bars: 2 s, 2  $\mu\text{m}$ .
- D. KIF16b localizes to a subset of Rab5-positive early endosomes. Confocal image of an Arpe-19 cell co-expressing mCherry-Rab5 (magenta) and mCitrine-KIF16b (green). Scale bar: 20  $\mu\text{m}$ .
- E. Late endosomes/lysosomes exhibit bidirectional, rapid movements interrupted by periods of little net movement. Arpe-19 cells labeled with either: mCherry-Rab7, RFP-Lamp1, Dextran-TMR, or LysoTracker Red were imaged at 20 fps. The images were contrast inverted and processed using background subtraction prior to generating kymographs. Scale bars: 4 s, 2.5  $\mu\text{m}$ .
- F. Trajectories of Rab5- and Rab7-positive endosomal populations in the same cell. The trajectories of all GFP-Rab5 (green) and mCherry-Rab7 (magenta) movements lasting longer than 5 s during a 45 s movie are shown (5  $\mu\text{m}$  scale bar, cell outline in black). The same cell and the same Rab5 trajectories used in Figure 1B are represented here to allow comparison to Rab7 punctae in the same cell. The inset (location is black box in the main panel) shows the maximum intensity projection of the movie with the tracks overlaid in white. Scale bar for inset: 2  $\mu\text{m}$ .

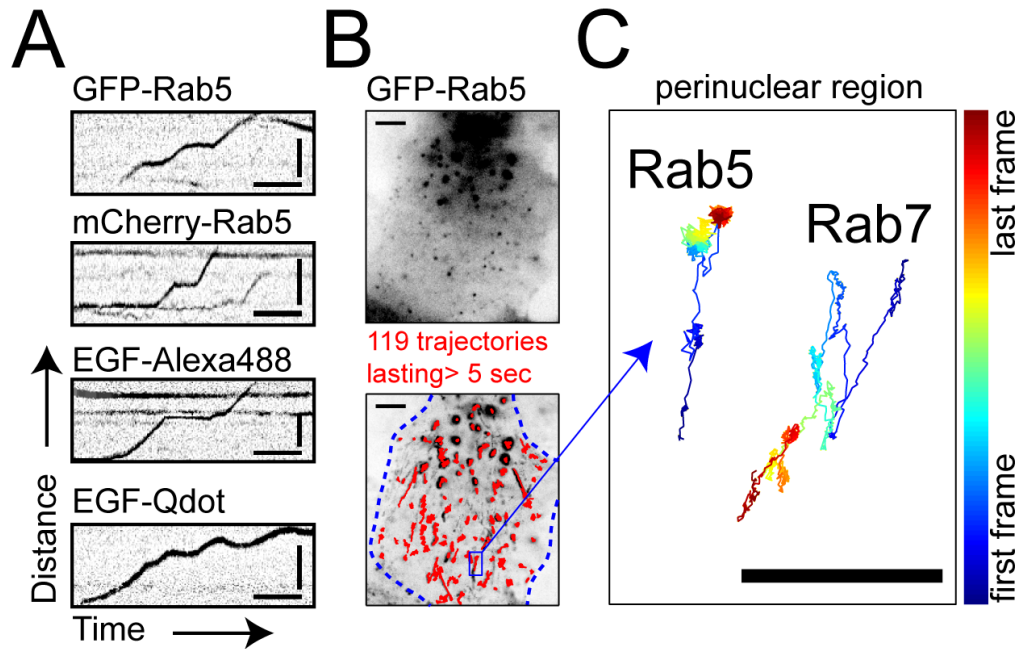


Figure 2. Motility in the early endosomal population

- A. Early endosomes move in rapid bursts towards the perinuclear region interrupted by periods of little net movement. Kymographs of early endosomes were contrast-inverted and background-subtracted. Scale bars: 2 s, 5  $\mu\text{m}$ .
- B. Tracking of GFP-Rab5 movements for analysis. GFP-Rab5-positive early endosomes (single frame in top panel). Bottom panel: maximum intensity projection of GFP-Rab5 movie (45 s) overlaid with trajectories (red) and cell outline (blue). Scale bars: 5  $\mu\text{m}$ .
- C. Early endosomes exhibit rapid movements towards the perinuclear region while late endosomes/lysosomes exhibit bidirectional rapid movements. Representative Rab5 and Rab7 trajectories from the cell in B, color-coded for time (first frame = blue, last

frame = red). Rab5 trajectory position in B (blue box). Scale bar: 2  $\mu\text{m}$ . See also Figure 1E,F, Table 1.

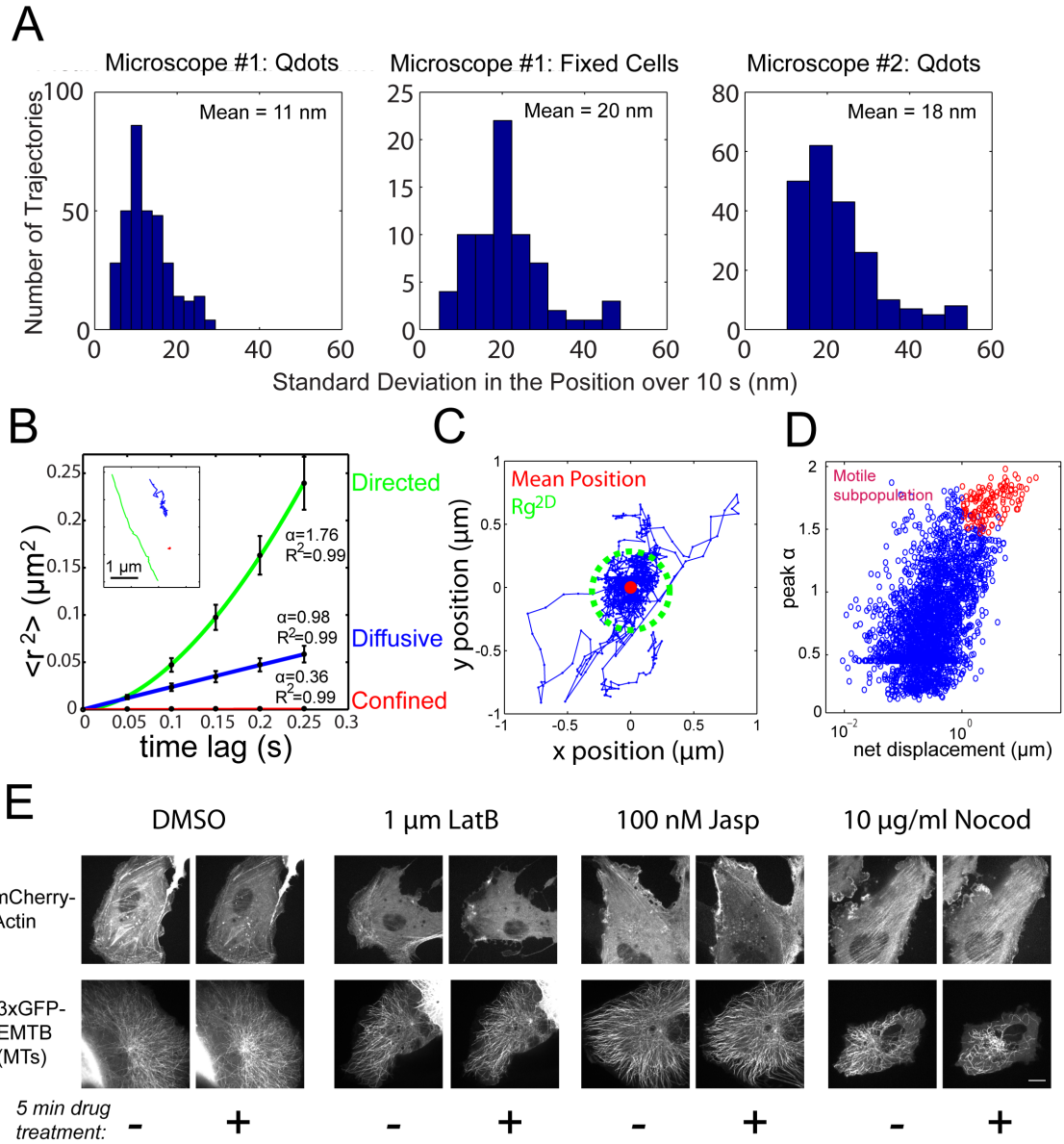


Figure 3. Early endosomal tracking and motion analysis.

A. Spatial resolution of EGF-Qdot tracking. EGF-Qdots that were adsorbed to glass (Qdots) or were inside early endosomes in fixed cells (Fixed Cells) were imaged under standard live-cell imaging conditions at 37°C. Two different microscopes were

- used for experiments in this study (as indicated in Materials and Methods, Microscope #1, Microscope #2). Particles were tracked with the same parameters used on live-cell movies (u-track (Jaqaman et al., 2008)), and trajectories lasting > 10 s were selected for analysis. The standard deviation of the position was calculated for each trajectory and the distribution of these standard deviations for each instrument is shown. The mean of each distribution is indicated in the histogram.
- B. MSD analysis of one example directed, diffusive, and confined 2.25 s period of an EGF-Qdot trajectory. The black circles represent the experimental values (mean  $\pm$  SEM) and the lines are fits to Eq.1. The inset shows the color-coded trajectories used in the MSD plot. Scale bar: 1  $\mu$ m.
- C. Measurement of the effective 2-dimensional radius of gyration ( $Rg^{2D}$ ). A sample EGF-Qdot trajectory is shown with the mean position indicated by the red circle.  $Rg^{2D}$  for this trajectory is indicated by the green dashed line. It is a radius-squared weighted average of the position (Eq.2).

$$Rg^{2D} = \sqrt{\left(\frac{1}{N} \sum_{i=1}^N (r_i - r_{mean})^2\right)}$$

- D. Motile early endosomes are defined by their large displacements and high MSD  $\alpha$  values. For each trajectory included in the analysis for Table 1 the net displacement is plotted versus the mean of the 20 largest  $\alpha$  values in the trajectory (peak  $\alpha$ ). The

motile subpopulation (net displacement  $> 1 \mu\text{m}$  over 30 s,  $\alpha > 1.5$  for 20 frames) is plotted in red.

- E. The degree of cytoskeletal disruption by drug treatment of Arpe-19 cells. Cells were transiently transfected overnight with mCherry-Actin or 3xGFP-EMTB to label MTs, serum-starved for 4 hours, and then imaged with a spinning disc confocal microscope. A single image was taken before drug treatment and after a 5 min incubation with the indicated drug. Actin perturbations did not lead to changes in MT organization. Scale bar  $10 \mu\text{m}$ .

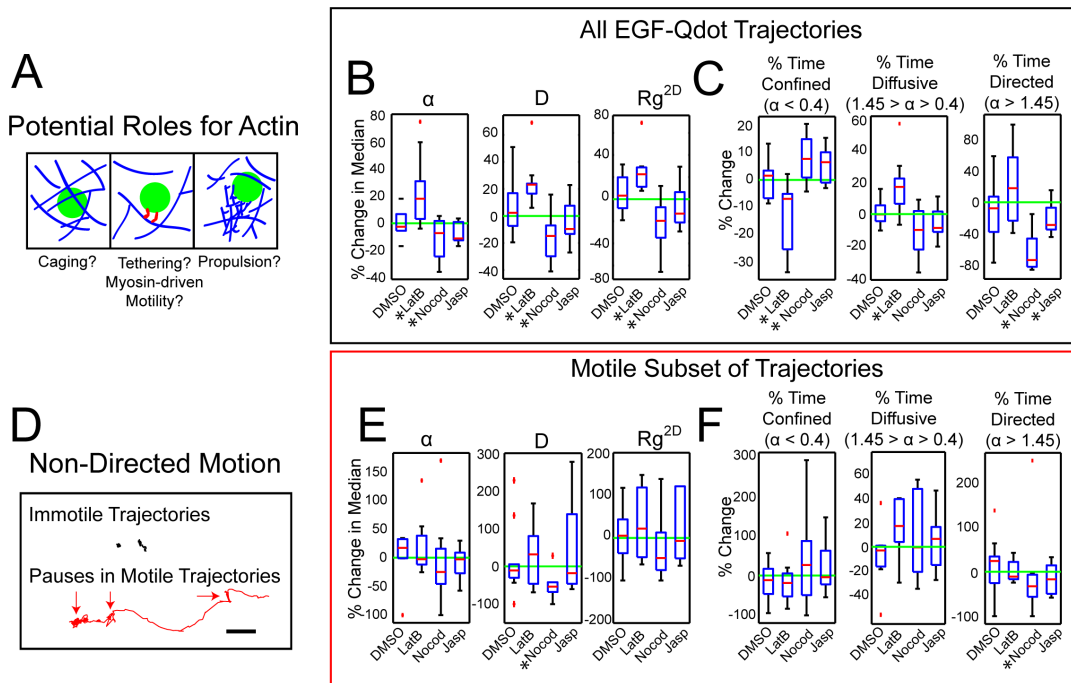


Figure 4. The effect of cytoskeletal disruption on early endosomal motion

- A. Potential roles for actin filaments in early endosomal movement. Early endosomes (green), actin filaments (blue), myosin motors (red).
- B. The effect of cytoskeletal perturbations on endosomal motion. All EGF-Qdot trajectories were analyzed for the indicated parameters using a sliding time window of 2.25 s and the % change in the median value per cell was calculated (n= 10 cells). DMSO: dimethyl sulfoxide control; LatB: 1  $\mu$ M latrunculin B; Nocod: 10  $\mu$ g/ml nocodazole; Jasp: 100 nM jasplakinolide. For all boxplots: medians (red lines), 25<sup>th</sup> and 75<sup>th</sup> percentiles (box edges), data extremes (whiskers), outliers (red crosses), 0% change (green lines). Significant changes (\*p < 0.05) were determined using a binomial test of the % change in the median. See also Table 3, Figure 3.

- C. The effect of cytoskeletal perturbations on the percentage of time EGF-Qdots spend confined, diffusive or directed.
- D. Early endosomal trajectories contain two types of non-directed movement. An immotile set of trajectories lacks directed movement for the entire period of observation. In contrast, motile trajectories contain periods of directed movement but also pauses (arrows). Scale bar: 2  $\mu\text{m}$ .
- E. The effect of cytoskeletal perturbations on the motion of the motile subset of trajectories.
- F. The effect of cytoskeletal perturbations on the percentage of time EGF-Qdots spend confined, diffusive or directed in the motile subset.

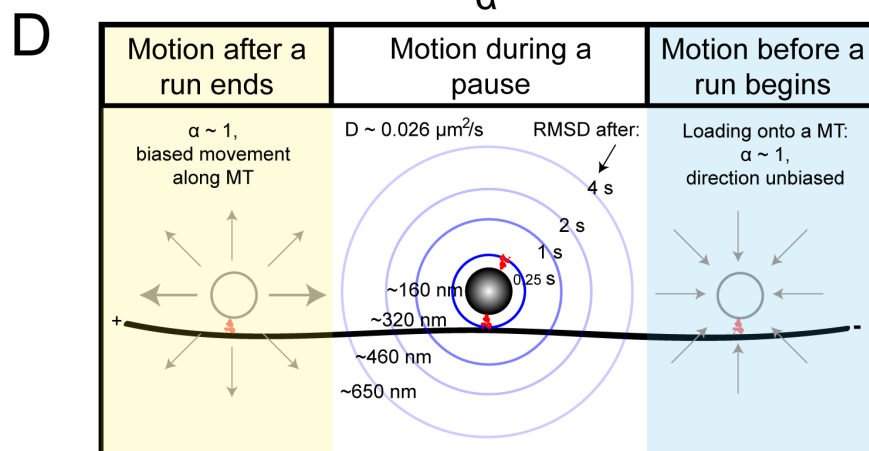
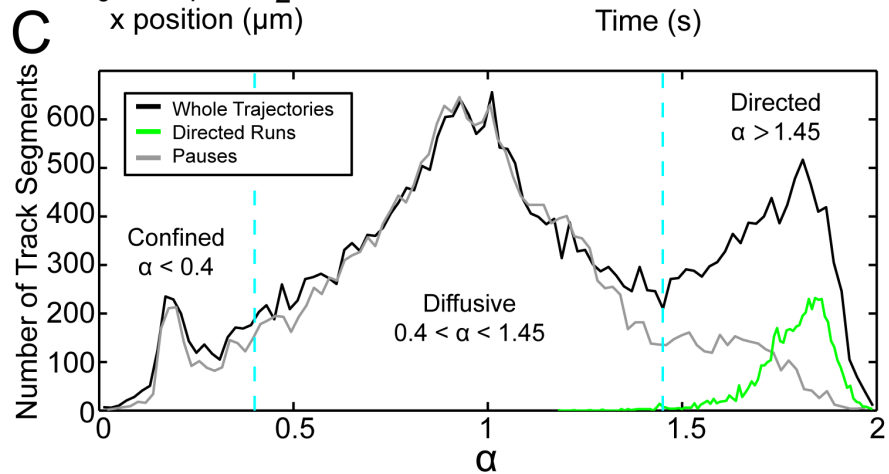
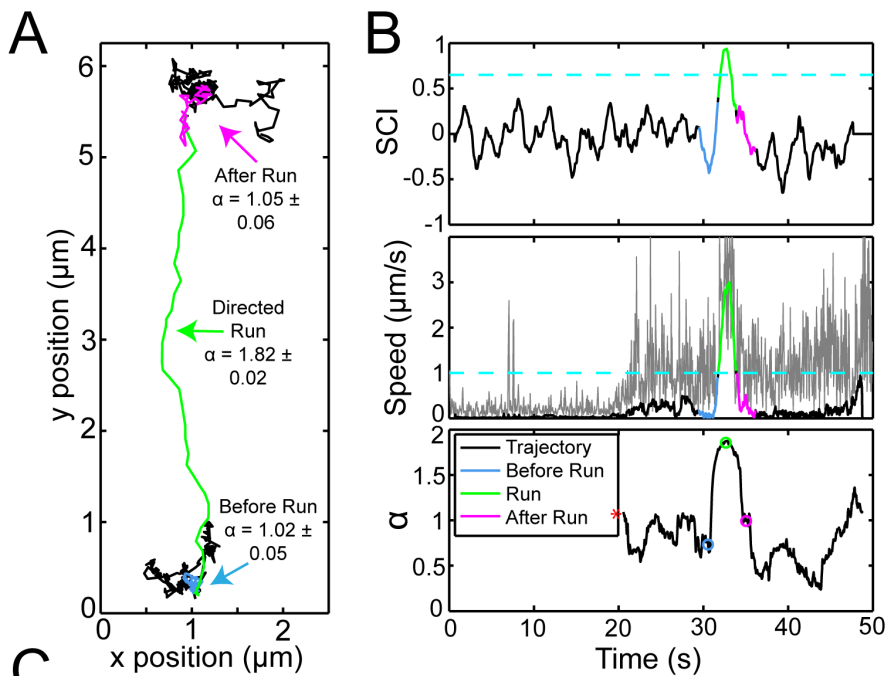


Figure 5. Parsing of trajectories into directed runs and pauses

- A. Early endosomal trajectories exhibited directed motion punctuated by pauses. A representative EGF-Qdot trajectory (black) with directed motion (green) and 2.25 s immediately before (blue) and after (magenta) the run highlighted. For  $\alpha$  values (means  $\pm$  SEMs),  $n=71$  before run,  $n=29$  directed run,  $n=54$  after run. See also Figure 6.
- B. Track parsing criteria and motion analysis. The directed movement criteria (SCI and instantaneous speed (position smoothed over 1.2 s; unfiltered data in grey)) and the MSD  $\alpha$  scaling exponent using a 2.25 s sliding window (Figure 3B, Table 2) are shown for the trajectory in A (5% false-positive thresholds in cyan (Figure 4C-E, Table 4)). Circles highlight the  $\alpha$  values immediately before and after the run and the run center. The  $\alpha$  values before the red asterisk were unreliable due to poor MSD fitting and are not plotted.
- C. MSD motion analysis of intact trajectories, directed runs, and pauses using a 2.25 s sliding time window. Whole tracks: 7% confined, 65% diffusive, 28% directed. Directed runs: 0% confined, 1% diffusive, 99% directed. Pauses: 7% confined, 82% diffusive, 11% directed.
- D. Characteristics of early endosomal motion after a run, during a pause, and before a run begins. Approximately scaled drawing of an early endosome ( $\sim 200$  nm diameter), its linkage to the MT track via dynein ( $\sim 70$  nm, adapted from (Vale,

2003)), and its predicted diffusion (root mean squared displacement (RMSD), blue circles) after different time intervals.

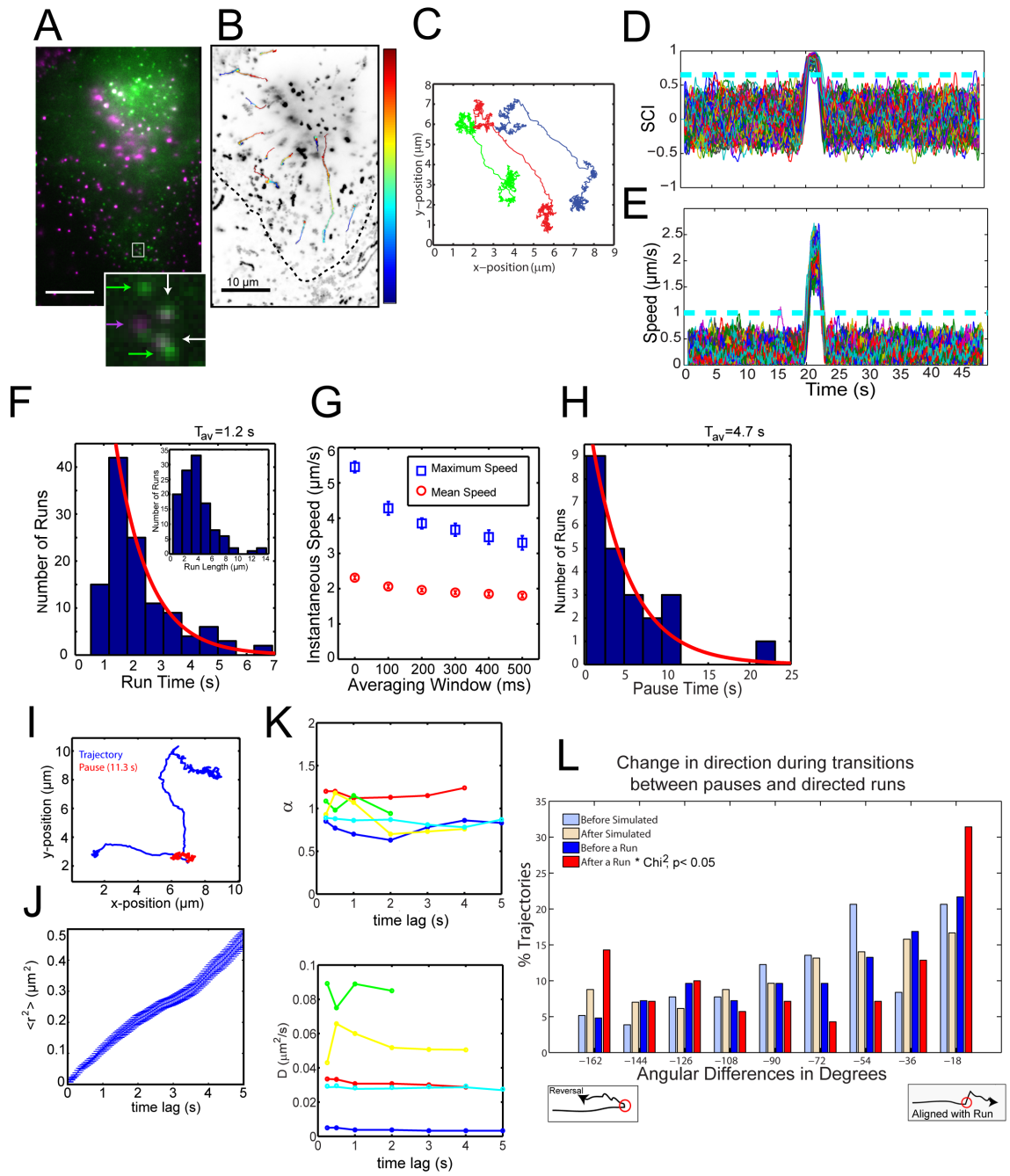


Figure 6. Analysis of motile trajectories.

- A. EGF-Qdots colocalize with GFP-Rab5 positive early endosomes. A single frame (50 ms) from a 50 s image sequence of GFP-Rab5 (green) and EGF-Qdots (magenta) 10 min after addition of EGF-Qdots. The zoomed inset in the bottom of the panel shows colocalization of EGF-Qdots and GFP-Rab5 (white arrows), EGF-Qdots not in early endosomes (magenta arrow), and GFP-Rab5 positive endosomes without EGF-Qdots (green arrows). Scale bar: 10  $\mu\text{m}$ .
- B. EGF-Qdots and GFP-Rab5 endosomes undergo correlated movement during directed runs and pauses. A contrast-inverted maximum intensity projection of the EGF-Qdots from the image sequence in A is shown with the outline of the cell drawn with a black dotted line. Trajectories that met the criteria for “motile” ( $> 2 \mu\text{m}$  net displacement, containing directed runs and pauses) and were GFP-Rab5-positive are overlaid, color-coded for time. Scale bar: 10  $\mu\text{m}$ .
- C. Three example simulated trajectories matching the speed and  $D$  of early endosomes and our imaging parameters. Simulations contain 20 s of diffusion ( $\alpha = 1$ ,  $D = 0.026 \mu\text{m}^2/\text{s}$ ), followed by 2.5 s of directed motion ( $2 \mu\text{m}/\text{s}$ ) with diffusion, followed by another 22.5 s of diffusion. Simulations also implemented 20 nm of positional uncertainty to match our tracking error.
- D. SCI analysis of simulated trajectories. Simulations with the parameters in C were analyzed for their SCI using a sliding time window of 4 frames. SCI traces were then smoothed over windows of 24 frames (1.2 s). Each trace represents one of 200

- simulations. The dotted cyan line (0.65) is the threshold that results in < 5% false positive identification of a directed run during the diffusive periods. See Table 4 for false-positive rates using different diffusion coefficients.
- E. Speed analysis of simulated trajectories. Simulations with the parameters used for C were analyzed for their instantaneous speed. First the position was smoothed over 24 frames (1.2 s) and then the frame to frame instantaneous speed was calculated. The dotted cyan line (1  $\mu\text{m/s}$ ) is the threshold that results in < 5% false positive identification of directed runs during the simulated trajectories. See Table 4 for false-positive rates using different diffusion coefficients.
- F. The duration and distance traveled during directed runs. The duration of the directed runs (based on parsing criteria in Figure 5B) was fit with a single exponential decay to determine the run lifetime ( $T_{av}$ ) of 1.2 s. For number of runs ( $N$ ) at time  $t$ ,  $N(t) = N_0 * e^{(-t/T_{av})}$ . The first bin was excluded from the fit since short runs are underrepresented. The inset shows the distribution of total distances traveled during the same directed runs. The position was smoothed over 6 frames (0.3 s) and the frame to frame displacements were summed over the entire run to calculate the distance traveled.
- G. Speed of directed runs. The position of the early endosome was smoothed over different time windows (Averaging Window) and then the instantaneous frame to frame speed was calculated. The maximum and mean speed was measured for each run. The mean  $\pm$  SEM is plotted.

- H. Duration of pauses. The duration of the pauses enclosed by two directed runs (position based on parsing criteria in Figure 5B) was measured. The distribution of pause times was fit to a single exponential decay as in F and resulted in an average lifetime ( $T_{av}$ ) of 4.7 s.
- I. An example trajectory containing a long pause in between two directed runs. The pause is one of the longest in our data set and is highlighted in red in the trajectory.
- J. MSD analysis of a long pause. The pause in I was analyzed for its mean-squared displacement ( $\langle r^2 \rangle$ , Eq. 1) over different time lags (mean  $\pm$  SEM). Since this is a long pause, we can observe longer time lags than in typical records. The relationship between MSD and time remains linear, or scales diffusively, over the whole time scale.
- K. MSD analysis results are consistent over long time lags. For 5 of the longest pauses (each color is one pause, the trajectory used in I and J is cyan), MSD analysis was performed to calculate  $\alpha$  and D over different time lags (ie, fitting Eq.1 to the data using different t). The resulting  $\alpha$  and D values are shown relative to the time lag used in the fitting.
- L. The motion after a directed run is preferentially aligned with the MT axis. The path of the directed run was assumed to be the axis of the MT. The net direction of the 0.75 s period immediately before or after a run was compared to the direction of the run. The absolute value of this angular difference was taken to simplify the measurement to range from reversals (-180 °) to aligned (0 °). Since errors in track

parsing will lead to regions of the directed run being included in the pause, this will lead to more alignment with the run than expected. To control for this, we compared analysis of simulated trajectories containing diffusion and directed runs. A  $\chi^2$  test comparing the distributions of angles before and after a run to their simulated counterpart was used to evaluate significance. A significant difference was found for the pause regions after a run ( $p < 0.05$ ). The % of trajectory segments after a run exhibiting either reversals or alignment with the directed run are considered to be aligned with the MT axis. This population is  $\sim 2$  fold higher than the simulated data. Before a run,  $N = 83$ . After a run,  $N = 70$ .

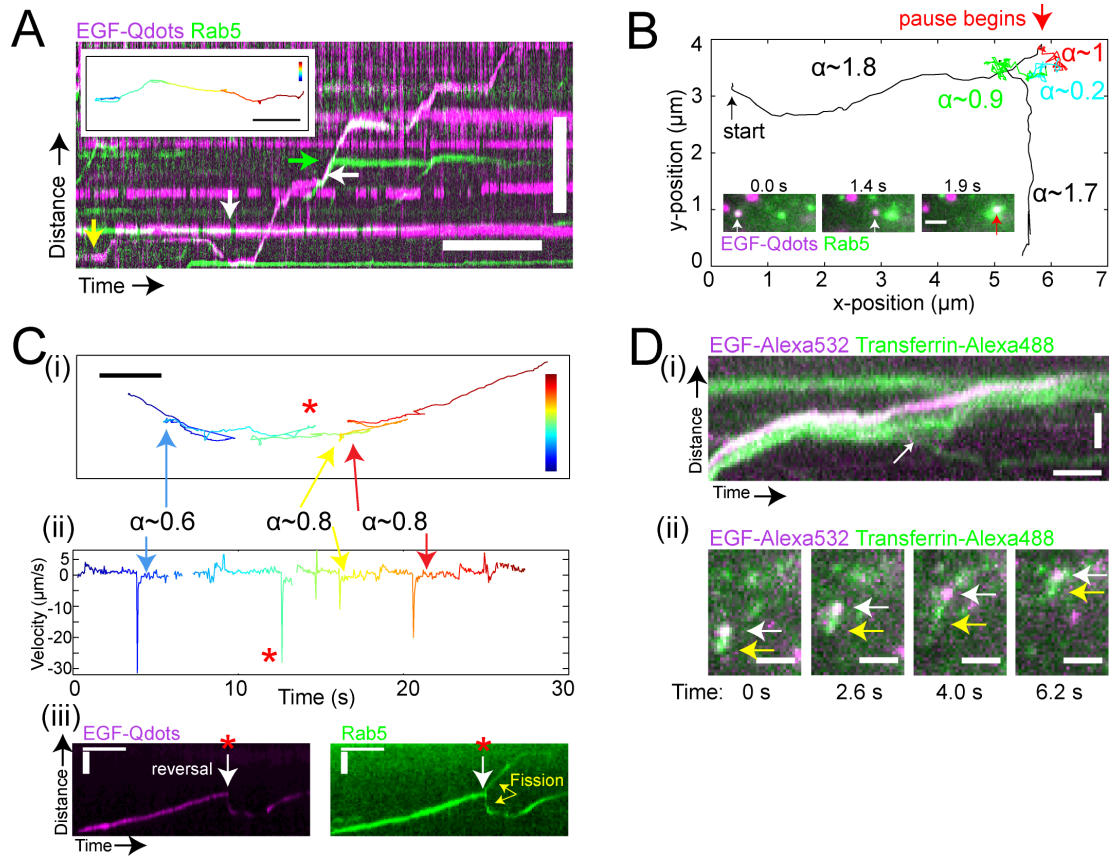


Figure 7. The motion of individual EGF-Qdot-containing early endosomes during encounters with other Rab5-positive early endosomes

- A. EGF-Qdots merge with and split away from other early endosomes during their trafficking. A kymograph showing an EGF-Qdot (magenta, yellow arrow) relative to several other GFP-Rab5 punctae (green) that merge (white arrows) and split away (green arrow). Scale bars: 5  $\mu\text{m}$ , 5 s. Inset: x,y trajectory color-coded for time (blue = first frame, red = last frame). Scale bar: 5  $\mu\text{m}$ .
- B. Pauses in early endosomal motility that occur during an encounter with another early endosome are mainly diffusive. The trajectory (black) of an EGF-Qdot that

- interacts with another endosome during a pause (3 time regions with distinct  $\alpha$  are color-coded on the plot during the pause- red, cyan, green). The inset images show the EGF-Qdot-containing endosome (magenta, white arrow) moving towards a large GFP-Rab5-positive endosome and pausing (red arrows). Scale bar: 2  $\mu\text{m}$ .
- C. An extreme example of a GFP-Rab5/EGF-Qdot particle snapping backwards after several periods of directed motion. (i) The trajectory is color-coded for time (blue = first frame, red = last frame). Scale bar: 5  $\mu\text{m}$ . (ii) The instantaneous velocity of the trajectory in (i). The  $\alpha$  values for three pause locations are indicated with arrows. (iii) The kymographs show one of the EGF-Qdot reversals (white arrow, red asterisk marks time-point of the reversals in (i) and (ii)) during which a puncta of GFP-Rab5 separates from the EGF-Qdot/GFP-Rab5 (yellow arrows) as the EGF-Qdot snaps backwards. Scale bar 2  $\mu\text{m}$ .
- D. Transferrin-positive tubules extend from motile, EGF-positive endosomes. (i) A kymograph showing a pause in EGF-Alexa532/transferrin-Alexa488 trafficking and a fission event (white arrow). Scale bars: 2  $\mu\text{m}$ , 1 s. (ii) A montage from the movie in (i) of EGF (magenta, white arrow) and transferrin (green, yellow arrow).

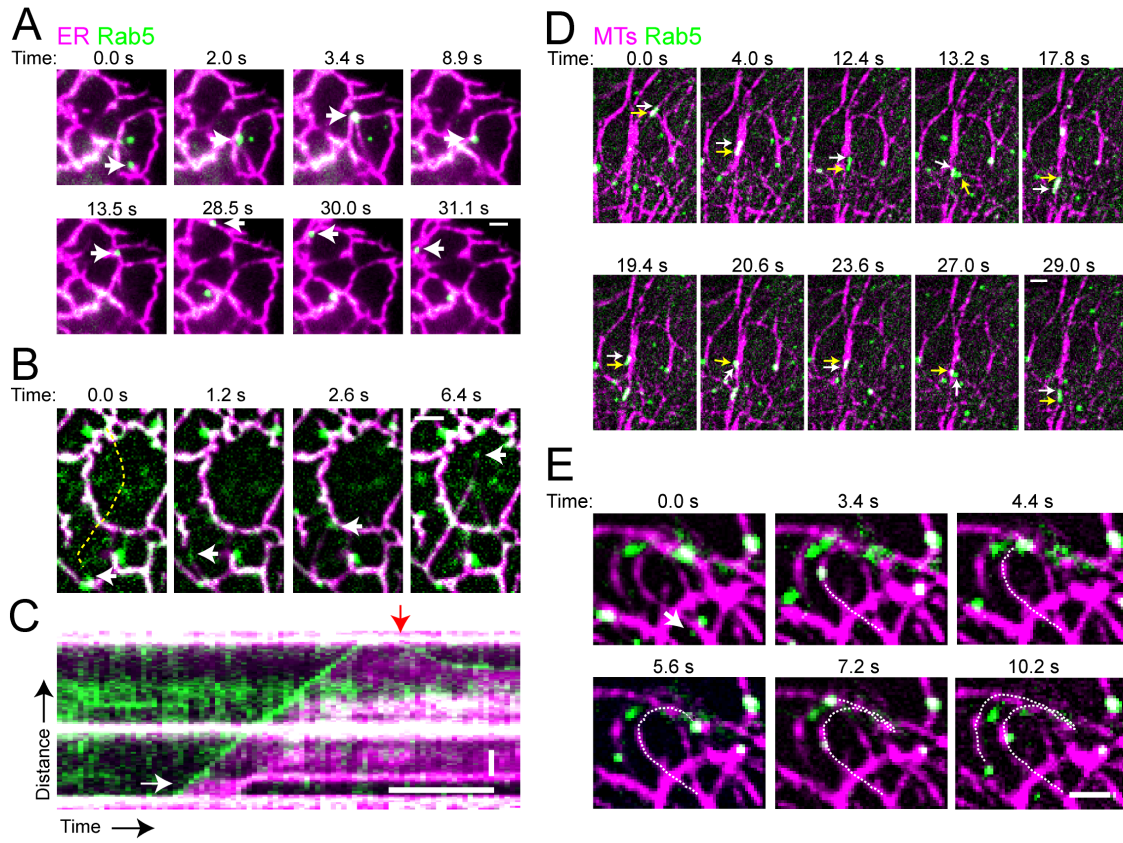


Figure 8. Early endosomal movement is affected by interactions with the ER and multiple MTs.

- A. Early endosomes remain attached to the ER for long periods during which repeated deformation of the ER occurs. The white arrow follows the same early endosome. Scale bar: 2  $\mu\text{m}$ .
- B. An early endosome appears to pull an ER tubule behind it during a directed run. The yellow-dotted line in the first panel indicates the trajectory used to generate the kymograph in C. Images are background-subtracted. Scale bar 2  $\mu\text{m}$ .

- C. The kymograph highlights the rapid ( $\sim 1.6 \mu\text{m/s}$ ) movement of the early endosome (green, white arrow) towards the perinuclear region followed by a slower reversal ( $\sim 0.7 \mu\text{m/s}$ , red arrow). Scale bars: 4 s,  $2 \mu\text{m}$ . See also Figure 9A.
- D. Pausing and rotation of two elongated early endosomes at a region of dense MTs. The white and yellow arrows indicate the two ends of an elongated early endosome (green) to highlight its rotation during the pause near dense MTs (magenta). The two rows show different early endosomes navigating the same region. Images are background-subtracted. Scale bar:  $2 \mu\text{m}$ .
- E. Rapid switch between 2 MT tracks by an early endosome. The dotted white line indicates the trajectory taken by the early endosome (green, arrow). Images are background-subtracted. Scale bar:  $2 \mu\text{m}$ . See also Figure 9B.

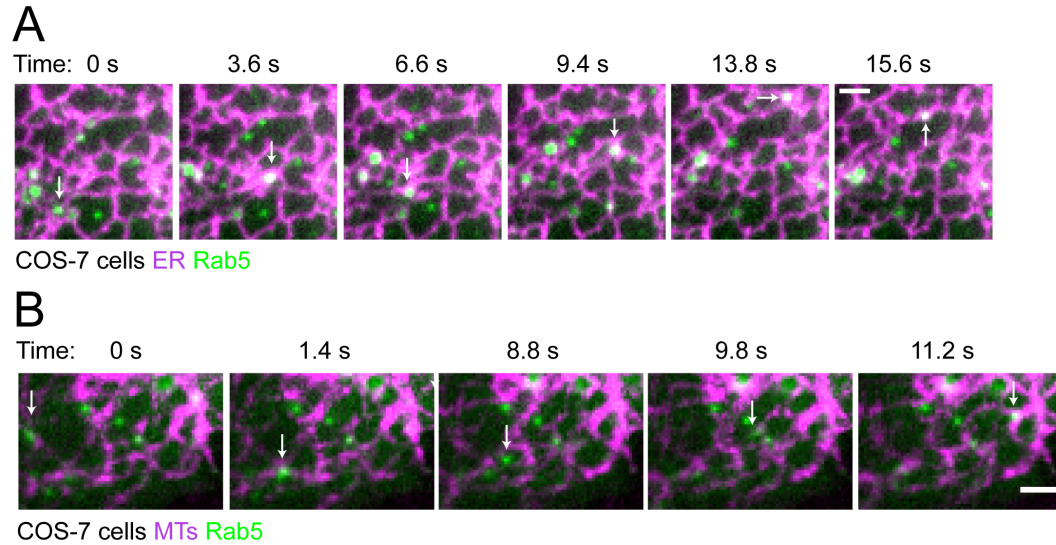
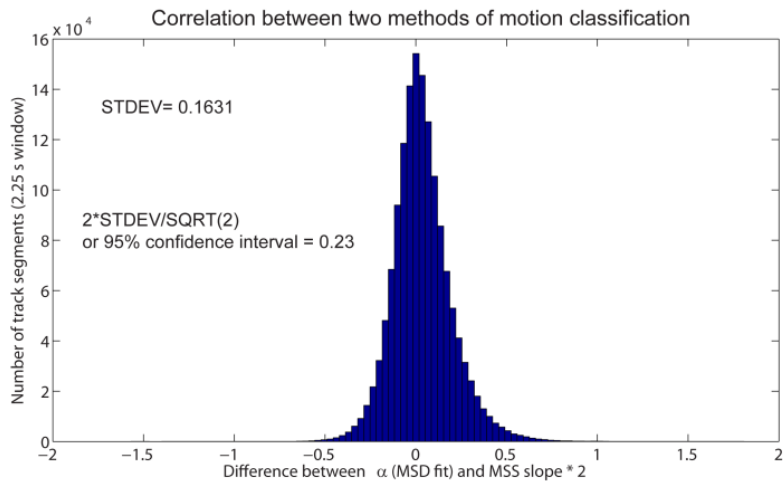
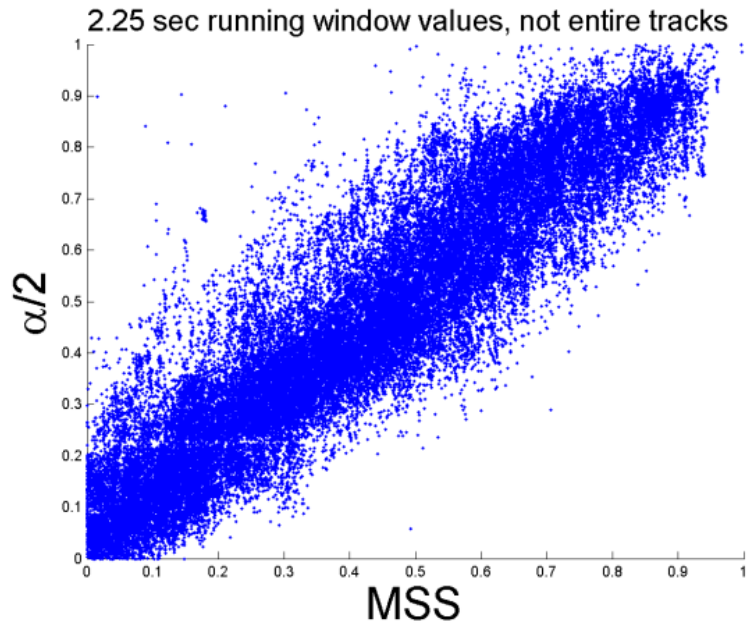


Figure 9. Interactions between early endosomes and the ER and between early endosomes and MT-dense regions are also observed in COS-7 cells.

- A. Rab5-positive early endosomes deform the ER during their movement and remain attached before, during, and after a pause, in COS-7 cells. A GFP-Rab5-positive early endosome (green), indicated by the white arrow, undergoes rapid movement towards the perinuclear region for 3.6 s during which time it seems to drag the ER (dsred2-KDEL, magenta) along with it. This is followed by 3 s during which both the Rab5 and ER slowly move in the opposite direction. The early endosome resumes perinuclear-directed movement, still attached to and deforming the ER, for the remainder of the movie. Scale bar: 2  $\mu$ m.
- B. Rab5-positive early endosomes pause at MT intersections in COS-7 cells. A rapidly moving GFP-Rab5-labeled early endosome (green), indicated by the white arrow,

moves into a region of dense, intersecting MTs (2xmCherry-EMTB, magenta) at 1.4 s and undergoes little movement for 7.4 s. Then it resumes rapid, perinuclear-directed movement for an additional 2.4 s before encountering another MT-dense region and pausing for the remainder of the movie. Scale bar: 2  $\mu\text{m}$ .

**A**



**B**

Figure 10. Comparison of MSD and MSS analysis to classify motion and estimate the uncertainty in  $\alpha$ .

- A. All of the EGF-Qdot data in Table 1 was analyzed using a 2.25 s sliding analysis window to calculate both the MSD  $\alpha$  exponent and the MSS slope. Since these two values are related by a factor of two the MSS slope for each track fragment was plotted vs the MSD  $\alpha$  measurement for that track divided by 2. The linear relationship across the entire spectrum of  $\alpha$  indicates the two independent methods arrive at the same classification.
- B. As a method to estimate the error in MSD  $\alpha$  we plotted the difference between the MSS slope, multiplied by 2 to scale it in terms of  $\alpha$ , and MSD  $\alpha$  for all track segments. The 95% confidence interval of this distribution would indicate the error in the measurement of  $\alpha$  if MSS slope had no error associated with it. Since we do not know how the error is distributed, we shared it equally between the two measurements. The 95% confidence interval for MSD  $\alpha$  is 0.23.

### 3.6 Tables

	<b>Immotile (net displacement &lt; 0.5 <math>\mu\text{m}</math>)</b>	<b>Speed &gt; 2 <math>\mu\text{m/s}^*</math></b>	<b>Minus-End Directed Runs*</b>	<b>Bidirectional Trajectories*</b>
<b>GFP-Rab5</b>	62 $\pm$ 2% (2,839 Tracks)	12 $\pm$ 2%	78 $\pm$ 4%	9 $\pm$ 2%
<b>mCherry-Rab7</b>	66 $\pm$ 2% (2,537 Tracks)	5 $\pm$ 1%	43 $\pm$ 3%	23 $\pm$ 4%

N=10 cells. Mean  $\pm$  SEM. \* p < 0.05, t-test. GFP-Rab5 data reproduced from text related to Figure 2 for comparison.

Table 1. Comparison of the motility of early endosomes and late endosomes/lysosomes.

Rab5-positive early endosomes are faster and more uniformly MT minus-end-directed than late endosomes/lysosomes. Trajectories of Rab5 and Rab7 particles in the same cell were analyzed for their speed and directionality. Trajectories are from movies acquired at 20 fps, over 45 s, in 10 cells. The analysis of the Rab5 tracks is the same as that described in the text related to Figure 2 and is reproduced here to facilitate comparison to Rab7. Percentages are the mean of the percentages in the 10 cells  $\pm$  SEM. \* p < 0.05 for a student's t-test comparing Rab5 and Rab7 values. See Materials and Methods for detailed criteria used in track classification.

	Simulation Parameters	Diffusive Period (2.25 s)	Before a Run (2.25 s)	After a Run (2.25 s)
$\alpha$	1	$0.80 \pm 0.02$ (20%)	$0.83 \pm 0.01$ (17%)	$0.80 \pm 0.01$ (20%)
$D$ ( $\mu\text{m}^2/\text{s}$ )	0.01	$0.0072 \pm 0.0004$ (28%)	$0.0088 \pm 0.0004$ (12%)	$0.0076 \pm 0.0003$ (24%)
$\alpha$	1	$0.90 \pm 0.01$ (10%)	$0.91 \pm 0.01$ (9%)	$0.88 \pm 0.01$ (12%)
$D$ ( $\mu\text{m}^2/\text{s}$ )	0.026	$0.022 \pm 0.001$ (15%)	$0.023 \pm 0.001$ (12%)	$0.022 \pm 0.001$ (15%)
$\alpha$	1	$0.93 \pm 0.01$ (7%)	$0.93 \pm 0.01$ (7%)	$0.91 \pm 0.02$ (9%)
$D$ ( $\mu\text{m}^2/\text{s}$ )	0.07	$0.060 \pm 0.002$ (14%)	$0.060 \pm 0.003$ (14%)	$0.062 \pm 0.004$ (11%)

For  $\alpha$ , mean  $\pm$  SEM (% difference from simulated  $\alpha$ ). For  $D$ , median  $\pm$  SEM (% difference from simulated  $D$ ).  
N=200 simulated trajectories with one directed run each.

Table 2. MSD analysis of simulated trajectories after parsing the trajectories into directed runs and pauses.

MSD analysis was performed on simulated trajectories containing diffusion with one directed run (Figure 6C). Analysis of simulations with a range of diffusion coefficients ( $D \sim 0.026 \mu\text{m}^2/\text{s}$  was measured for early endosome pauses) is shown here to indicate our MSD analysis is also appropriate for smaller or larger  $D$  values. Analysis was done on

2.25 s periods during a known period of diffusion (Diffusive Period). To obtain 2.25 s regions before and after a run, the simulations were analyzed using the same parsing criteria as for EGF-Qdot data in cells (Figure 5B, Figure 6D,E). The recovered  $\alpha$  (mean  $\pm$  SEM) and D (median  $\pm$  SEM) are shown as well as the percentage by which they differ from the simulated values.

	$\alpha$	D ( $\mu\text{m}^2/\text{s}$ )	Rg <sup>2D</sup> ( $\mu\text{m}$ , over 0.75 s)	Confined ( $\alpha < 0.4$ )	Diffusive ( $0.4 < \alpha < 1.45$ )	Directed ( $\alpha > 1.45$ )
<b>All Trajectories</b>	0.32 ± 0.09	0.006 ± 0.001	0.0016 ± 0.0003	59 ± 9%	39 ± 9%	2 ± 1%
<b>Motile Trajectories</b>	0.84 ± 0.24	0.024 ± 0.023	0.0067 ± 0.0055	25 ± 13%	52 ± 12%	23 ± 8%

N=40 cells. Median  $\alpha$ , D, Rg<sup>2D</sup> calculated for each cell. Mean ± SEM presented in table.

Table 3. Motion characteristics of EGF-Qdots

MSD and Rg<sup>2D</sup> analysis was performed on EGF-Qdot trajectories from 30 s movies (acquired at 20 fps) in 40 cells using a 2.25 s sliding time window (analysis description in Figure 3B,C). The median values of  $\alpha$ , D, and Rg<sup>2D</sup> were calculated for each cell; table values are (means ± SEMs) for all cells.

<b>D (<math>\mu\text{m}^2/\text{s}</math>) in simulation</b>	<b>SCI</b>	<b>Speed</b>
<b>0.010</b>	1.5%	0.0%
<b>0.026</b>	2.5%	0.5%
<b>0.070</b>	3.0%	63.5%

% of simulated trajectories with a false-positive directed run.  
N=200 simulated trajectories with one true directed run each.

Table 4. The false-positive rate in determination of directed runs using individual parsing criteria.

Simulations of diffusion with 1 directed run (Figure 6C) were subjected to SCI and velocity track parsing analysis as described in Figure 6D,E. The percentage of simulated trajectories that contained a false-positive directed run using either the SCI or Speed analysis is indicated. Analysis of simulations with a range of diffusion coefficients ( $D \sim 0.026 \mu\text{m}^2/\text{s}$  was measured for early endosome pauses) is shown here to indicate our track parsing criteria are also appropriate for smaller or larger  $D$  values. In data analysis, both criteria had to be met to determine a directed run, so the large false-positive rate using the speed criteria when the diffusion coefficient =  $0.07 \mu\text{m}^2/\text{s}$  will not lead to that false-positive rate in data analysis.

	$\alpha$	D ( $\mu\text{m}^2/\text{s}$ )	Rg <sup>2D</sup> ( $\mu\text{m}$ , over 0.75 s)	# Trajectory Segments
<b>Before a Run</b>	1.13 $\pm$ 0.25	0.047 $\pm$ 0.020	0.07 $\pm$ 0.03	83
<b>Middle of a Run</b>	1.98 $\pm$ 0.29			105
<b>After a Run</b>	1.08 $\pm$ 0.40	0.104 $\pm$ 0.03	0.10 $\pm$ 0.03	70

For  $\alpha$  and D, mean  $\pm$  SEM. For Rg<sup>2D</sup>, median  $\pm$  SEM.

Table 5. Alternative MSD analysis using concatenated 0.75 s trajectory segments.

As an alternative method to analyze small track segments immediately before and after a directed run, we collected all the 0.75 (15 frame) segments before or after a directed run in our data. We concatenated each set into one long trajectory and then performed MSD (Figure 3B) and Rg<sup>2D</sup> (Figure 3C) analysis on that trajectory. Creating one long trajectory increases the number of measurements of the squared displacement at different time lags. The SEM was calculated by bootstrapping. Briefly, 100 random samples of the trajectory segments in random order were concatenated and analyzed to calculate the error in the measurement.

	<b>Spatial Overlap with Rab5 Pauses</b>	<b>Spatial Overlap with Random Locations</b>	<b>Number of Pauses Scored</b>
<b>Rab5*</b>	25 ± 12 %	11 ± 4 %	89
<b>Late endosomes/lysosomes</b>	21 ± 9 %	25 ± 6 %	110
<b>Mitochondria</b>	5 ± 4 %	12 ± 8 %	90
<b>Golgi</b>	4 ± 4 %	6 ± 7 %	90
<b>ER*</b>	39 ± 13 %	23 ± 8 %	76

Pauses scored in 10 Rab5 tracks per cell, 5 cells. Mean ± SEM. \* p < 0.05 for t-test comparing Rab5 and random distributions.

Table 6. Spatial correlation between Rab5-positive endosomal pauses and organelle positions

The cellular location of pauses in GFP-Rab5 positive early endosomal directed runs was determined and scored for the presence of the indicated organelle (see M&M for organelle constructs). Mean % ± SEM, n= 5 cells. Statistical significance (\* p < 0.05) was determined by comparing the % of endosomal pauses that correlated with the location of each organelle to the % of randomly chosen locations that correlated with that organelle.

## Chapter 4. Discussion

Analysis of the motion within the early endosomal compartment has given us a framework of the types of motion observed during early endosomal trafficking and how types of motion correlate with cellular structures. This characterization sets boundaries on which models for motor regulation could be occurring in the cell.

The types of movement observed in this study also raised several new questions about how and why early endosomes move in the way we observed. Why do individual early endosomes exhibit distinct types of movement when they are all members of the same organelle? In motile early endosomes, what causes the pauses in directed motion and what is occurring during the pauses? Are the pauses in directed motion beneficial to early endosomal function or just a consequence of roadblocks in the cell? Is the saltatory movement observed in other organelles also caused in some part by MT intersections and interactions with other organelles? Does interaction with the ER create enough of a resistive force to influence directed transport? Does ER contact by other organelles lead to similar pauses in directed transport?

The results of this study of early endosomal motion will be summarized, these outstanding questions discussed in more detail, and future directions proposed in the following sections of this chapter.

## **4.1 Heterogeneity in the movement of different early endosomes**

Analysis of the movement of GFP-Rab5 punctae and endocytosed EGF-Qdots indicated that there are at least two distinct groups of early endosomes based on motion: early endosomes that are immotile (defined as moving  $< 0.5 \mu\text{m}$  over 30s), and endosomes that are motile but contain many pauses (have some period of rapid, directed motion). Notably, the immotile early endosomes are confined to a degree controlled in part by the density of the actin network, while pauses in the motile tracks are diffusive and not affected by actin perturbations. This suggests that the immotile early endosomes are not an extended pause in directed movement. Several factors may contribute to the different types of motility, including: (1) artifacts introduced from imaging conditions, (2) heterogeneity within the early endosomal population, and (3) spatial variation in cell organization. Future experiments can be done to address the contributions of each of these factors.

### **4.1.1 Imaging time affects interpretation**

In order to obtain high-resolution trajectories we sacrificed long observation periods, precluding motion analysis over the complete lifetime of an individual EGF-Qdot. Therefore, the immotile and motile early endosomes may maintain these motion differences for their lifetime, or may be types of movement that all early endosomes switch back and forth between. Alternatively, since early endosomes are a

compartment that matures over time our data likely contains early endosomes at a mixture of maturation states. Different types of motion may correlate with different maturation stages of early endosomes.

#### **4.1.1.1 Future experiments**

The exploration of organelle and cargo movements over different time scales is necessary to gain a full picture of how an organelle moves and maintains its structure. Using low-intensity illumination should allow longer imaging periods of EGF-Qdots, but with a loss of high-resolution information. Alternatively, the use of EGF conjugated to gold nanoparticles (Gu et al., 2012) would allow a large increase in acquisition rate (< 2ms per frame) using video-enhanced differential interference contrast microscopy (DIC), without a loss in resolution, and would reduce the damage to cells from short-wave length laser illumination.

#### **4.1.2 Differences in effectors and motors exists within Rab5 compartment**

Some studies have found that different cargos segregate into distinct subsets of early endosomes (Lakadamyali et al., 2006; Leonard et al., 2008; Warren et al., 1997). Rab5 is necessary for the existence of the early endosomal compartment, and its many effectors biochemically define the early endosome (Zeigerer et al., 2012). Some Rab5 effectors are found on only a subset of early endosomes and are thought to represent

different maturation states or different trafficking routes within the early endosomal compartment.

A subset of endocytosed material from both clathrin-dependent and clathrin-independent endocytosis enters early endosomes that are positive for Rab5 and its effector APPL1/2 but negative for the Rab5 effectors PI(3)P and EEA1 (Zoncu et al., 2009). APPL positive endosomes either convert to WDFY2 positive endosomes (Hayakawa et al., 2006), another recently identified subpopulation of early endosomes, or mature into EEA1/PI(3)P positive endosomes (Zoncu et al., 2009). WDFY2 containing endosomes ultimately convert to EEA1/PI(3)P positive endosomes as well (Zoncu et al., 2009).

A critical regulator of the switch from APPL positive to EEA1 positive early endosomes is the depletion of PIP<sub>2</sub> and the accumulation of PI(3)P (Zoncu et al., 2009). Inhibiting PI(3)P accumulation on early endosomes blocks them in an APPL positive state associated with increased EGFR signaling (Zoncu et al., 2009). APPL1/2 contain BAR, PH, and PTB domains, allowing them to interact with both lipids and activated RTKs (Li et al., 2007; Miaczynska et al., 2004; Zhu et al., 2007). The distinct roles for APPL and WDFY2 endosomes are unclear. APPL positive endosomes have been proposed to represent the “signaling endosome” compartment based on the high levels of EGFR signaling when this compartment is expanded (Zoncu et al., 2009). However, another study implicated

APPL1 endosomes not in signaling, but in transport of endocytosed cargo to autophagosomes (Tumbarello et al., 2012).

Our study has confirmed that at least two motors are present on only a subset of early endosomes, myosin VI and KIF16b (Aschenbrenner et al., 2003; Hoepfner et al., 2005). Importantly, these motors can be visualized on early endosomes in live cells, unlike the other motors implicated in early endosomal transport. Myosin VI is likely involved in early stages of early endosomal motion. It is on a subset of Rab5-positive endosomes (Aschenbrenner et al., 2003) enriched in the periphery of the cell where actin density is the highest, and its binding partners Tom1 and GIPC can recruit it to APPL positive endosomes (Tumbarello et al., 2012). In contrast, KIF16b binds tightly to PI(3)P and colocalizes with EEA1 positive early endosomes, suggesting it is recruited later in endosomal maturation than myosin VI (Blatner et al., 2007; Hoepfner et al., 2005).

#### **4.1.2.1 Future directions**

The ability to visualize different endosomal populations and molecular motors would allow us to test the relationship between early endosome maturation state, motor recruitment, and motion. One hypothesis would be that as Rab5 effectors change, the motors change, and that this correlates with changes in the type of early endosomal motion.

##### **4.1.2.1.1 Myosin VI**

I would hypothesize that the early, APPL positive early endosomes are part of the immotile population of early endosomes because they are enriched within the first 100 nm of the plasma membrane relative to EEA1-positive early endosome (Hayakawa et al., 2006), suggesting they are in the actin rich cortex. Measuring the kinetics of myosin VI recruitment to early endosomes relative to APPL and PI(3)P/EEA1 would tell us if myosin VI follows a similar maturation pathway. However, recruitment of myosin VI does not necessarily mean it is actively engaged in moving the endosomes.

A related question is whether myosin-based transport affects the rate at which APPL1 endosomes acquire PI(3)P and EEA1. If there is feedback from the change in transport to the rate of Rab5 effectors changing, I would expect that APPL endosomes would exist longer and that EGFR signaling would increase as it does when PI(3)P levels are inhibited (Zoncu et al., 2009). Myosin VI has many binding partners in the cell for diverse cellular processes (Buss and Kendrick-Jones, 2011). To specifically inhibit myosin VI recruitment to APPL endosomes, mutations in myosin VI or Tom1 that disrupt this interaction should be cleaner. Additionally, mutations in the myosin VI motor domain can be used that would allow recruitment of myosin VI but block motor activity.

Tracking the movement of these organelles in live cells and the fate of signaling cargo like EGF will be informative. Since APPL1 has now been proposed to identify both a signaling endosome (Schenck et al., 2008; Zoncu et al., 2009) and a transport pathway for autophagy (Tumbarello et al., 2012), there may still be further subsets of APPL1

endosomes. Since Tom1 was essential for myosin VI recruitment to APPL positive endosomes, but GIPC was only partially involved (Tumbarello et al., 2012), comparison of the movement of GIPC and Tom1 positive early endosomes would be a good first test that there are further subdivisions of early endosomes.

#### **4.1.2.1.2 KIF16b**

KIF16b can also be visualized in live cells on early endosomes. Since KIF16b localization to early endosomes requires its PX domain, which binds tightly to PI(3)P (Blatner et al., 2007), I would hypothesize that this motor is not present on APPL positive endosomes and is recruited over time as PI(3)P levels rise, perhaps showing an inverse correlation with myosin VI recruitment times. It will be interesting to see how this motor's presence correlates with the presence of directed motion since it is a plus-end directed MT-based motor, but directed motion occurs predominantly towards the MT minus-end. This leaves open the possibility that KIF16b recruitment to the early endosome serves a different purpose and does not correlate with the presence of directed runs.

#### **4.1.2.1.3 Dynein/dynactin**

To address when dynein/dynactin is recruited, we are not able to use visual recruitment of labeled motor proteins. Previous work inhibiting dynein through knock-down or injection of the DN CC1 (Driskell et al., 2007) demonstrated almost complete loss of

directed motion. However, even the 4 hr treatment period with the DN construct is long-term inhibition relative to the rate that cargo and endosomes mature and renew the compartments. The use of the new chemical inhibitor of dynein, ciliobrevin (Firestone et al., 2012), should be instrumental in assigning a role for dynein activity in different types of endosome movement and at different stages of endosomal maturity.

Another route to more specifically interrogate dynein's role in early endosomal motion and maturation is to try to block dynein's recruitment specifically to early endosomes. The studies in *Aspergillus nidulans* (Zhang et al., 2011) and COS-7 cells (Yeh et al., 2012) suggest that the p25/p27 pointed end complex in dynactin mediates the interaction with early endosomes without affecting several other known roles for dynein. Further study of this interaction and development of reagents to specifically disrupt dynein at this compartment would create useful tools to study early endosomal motility in a normal cellular context.

#### **4.1.2.1.4 Parallel studies in neurons**

Although large, flat tissue culture cells, such as Arpe-19 cells, provide an ideal morphology for imaging clathrin-coated pit dynamics and the early stages of endosomes moving in the cell periphery, at later times early endosomes become a dense cloud of overlapping trajectories. Conversion of Rab5 to Rab7 in Arpe-19 cells occurs after early endosomes have already reached the perinuclear region when endosomes are so

clustered that following many individual endosomes with confidence becomes nearly impossible.

Extending these types of studies correlating markers for subsets of early endosomes with motion, position in cell, and the recruitment of different motors in an elongated cell like a neuron would allow better spatial separation of the endosomal compartments once MT-based trafficking commences. Treatment of neurons with NGF activates the TrkA tyrosine kinase receptor (Jing et al., 1992), which passes through the endosomal pathway. TrkA receptors are found in early endosomes containing APPL1, GIPC, and myosin VI (Lin et al., 2006; Varsano et al., 2006). Myosin VI and GIPC are also required for normal BDNF-induced TrkB signaling (Yano et al., 2006). These studies suggest that the NGF or BDNF pathway can be used in neurons to test in parallel many of the same questions explored using EGF in tissue culture cells.

#### **4.1.3 Physically distinct areas of the cell**

Early endosomes are scattered throughout the cell, creating another potential source for the differences in motion between early endosomes. The viscoelastic properties vary in different regions of the cell (Tseng et al., 2002). Therefore, the decrease in the confinement of early endosomes when actin filaments were disrupted could be interpreted in two ways. Early endosomes may have a direct and specific coupling to actin filaments that leads to confinement (Provance et al., 2008). Alternatively, the

early endosomes may be confined non-specifically by the density of the actin network relative to their size (Aschenbrenner et al., 2004). A dense network of actin would correlate with an increased elastic modulus locally.

#### **4.1.3.1 Future Directions**

##### **4.1.3.1.1 Super-resolution mapping**

Further investigation of the organization of the cytoskeleton relative to early endosomes at higher spatial resolution is needed to understand how they contact the cytoskeleton. High speed imaging, followed by rapid fixation and correlative super-resolution imaging may provide better insight into the organization of actin around immotile early endosome or paused early endosomes. The use of platinum replica EM is also possible, although more technically challenging.

##### **4.1.3.1.2 Two point microrheology**

The mechanical properties of the cell can be mapped using two point microrheology (TPM) (Wirtz, 2009). In this approach passivated beads are injected into the cell as tracers and their motion tracked. How the motion of pairs of beads correlates can be used to get information about the material between the two beads. With a very high bead density, fine mapping of cellular mechanics is possible (Tseng et al., 2002). This approach would allow us to use passivated beads matching the size of early endosomes

to see how much variation there is in the cell viscoelastic properties on the size scale of early endosomes. Since this is a tracking based approach, endosomes can be simultaneously imaged. This is important because we expect these domains to change over time. Additionally, repeating the cytoskeletal disruption experiments while performing TPM will allow us to assess whether the degree of actin disruption was enough to change the mechanical properties of the cell or was minor enough to indicate a more specific linkage to actin might be involved in early endosomal confinement.

In our original studies, we did not find that early endosomes that were confined were closer to the actin-dense cell edge than motile early endosomes. However, the way this data was collected does not give us a representative slice of the cell. We used low angle oblique illumination, limiting our depth of view to the bottom of the cell where the actin cortex lies. Additionally in order to obtain 2 channels simultaneous at high magnification our field of view was limited to roughly  $\frac{1}{4}$  of the cell area, meaning that as cells varied in morphology, we could not easily define regions of the cell.

Employing strategies to standardize cell shape and imaging could allow us to look for spatial difference in motion more reliably. The use of micropatterns of adhesive proteins can constrain cells to the same shape, which tends to lead to a more stereotypic cytoskeletal arrangement from cell to cell (They et al., 2006). Switching to spinning disk confocal would allow measurement within the center plane of the cell, and using the full camera frame so that we can see the whole cell either by limiting

ourselves to a single channel or using two cameras will allow us to compare motion spatially across many cells.

#### **4.2. Heterogeneity in motion within individual tracks**

Individual early endosomes pause for several seconds in between short directed runs of  $\sim 1$  s towards the perinuclear region. Analysis of the motion specifically during the pause periods indicated that the motion is diffusive, or randomly directed. Additionally the motion immediately before and after a directed run (within a 2.25 s analysis window) was not significantly different from the motion during pauses as a whole, indicating that transitions into and out of directed motion are not marked by a unique motion signature on this time-scale. However, analysis of the direction of the motion before and after a run indicated that there was a significant enrichment in movement along the axis of the MT after a directed run.

This combination of movements within individual trajectories led us to propose a model in which early endosomes bind to MTs and initiate directed transport from a 2 dimensional diffusive state, undergo dynein-driven directed movement for  $\sim 1$  s or 2-3  $\mu\text{m}$ , then pause and diffuse in 2 dimensions. Prior to release from the MT, there is evidence of 1 dimensional diffusion in some tracks. This indicates a continued attachment to the MT such as a bidirectional tug of war between motors or diffusion of

a motor or MAP along the MT occurs prior to 2 dimensional diffusive movements at the end of a directed run.

#### **4.2.1 Pausing due to engagement of an opposite polarity motors**

Most cargoes and organelles contain several motors of opposing polarities. The saltatory and bidirectional motion of these cargoes is thought to arise in part from the opposing forces of these motors (Hendricks et al., 2010; Muller et al., 2008; Soppina et al., 2009), or coordination of the activity of opposing motors (as reviewed (Gross, 2004)). Modeling of a tug-of-war between motors can result in either bidirectional movement or unidirectional runs with pauses depending on the properties of the motors (Muller et al., 2008).

Early endosomes are thought to contain many different types of motors with different polarities. We did not conclude that a tug-of-war is the best explanation for pauses in early endosomal motion during the pauses because the motion is in 2 dimensions, not one dimension along the MT axis, and covers enough distance to suggest it uses another MT for the next directed run. Although this is our working hypothesis, there are several assumptions made in this reasoning and more information is needed to understand the source of the motion we observed.

##### **4.2.1.1 Improve imaging resolution**

The argument against a tug-of-war during the pauses rests on the accuracy of the MSD analysis showing 2-dimensional diffusion. Additionally our MSD analysis is currently limited to evaluating motion over 2.25 s periods so shorter time periods containing distinct types of motion could be lost. In order to further validate our results and extend our analysis to shorter time periods, improving the spatial and temporal resolution of our tracking is necessary.

The use of a system with less mechanical noise and a faster camera would improve our spatial and temporal resolution and allow motion analysis over a smaller time window. These implementations would likely allow us to use the same experimental conditions with EGF-Qdots. Alternatively using EGF conjugated to gold for imaging using video enhanced DIC imaging (Fujiwara et al., 2002), or for tracking using a photodiode detector could provide marked increases in temporal and spatial resolution (25  $\mu$ s and 1.5 nm in (Nan et al., 2008)) and would prevent the loss of frames due to blinking of Qdots.

Additionally, we have been tracking 3 dimensional movement projected onto a 2 dimensional surface. Since we lose particles as they move out of the focal plane (for an 100x objective, NA 1.49, focal plane is  $\sim$  200 nm) we are not collapsing large z movements, but we are potentially altering motion on the scale of our resolution ( $\sim$ 20 nm) and we are ignoring all trajectories that leave the focal plane. The use of parallax imaging (Sun et al., 2009), a cylindrical lens to introduce astigmatism (Kao and Verkman,

1994) , or other 3 dimensional imaging systems could also be useful in improving spatial resolution.

#### **4.2.1.2 Linkage between cargo and motor**

Our interpretation that the cargo detaches during pauses due to the large area it explores assumes that the linkage between the endosome, which is what we are tracking, and the MT is smaller than the maximum distance traveled. If the cargo was attached to the MT via an extended adaptor protein, linked to dynactin, then linked to dynein, it could be several hundred nms away from the MT. In this scenario, if dynein is in rigor bound to the MT and the attached vesicle could move around on this long tether, we may not be able to detect confinement over short time periods. One study points to this type of tethering during pauses in transport (Gu et al., 2012). Endosomes containing an elongated gold rod coated with transferrin were tracked and the polarization of the rod was used to determine how the cargo was rotating during transport. During pauses in directed motion, the rod rotated, but not in 3 dimensions, only in 2. This motion was interpreted as confinement due to continued tethering to the MT. Future studies of cargo motion using other readouts like this type of polarization can aid in determining how cargo is moving. One caveat to many of these studies is that we are tracking an artificially large or oddly shaped cargo that is in a vesicle, potentially quite far from the site of the motor walking. However, studies of peroxisomes (Kural et al., 2005), melanosomes (Kural et al., 2007), and endosomal

compartments (Nan et al., 2008) at very high time resolution did reveal step-like advancement of the cargo matching known motor step sizes, indicating that the body of the cargo can read out what the motor is doing during active transport.

#### **4.2.1.3 Distinct classes of motion**

There appear to be differences between the motion of individual motile early endosomes, even within the same cell. I hypothesize that there are different types of motion before and after a run that are averaged in our current analysis. There is not currently enough data to look for distinct classes, but improving the imaging and analysis workflow to increase the dataset of motile trajectories would allow us to look for discrete types of events during pauses.

For example, imaging of the pause locations of GFP-Rab5 punctae relative to organelles and MT intersections has suggested that several interactions influence pausing. We would not necessarily expect all these interactions to lead to the same type of motion at the end of the run or during the pause. For example, in regions of the cell with well-defined MTs we observed endosomes moving back and forth between several different MTs that appear to intersect during a pause. This appears to be a case of a tug of war between MT motors, potentially dyneins engaged on different MTs, that lasts until the beginning of the next directed run. This particular case seems unlikely to be an event where the endosome detaches from the MT and undergoes 2 dimensional diffusion.

MSD analysis of bidirectional motion will look like diffusive scaling with a higher diffusion coefficient than the organelle would experience without active motion. If we collect a large enough set of data, we may be able to separate this type of motion based on differences in diffusion coefficient.

The development of different classes to describe endosomal motion during pauses would be helpful for assessing how different perturbations affect early endosomal motion. In many cases, the assessment of how a particular protein affects transport is how quickly a cargo gets recycled or gets degraded in the lysosome when that protein is absent. Being able to see how classes of motion are differentially populated after a perturbation will allow us to focus on the mechanism by which different proteins affect cargo trafficking in early endosomes. Additionally, the endosomal system is robust and some perturbations to the system, such as depletion of clathrin machinery, result in cargo using different endocytic pathways and little discernable defects. More detailed analysis of shifts in motion would be useful in looking for changes in cargo routes in response to the loss of some machinery as well.

#### **4.2.2 Motion during pauses**

This thesis has focused on the role of cell organization on the location of pauses. Future studies should also follow up on understanding the coordination between the motors

present on early endosomes. As already discussed, identifying which motors are present together on individual early endosomes is key.

#### **4.2.2.1 Dynein's diverse motion repertoire**

##### **4.2.2.1.1 Dynein switches between diffusion and directed motion**

One alternative hypothesis is that the motile trajectories are an example of dynein switching between a directed and diffusive state. In vitro studies of purified dynein have shown it can undergo diffusion and directed motion in either direction (Mallik et al., 2005; Ross et al., 2006). Dynein interaction with Num1 in fission yeast is correlated with its switch from diffusive to directed motion (Ananthanarayanan et al., 2013).

Does a dynein binding partner determine the switch between directed runs and pauses?

Perhaps, but it is unlikely we could ever visualize a dynein interacting protein binding and unbinding to early endosomes in live cells. A more feasible alternative is to purify early endosomes and reconstitute their motility in vitro. In this system high concentrations of different dynein regulators can be added and changes in motility assessed. Previous studies using purified early endosomes in in vitro motility assays have mostly relied on pulsing cells with a labeled endocytic cargo, enriching for light vesicles, and visualizing the endosomes using the cargo signal (Bananis et al., 2003; Gorvel et al., 1991; Loubery et al., 2008; Nielsen et al., 1999). These studies saw bidirectional early endosomal motion, but could have contained other types of

endosomes. Reconstitution of motion matching early endosomal motion in cells would need to be demonstrated first.

#### **4.2.2.1.2 How does the dynein motor domain respond to the MT code?**

From the other perspective, how does dynein movement as a single molecule inside mammalian cells compare to the movement of early endosomes?

In vivo tracking of motors that lack the ability to bind cargo has been done with kinesin (Courty et al., 2006) and myosin (Nelson et al., 2009; Pierobon et al., 2009), but not for dynein. Since yeast dynein dimers created with artificial dimerization domains that remove endogenous cargo binding sites are motile in vitro, with similar stepping behavior to endogenously purified dynein (DeWitt et al., 2012; Reck-Peterson et al., 2006), this strategy could be used to generate a mammalian dynein unable to attach to cargo in cells. An alternative strategy is to add labeled dynein to extracted cytoskeletons (Brawley and Rock, 2009). This would allow use of endogenously purified dynein and remove potential cellular binding partners. However, the cytoskeletal dynamics and 3D spatial organization will be lost during extraction. Additional information on how dynein motion alone compares to early endosomal motion will be necessary to understand the source of the directed runs and pauses.

#### **4.2.2.2 Spatial organization of motors on cargo**

The spatial organization of motors on a cargo affects its motion (Erickson et al., 2011). Understanding how many motors are on an early endosome and how they are spatially arranged can be used to distinguish between causes for pauses at MT intersections. For example, if all motors are clustered near the MT being used for transport, it is unlikely that motors will engage other nearby MTs during transport. Since we see MT switching and MT buckling as endosome pass, this suggests there are some active motors scattered around the surface of the endosome. However, EM studies have previously shown cross bridges between vesicles and cytoskeletal filaments accumulated mainly near the filaments (Ashkin et al., 1990; Miller and Lasek, 1985).

Since early endosomes are near the diffraction limit of light microscopy, the mobility of motors on the endosomal surface using standard imaging techniques is not feasible. A technical advance in studying the mobility of membrane attached proteins in small areas has been made recently by combining fluorescence correlation spectroscopy (FCS) with STED (Mueller et al., 2013). FCS volumes alone would encompass the whole early endosome, but STED illumination can be limited to 20 nm (Fabian Gottfert, 2013) , perhaps allowing us to probe fluorescently-labeled motor mobility and clustering on isolated early endosomes. A strategy to immobilize organelles using affinity purification on a glass coverslip for single molecule imaging has been demonstrated to work for mitochondrial purification (SimPull (Jain et al., 2011)) and could be extended to purify early endosomes for FCS-STED analysis.

#### **4.2.2.3 Number of motors engaged in force production**

Counting the number of motors on an endosome does not tell us how many motors are actively engaged in generating force. The use of optical trapping in live cells has been used to measure the force a cargo can generate for comparison to the known motor stall forces *in vitro*. The first organelles optically trapped *in vivo* were in the giant amoeba *Reticulomyxa* (Ashkin et al., 1990) followed by lipid droplets in *Drosophila* (Shubeita et al., 2008). Recently several groups have examined the force generated by phagocytosed beads, which allows introduction of materials with a higher refractive index well-suited for optical trapping into endogenous organelles (Blehm et al., 2013; Hendricks et al., 2012a; Rai et al., 2013). Since early stages of phagosome maturation also contain Rab5, analysis of phagosome-generated forces at early times after internalization will be a useful first step in understanding how much force is generated on Rab5-positive compartments.

#### **4.2.2.4 KIF16b**

Finally, there is one candidate plus-end directed kinesin that we can visualize in live cells to gain insight into whether or not it is present at a time and place on early endosomes when it could engage in a tug-of-war with dynein to induce pausing in directed transport. Preliminary *in vitro* experiments demonstrated that it could move processively in an ensemble (Hoepfner et al., 2005), but little is known about its

mechanical properties so it is difficult to explain why it would be highly localized to an endosomal compartment that only exhibits directed motion towards the MT minus end unless its activity is regulated.

#### **4.2.2.4.1 In vitro characterization**

KIF16b has been successfully purified and used for ensemble motility assays in vitro (Hoepfner et al., 2005). Purification and characterization of the mechanical properties of KIF16b will provide some insight into how it would affect dynein motility. Additionally, studying the effects of combining purified dynein and KIF16b on the same cargo in vitro can be used as a comparison to early endosome motility.

#### **4.2.2.4.2 Preliminary in vivo characterization**

In previous studies, KIF16b was shown to affect transferrin recycling (Hoepfner et al., 2005), suggesting that it might assist in sorting cargo and transporting it from early endosomes to recycling endosomes.

Preliminary experiments demonstrate KIF16b is highly enriched on Rab5 positive early endosomes (Figure 1). To address whether or not KIF16b could generate MT plus-end directed movement of early endosomes, we overexpressed KIF16b in cells. KIF16b overexpression resulted in clustering of early endosomes in the cell periphery (Figure 1), indicating that it is capable of moving early endosomes towards the plus ends of MTs or

interfering with dynein activity. This is somewhat surprising since when dynein is inhibited, there is not any aggregation of early endosomes near cell edges. Lysosomes, which do exhibit bidirectional motility normally, collect in the cell periphery when dynein is inhibited (Caviston et al., 2011; Yi et al., 2011).

In some early endosomes we observed faint tubular-looking extensions containing KIF16b from early endosomes. To obtain better spatial resolution, we used overexpression of mCherry-Rab5 to generate enlarged early endosomes (Skjeldal et al., 2012). We found that KIF16b had a patchy distribution on the body of early endosomes and that its intensity inversely correlated with Rab5 intensity (Figure 2). This patchiness has been seen for other PI(3)P binding proteins (Hu et al., 2002). Strikingly, KIF16b was also present on tubules that were continuously being formed on the Rab5 endosome, undergoing fission, and being rapidly moved towards the cell periphery (Figure 3). These tubules were for the most part Rab5 negative and we speculate that they are recycling compartments based on the previous studies implicating KIF16b in transferrin recycling, and more recently in Rab11-mediated transcytosis (Perez Bay et al., 2013).

Longer term imaging of the Rab5 positive endosomes containing KIF16b tubules revealed a potential way to reconcile why there is not bidirectional motion of early endosomes normally, but overexpression of KIF16b over long periods leads to accumulation of early endosomes in the cell periphery. As a new tubule grew out of the endosome, the body of the endosome slowly followed (Figure 4). When a tubule grew

out of the endosome in a different direction, it was slightly pulled that way. Since the tubules are presumably driven by KIF16b, a plus-end directed motor, the excessive tubule formation likely drags the body of the endosome slowly towards the edge of the cell until fission of the tubule occurs. Under normal expression levels of KIF16b, there likely is not enough tubule formation to move the endosome body. However, it remains unclear why KIF16b is highly concentrated on the body of the early endosome but appears to be mainly active in the extending tubules.

#### **4.2.2.4.3 Future directions**

I propose a model in which spatial segregation of dynein motor activity on the body of the early endosome and KIF16b activity on tubular extensions containing recycling cargo prevent a tug-of-war between the two motors. KIF16b has been shown to interact with GTP-Rab14 *in vitro*, indicating it may have other binding partners that may be necessary to activate its motor activity on subdomains of early endosomes (Ueno et al., 2011).

The movement of the body of the early endosome when tubulation was upregulated by KIF16b overexpression also suggests a potential role for myosins on early endosomes. Since several of the myosin isoforms found on early endosomes have been proposed to act as tethers (Provance et al., 2008; Raposo et al., 1999), their role may be to anchor the body of the early endosome during KIF16b-mediated tubule extension. Further

work assessing when motors are present on the same early endosomes is needed to know if myosin 1b or myosin Vb could be serving as anchors against KIF16b activity.

### **4.3. What are the benefits of saltatory motion for early endosomes and other organelles?**

#### **4.3.1 Sorting**

Is saltatory motion a mere consequence of the crowded cellular environment or does it functionally contribute to some aspects of endosomal function or maturation?

In this study we investigated the hypothesis that saltatory motion could contribute to sorting in early endosomes. We observed deformation and fission of vesicles during pauses in motion. We hypothesize that motor activity on Rab5 positive endosomes is tuned to be near stalling so that the endosomal membrane can be placed under tension during transport. Since fission of transferrin positive vesicles away from EGF containing endosomes was observed, we speculate that this tension can facilitate the fissions necessary for cargo sorting for recycling or transport to the Golgi.

#### **4.3.2 Facilitating membrane sculpting**

During pauses and resumption of directed trafficking, the motors may deform the membrane cyclically. In many electron micrographs of vesicles with cross bridges

attached to the MTs the vesicle is elongated along the MT (Hirokawa, 1998; Miller and Lasek, 1985), suggesting that during trafficking the membrane may be deformed. Most sorting events involve proteins with membrane sculpting or curvature recognition domains (Elia et al., 2011; Galic et al., 2012; Shimada et al., 2007) that take advantage of fluctuations in normal membrane curvature to bind and stabilize their preferred curvature. For example, the SNX-BAR family of sorting nexins is involved in endosomal sorting (van Weering et al., 2012). Putting the membrane under cycles of tension and relaxation may allow endosomal membranes to sample different curvatures at a higher frequency and facilitate binding of curvature sensing proteins. One piece of experimental cell data that fits with this line of thought, is that dynein is needed for efficient sorting of receptors in the early endosome (Driskell et al., 2007).

In vitro, changing the membrane curvature affects binding of curvature sensing proteins (Capraro et al., 2010; Ramesh et al., 2013). Altering this experimental approach to cyclically deform lipid vesicles could explore whether membrane deformation enhances recruitment or tubulation driven by curvature sensing proteins. Since their preferred curvature will not always be present, the constant movement could be hypothesized to inhibit binding. However, many of these proteins oligomerize into higher order structures (Frost et al., 2008) and form domains with local changes in curvature to allow budding or invagination, so increasing the initial binding/nucleation event may be sufficient to enhance oligomerization of curvature sensing proteins.

### 4.3.3 Decreasing search time

Early endosomes undergo homotypic fusion and get larger as they mature and are transported towards the perinuclear region (Simonsen et al., 1998). If we assume that fusion of early endosomes is necessary for normal function, then the chances of two early endosomes finding each other to fuse will affect their maturation or function. Uninterrupted dynein-driven transport of an early endosomes from the plasma membrane to the center of the cell would only take a few seconds and would not give endosomes much opportunity to contact each other.

There are different types of random walks with features that make them optimal for different types of movement (Codling et al., 2008). The Levy flight is a type of random walk where the distribution of step sizes has a heavy tail, or population of very large step sizes. This leads to a random walk containing regions where large distances are covered. The Levy flight is studied as an effective random search strategy and has been applied to explain patterns of animal foraging behavior (Humphries et al., 2012) and more recently the migration of T-cells in the brain searching for a pathogen (Harris et al., 2012). In the motile trajectories, the distribution of step sizes does have a large tail. However, the methods for determining whether a dataset is described by a Levy flight are beyond the scope of my knowledge. Determining if there is a model that describes the saltatory endosomal motion could be useful for hypothesis generation if the model has known benefits, such as the Levy flight's optimal search time.

#### **4.4 Relevance to the transport of other cargos and organelles**

Is this study of early endosomal motion relevant to other cargoes and organelles? Most long-distance transport is MT-based so MT intersections and local changes in MT density are likely to affect many cargos undergoing long distance transport. In addition, many organelles make contacts with the ER so understanding how the ER affects motility is applicable to the nucleus, early endosomes, lysosomes, the Golgi, peroxisomes, autophagosomes, and mitochondria. Other types of organelle-organelle contacts such as the one observed between different Rab5 positive early endosomes in this study will likely be organelle-specific.

##### **4.4.1 MT intersections**

Several studies indicate that trafficking cargo can switch MTs during transport. TrkA-positive endosomes labeled with NGF-Qdots exhibited lateral displacements suggestive of MT track switching during transport in axons (Mudrakola et al., 2009). In COS-7 cells, peroxisomes induced to accumulate dynein were shown to switch between MTs, although this is not a normal cargo/motor setup (Kapitein et al., 2010).

Finally, a very elegant study using live-cell imaging of lysosomal trafficking followed by correlative 3D super-resolution (STORM) imaging of the MTs provided new insight in the constraints MT organization places on organelle motility (Balint et al., 2013). The authors found that lysosomes that reached a MT intersection could pass, pause, or

switch MTs. However, nearly all lysosomal pauses occurred when the MTs were less than 300 nm apart in z. Since lysosomes can be larger than 300 nm in diameter, a more careful examination of lysosome height would be useful to know if the z requirement stems from the lysosome needing to contact the upper MT to allow a motor to engage on the upper MT, or whether 300 nm is the cutoff at which a lysosome cannot squeeze under an intersecting MT.

As improvements in rapid STORM and SIM techniques continue, live super-resolution imaging of MTs relative to cargo movements will be helpful in determining how MT intersections contribute to pauses in transport.

#### **4.4.2 Organelle-organelle interactions**

I hypothesize organelle interactions with each other would be organelle-specific. However, I propose that altering the organelle lipid composition, in particular by changing the type of PIPs, is a general mechanism to regulate motors on an organelle in trans. This is a very speculative hypothesis, but the large literature on PIPs regulating organelle identity, and the recent flux in papers on organelle-organelle contacts suggest this mechanism is worth exploring (Di Paolo and De Camilli, 2006).

Since PIPs are generated by kinase activity, and removed by phosphatase activity, very rapid shifts in concentration can occur specifically on the membrane without the need for transport. Depletion of the parent lipid can occur under high stimulation conditions

(Kim et al., 2011), but these are unlikely to be physiological. PIPs are often affected by signaling pathways, so using them to affect motors is a way of coupling motility to signaling. In fact, lipid levels are more sensitive than mRNA transcript or protein level changes for inflammatory signaling (Tam et al., 2013).

There are several examples of lipids on a neighboring organelle affecting motor attachment on another organelle. On the lysosome, dynactin attachment is regulated by the levels of cholesterol in the ER (Rocha et al., 2009). Dynein is attached to retromer vesicles via an interaction between dynactin and SNX6 is disrupted by PI4P on the Golgi membranes (Niu et al., 2013). Importantly, these interactions have been demonstrated using in vitro mixtures of proteins and lipids. This suggests that the ability of PIPs to alter organelle movement can be tested on purified organelles in vitro.

#### **4.5 A potential role for the ER in regulating transport?**

This study demonstrated that contacts between the early endosome and the ER are not merely static binding events. As early endosomes move, the attached ER gets dramatically rearranged. This result raises several questions. What is connecting the two organelles? What is the effect of this attachment on endosome trafficking? What is the effect of endosome movement on ER structure? Does this type of coordinated movement and rapid ER deformation occur with other ER-organelle interactions? In

order to address these questions, future studies are needed to determine the proteins mediating attachment and the mechanics of the ER in vivo.

#### **4.5.1 Introduction to the ER**

The endoplasmic reticulum is involved in a diverse set of functions in the cell. It forms the nuclear envelope (Wandke and Kutay, 2013), synthesizes lipids (Fagone and Jackowski, 2009), is a major site of protein synthesis and folding (Araki and Nagata, 2012), sorts proteins for export to their proper locations in the cell (Watanabe and Riezman, 2004), and stores calcium (Berridge, 2002).

##### **4.5.1.1 ER membrane contact sites**

The ER works in conjunction with other organelles to carry out these functions. Instead of using vesicular transport of material between organelles, close contact between the ER membrane and the membrane of the coordinating organelle is involved in the processes listed above (4.5.1). These membrane contact sites (MCSs) are defined at the ultrastructural level by the two membranes being separated by less than 30 nm (Elbaz and Schuldiner, 2011).

Two of the most studied ER MCSs are with mitochondria and the plasma membrane. These mediate lipid synthesis and store-operated calcium re-entry. However, several

studies indicate these MCSs play several different roles, some of which involve organization of domains on organelles or in the cell.

In addition to lipid metabolism, the contact between the ER and the mitochondria is involved in organizing and constricting sites of mitochondrial division (Friedman et al., 2011; Korobova et al., 2013). At PM-ER MCSs, a number of proteins are enriched, such as VAMP (vesicle-associated membrane-associated)-associated protein A (VAPA). VAPA mutations were recently identified as a suppressor of a mutation in fission yeast that causes abnormally slow clustering of actin foci into a cytokinetic ring. The lack of VAPA was hypothesized to rescue this defect by removing ER barriers to these clusters congressing. Creation of an artificially high amount of ER-PM contacts inhibited WT cytokinetic ring formation, leading the authors to speculate that the ER takes on a tubular morphology to prevent large physical barriers from forming (Zhang et al., 2012). The early endosome-ER contact was previously known to mediate PTP1B interaction with EGFR (Haj et al., 2002), but may also serve a role in regulating motility.

#### **4.5.1.2 ER structure and maintenance**

The endoplasmic reticulum adopts two general shapes, sheet-like domains, and tubular domains, both thin in diameter, distributed throughout the entire volume of the cell, and undergoing continual rearrangement while maintaining a common lumen (Shibata et al., 2006). The tubular ER, the focus in this study, is distributed through at least 3

mechanisms (Waterman-Storer and Salmon, 1998). The ER can be stably attached to a MT and undergo retrograde flow with the cytoskeleton. The plus-tips of newly growing MTs can attach to the ER and pull ER tubules as the MT grows, a process requiring EB3 and STIM1 (Grigoriev et al., 2008). Or molecular motors can drive extension of ER tubules (Wozniak et al., 2009). This is primarily dependent on MT motors, but myosin V can also extend ER tubules (Wagner et al., 2011). Maintenance of the ER tubular morphology also requires curvature stabilizing proteins (reticulon proteins (Voeltz et al., 2006)), anastomosis of new tubules (Alastin GTPases (Moss et al., 2011)), and attachment to the MTs (CLIMP-63, (Klopfenstein et al., 1998)). In summary, at least two things are needed for ER tubular structure, force dependent extension of ER tubules and stabilization of the resulting tubular structure.

#### **4.5.2 Future Directions**

##### **4.5.2.1 Is ER deformation by organelles a common effect of MCSs?**

The movement of the tubular ER relative to several other organelles was investigated using simultaneous 2-color live-cell imaging at 20 fps in Arpe-19 cells. We observed little association between the cis-Golgi marker GPP1 and the ER in the tubular network that we can visualize in the edge of the cell. Mitochondria colocalized extensively with the ER, as previously reported. Mitochondrial movements were slower than early endosomes and the extension speed of newly growing ER tubules. However, when

small, rapidly moving mitochondria were observed, they did deform the ER during their movement.

Lysosomes had extensive colocalization with the ER (> 90%), which was statistically significant in comparison to randomly chosen locations, and higher than the overlap between early endosomes and the ER (Figure 5A). In addition, lysosomal movements are rapid and bidirectional, caused dramatic remodeling of the ER and new tubule formation (Figure 5C). To test that connections between the late endosomes/lysosomes and the ER were not a result of overexpression of the GTPase Rab7, we confirmed these results using the transmembrane resident late endosomal/lysosome protein Lamp1, the dye LysoTracker Red, and endocytosed TMR-dextran that was chased for 24 hours to allow accumulation only in lysosomes.

Similar reports of colocalization between the ER and lysosomes were published in the past year (Friedman et al., 2013; Kilpatrick et al., 2013; Sivaramakrishnan et al., 2012). Additionally, at the ultrastructural level, in both thin section EM (Kilpatrick et al., 2013) and high pressure frozen cryo-electron tomography of mammalian cells (Friedman et al., 2013), membrane contact sites between the ER and lysosomes were observed. The EM studies indicate that the colocalization in light microscopy studies are MCSs and that fusion between the two organelle membranes is not occurring. The lysosomal-ER contacts play a role in mediating bidirectional calcium signaling between the two organelles (Morgan et al., 2013).

We previously asked if the presence of the ER correlated with changes in early endosomal motion. To test the hypothesis that the newly growing ER tubules that have an endosome (early and/or late) leading the way behave differently than ER tubules without an endosome, we investigated the speed of ER extension and the fate of new extensions.

Although the motors on endosomes and the ER could be the same, if the motors are on a different type of cargo with other scaffolds or regulatory factors, motion could be affected. However, for both early and late endosomes, there was not difference in extension speeds (Figure 5B).

Roughly half of new ER tubules in Arpe-19 cells had a lysosome associated with them. The fate of new ER tubules can be divided into 3 categories visually: (1) ER tubules abruptly retract (2) ER tubules contact another region of ER and then retract back (3) ER tubules contact another ER region and remain stable and perhaps merge with the network. Looking at pictures of growing ER tubules, the tip is often thinner than the bulk of the tubule, suggesting it is getting stretched and covers a small area. The lysosome in contrast is large globular vesicular structure, capable of spanning an area containing multiple MTs. Since the lysosomal connection increases the area that a motor could attach to a MT, we hypothesized that the number of retraction events in lysosome-associated ER tubules would be reduced.

We scored the fate of all growing ER tubules in 5 cells and retrospectively looked for the presence of a lysosome at the tip. We found a 2 fold increase in the percentage of ER tubules that contacted another ER tubule and remained stable, and very few ER tubules that spontaneously retracted. This suggests lysosome-ER attachments may stabilize ER extensions. This could be important for maintenance of the ER structure, especially in large cell types like neurons. However, this observation reflects only 5 cells and should be repeated.

We extended these studies to other cell types to see if these endosomal-ER connections were conserved. We observed early endosome and late endosome/lysosome connections to the ER that were associated with ER deformation and tubulation in COS-7 and HeLa cells. However, in COS-7 cells, which have an easily visible reticular ER and contain many dynamic ER tubules, we found that lysosomes were found on <<50% of new ER extensions, indicating there are differences in the usage of ER distribution mechanisms between cell types. This is perhaps not surprising since cell type-specific differences in the MT motors used for ER distribution have been found, leading to the idea that dynein was not even involved in ER transport until a few years ago (Wozniak et al., 2009). In COS-7 cells, another Rab protein, Rab10, which has previously been found associated with post-Golgi carriers (Liu et al., 2013) and Glut4 containing vesicles (Chen et al., 2012), was found to associate with the ER and be enriched in the tips of growing ER tubules (English and Voeltz, 2013). These tips excluded normal ER markers like Sec61 $\beta$ , but the authors hypothesized these Rab10 areas are a specialized ER domain

and not a MCS. Future investigation of different modes of ER distribution across cell types and under different stress conditions will likely be necessary to understand the role of each type of ER attachment.

#### **4.5.2.2 What is the connecting complex?**

Visualization of the connection between early endosomes and the ER and between lysosomes and the ER using TEM has revealed that protein fibrils bridge the two organelles (Eden et al., 2010; Kilpatrick et al., 2013). PTP1B was found in early endosome-ER MCSs using immuno-EM, but it was not required for the contact to form (Eden et al., 2010). Similarly the contact between the mitochondria and the ER contains protein fibrils of unknown composition, although many proteins involved in the contact are known (Kornmann et al., 2009).

We tested for enrichment of several ER proteins involved in MSCs at either early endosome-ER contacts or ER-lysosome contacts, but did not find any enrichment of PTP1B, STIM1, or VAPA. Although, we should note that the enrichment of these proteins at MCSs was previously visualized using FRET (PTP1B (Haj et al., 2002)), in punctae near calcium bursts (STIM1 (Nunes et al., 2012)), or in the same region of fixed cells (VAPA (Rocha et al., 2009)), indicating a clear enrichment does not rule out these proteins' involvement.

A biochemical approach to identify proteins at ER MCSs may be feasible using new biotinylation labeling strategies targeted to subcellular compartments (Rhee et al., 2013; Roux et al., 2012). Since prior work has shown PTP1B is found in early endosome-ER contacts, PTP1B can be used to target a promiscuous biotin ligase to these sites. Subsequent fraction of the cells to enrich for ER membranes followed by purification and identification of biotinylated ER proteins may provide candidates for this MCSs linkage. Investigating this contact in live cells will be interesting because the two organelles are mobile relative to each other, yet maintain contact for long times.

#### **4.5.2.3 How do the mechanical properties of the ER affect endosome/lysosome movement?**

Based on the correlation between early endosomal pause sites and the deformation of the ER during endosome movement, we hypothesized that the force to deform the ER may affect the motors moving the early endosomes. In order to know if this tension would impact motors on early endosomes or lysosomes, we need to know (1) how much force the motors on the endosomes can generate and (2) how much force it takes to deform the ER.

Bilayers deform easily because lipids can flow within them. However, in comparison to a model bilayer of pure lipid, the ER contains many transmembrane proteins and cholesterol, which are known to rigidify membranes. One in vitro study directly

measured the force required to hold a static ER tether in an optical trap. This force was ~20 pN at room temperature, and was significantly higher than the force required to hold a tether made from Golgi membranes, indicating that the ER is on the rigid spectrum of intracellular membranes (Upadhyaya and Sheetz, 2004). However, temperature, the size of the attachment site on the membrane (Koster et al., 2005), and the presence of curvature stabilizing proteins would all be expected to affect the force to extend an ER tubule in the cell.

In vitro, the ability to pull tubules from a bilayer GUV required multiple kinesin-1 motors (6 pN of force each, subadditive stall force) suggesting higher forces are required (Koster et al., 2003). However, multiple kinesins may also be acting to stabilize the tubule along its length, a process that in the cell could be done by non-motor proteins.

The ER has not been characterized mechanically in the cell. The use of a similar optical trap setup in live cells to measure the force to pull an ER tubule would be ideal. Adam Hendricks in the Goldman and Holzbaur lab has demonstrated that beads phagocytosed by Arpe-19 cells moved along the ER, similar to phagosomes in macrophages, and is able to optically trap beads in these cells, suggesting it may be possible to measure this directly. However, moving a large bead/phagosome through the cell with the optical trap will likely be resisted not only by the ER but also the surrounding cytoskeletal structures, making it challenging to isolate the ER contribution.

Another way of estimating the force required to deform the ER in cells is to compare other causes of ER deformation. The ER is attached to growing MTs in cells and can be extended as they grow. The force-velocity relationship for MT growth has been measured in vitro (Dogterom and Yurke, 1997). MTs stop growing nearly completely with the application of 4 pN of force. Measurements of the speed of growing MT plus-tips in cells showed no significant difference between the speed of plus-tips with associated ER tubules and those without ER (Grigoriev et al., 2008). If MT growth stalls under 4 pN in the cell, this would suggest deforming the ER takes less than 4 pN. However, in the cell there are many MT binding proteins at the plus-tip that change polymerization speeds and whose effects on the force-velocity relationship are unknown. In addition, the amount of force it takes to deform a membrane depends on the rate it is pulled. Since early endosomes and lysosomes extend the ER 10 fold faster than MTs grow, the force required would be expected to be higher.

One way to address how the ER affects the motility of motor-driven cargoes, is to reconstitute a reduced complexity system in vitro. Purification of ER membranes and reconstitution of ER motility in vitro has been done for several decades (Vale and Hotani, 1988). To test the hypothesis that the ER would impede the movement of a model cargo, a bead coated with different numbers of motors could be placed on a MT using an optical trap and its speed measured before and after contact with the ER network. Additionally complexity could be added to the system by creating an artificial attachment between the ER and beads (Upadhyaya and Sheetz, 2004), or by purifying

an organelle that natively attaches to the ER like latex bead derived phagosomes (Nunes et al., 2012). Comparison of beads transported by either dynein or kinesin-1 will be informative since dynein has properties including backwards stepping and becoming a gear under load, that we hypothesized may allow it to maintain attachment to MTs under tension better than kinesin-1.

#### **4.5.2.4 How does organelle- driven movement affect the ER?**

In Arpe-19 cells, a large number of ER tubules are associated with EE or LE/L. Are these connections playing an important role in the structure of the ER or just byproducts of the connection? The mechanism of attachment of motor to the ER is unknown, leaving open the possibility that motor attachments are indirect through other organelles or specialized ER domains devoid of normal ER proteins (English and Voeltz, 2013). In vitro, purified ER membranes can form a network on MTs in the presence of ATP, suggesting that the ER alone contains the motors necessary to move it. However, it is important to note that ER “purification” or “enrichment” involves vesiculating the ER and collecting fractions based on the density of the membranes. Contamination of these preps with lysosomal and endosomal proteins is seen biochemically. Imaging of ER motility in vitro indicated globular domains enriched in secretory proteins collected at the tip of new ER tubules (Allan and Vale, 1994; Waterman-Storer et al., 1995). Therefore, it remains possible that organelles with their associated motors co-purify with the ER.

Speculatively, why would organelle movements along ER benefit the ER? It would provide early endosomes and late endosomes/lysosomes, which are involved in signaling and trafficking decisions, a method to integrate signaling with the ER. Structurally, it may maintain the ER tubular integrity as preliminary data indicated tubules associated with lysosomes are more stable. Finally, organelle movement while attached to the ER presumably moves the contact site through the ER membrane. Many of the proteins involved in ER bridging interactions, between ER sheets or with MTs, form low affinity interactions. However, overexpression of these proteins in cells lead to massive crystalline arrays of packed ER membranes (Gong et al., 1996; Korkhov and Zuber, 2009; Ohkuma et al., 1995; Park et al., 2010; Profant et al., 1999; Renvoise and Blackstone, 2010; Sandig et al., 1999; Shibata et al., 2008; Snapp et al., 2003; Takei et al., 1994; Vergeres et al., 1993; Volkova et al., 2012; Yamamoto et al., 1996). The constant movement of domains through the ER may mitigate this tendency to oligomerize, particularly in post-mitotic cells.

Mutations in several ER proteins (VAPA, reticulons, REEP) are associated with neurodegenerative diseases (Park et al., 2010). Since the ER has many functions it is difficult to point to the mechanism of disease, but the fact that these proteins all are required to maintain the tubular structure of the ER suggests (1) ER tubular structure is important for its function (2) and the late-onset of these diseases in neuronal cells indicates that only subtle changes in cell health may be induced by ER structural defects and will require very careful observation.

#### 4.6 Figures

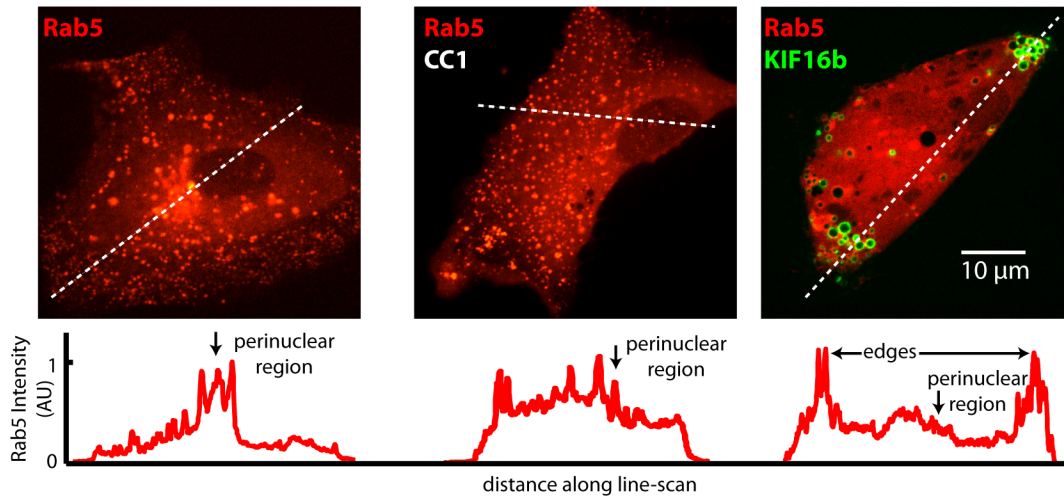


Figure 1. Rab5-positive early endosomal positioning depends on dynein/dynactin and KIF16b.

Arpe-19 cells were transiently transfected with mCherry-Rab5 and either mCherry-CC1 or mCitrine-KIF16b. A line scan (dotted white line) from the cell edges through the cell nucleus demonstrates that the Rab5 intensity is highest in the perinuclear region in control cells, mostly uniformly dispersed in CC1-expressing cells, and clustered in the cell periphery when KIF16b is overexpressed. This suggests that both dynein/dynactin and KIF16b can move early endosomes, but that in the absence of dynein/dynactin, normal levels of KIF16b are not sufficiently active to cluster the early endosomes in the cell periphery. Scale bar: 10 μm.

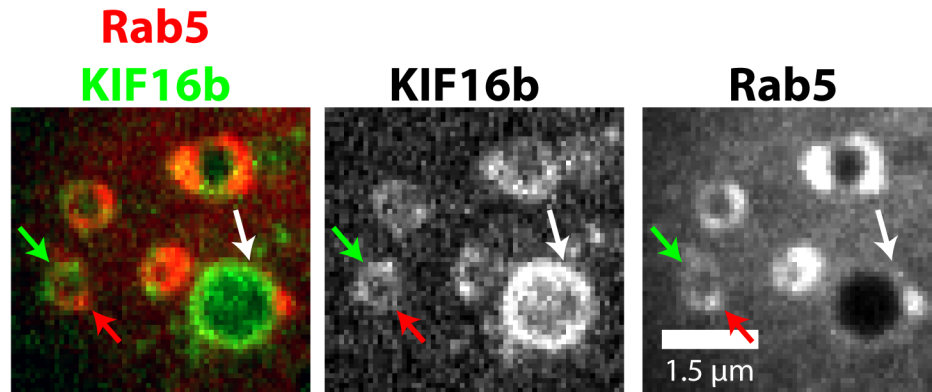


Figure 2. KIF16b localizes to a subset of Rab5-positive early endosomes, often in patches.

Arpe-19 cells transiently expressing mCherry-Rab5 and mCitrine-KIF16b were imaged with a spinning disc microscope. The green arrow indicates an enrichment of KIF16b on one side of an endosome and the red arrow indicates a high Rab5 level on the other side. The white arrow indicates an early endosome with high KIF16b levels but little Rab5. Scale bar: 1.5  $\mu\text{m}$ .

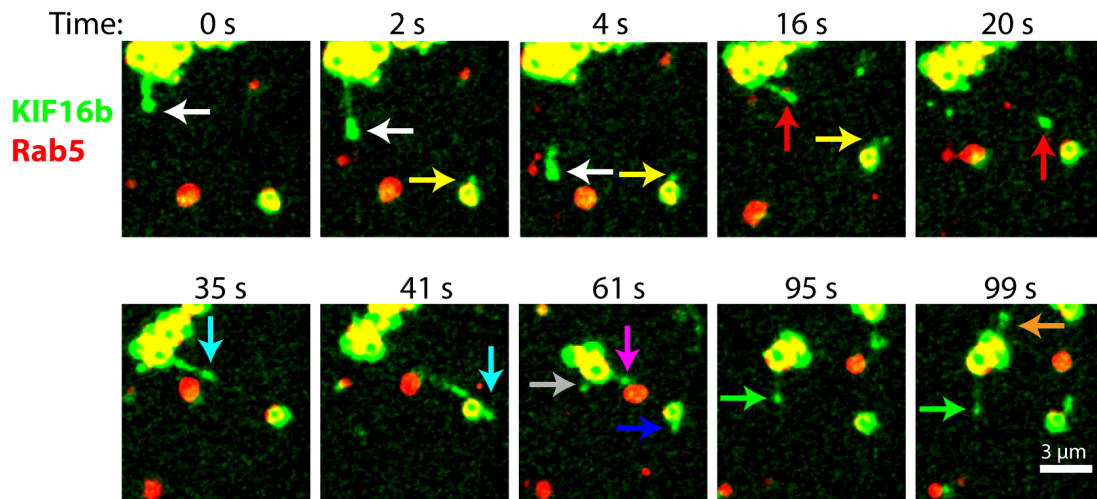


Figure 3. KIF16b continuously generates tubules that pinch off Rab5-positive early endosomes and travel rapidly towards the cell periphery.

Arpe-19 cells overexpressing mCitrine-KIF16b and mCherry-Rab5 were imaged with a spinning disc microscope. Each different color of arrow follows a different tubulation event. Scale bar: 3 μm.

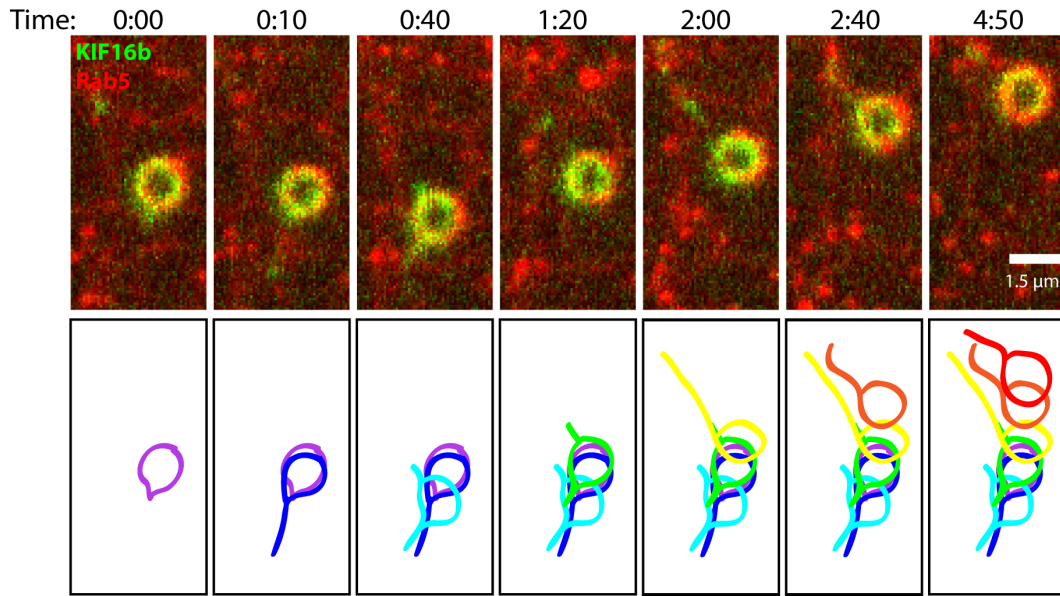


Figure 4. The growth of new KIF16b tubules moves the Rab5-positive endosome body with it.

Arpe-19 cells expressing mCherry-Rab5 and mCitrine-KIF16b were imaged with a spinning disc microscope. The montage shows a KIF16b-positive tube form and extend from the bottom of the endosome, moving the endosome with it. A new KIF16b-positive tubule then forms at the top of the endosome and moves it in that direction as the tubule extends. The outline of the endosome is drawn below each panel to highlight the length of the tubule and the position of the body of the endosome. Scale bar: 1.5 μm.

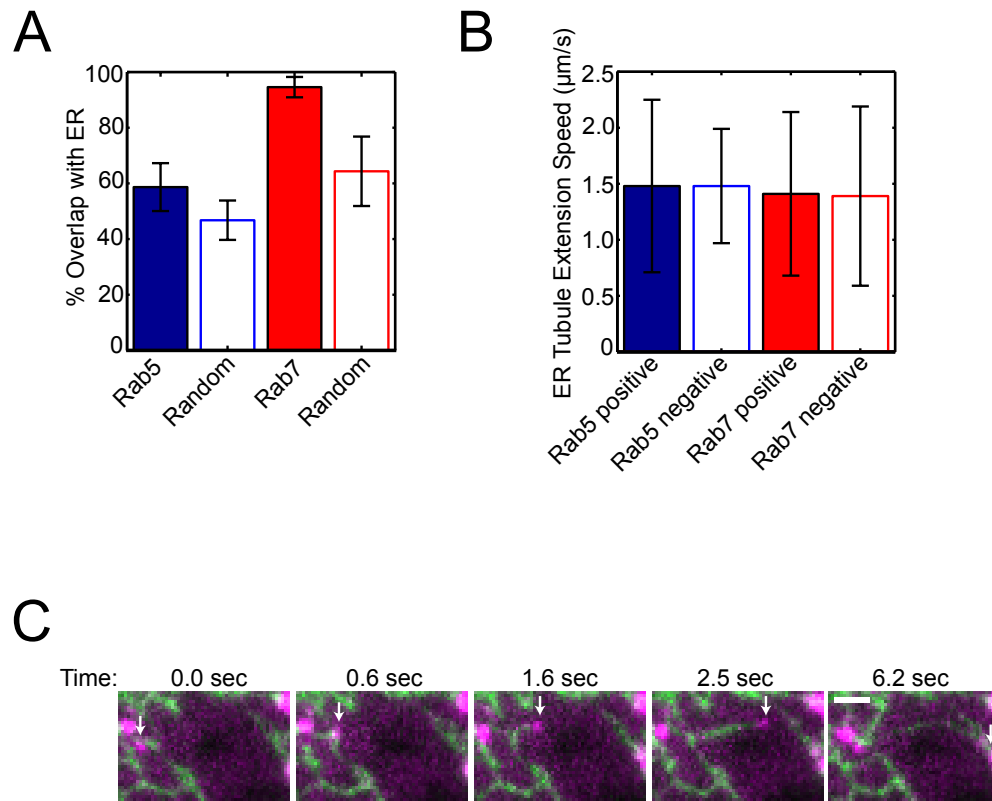


Figure 5. Nearly all late endosomes/lysosomes associate with the ER and deform the ER during movement.

- A. The overlap early endosomes (GFP-Rab5) and late endosomes/lysosomes (mCherry-Rab7) with Sec61 $\beta$ -labeled ER tubules was scored relative to randomly chosen locations. All Rab5 and Rab7 punctae were scored in 5 different frames of a time-lapse. 5 movies per condition were used. Mean  $\pm$  SEM.
- B. The speed of ER tubule extension was measured for all growing tubules in 5 cells per condition. The presence of Rab5 or Rab7 at the tip of the ER was scored

retrospectively and the speeds parsed based on the presence of absence of an endosome. N=5 cells. Mean  $\pm$  SEM.

- C. Time-lapse of an mCherry-Rab7 (magenta) positive late endosome/lysosome movement that correlates with buckling of the ER (GFP-Sec61 $\beta$ , green) at 0.6 sec, followed by extension of the ER and stable docking of the new ER tubule through the end of the movie. 2-color images were collected simultaneously using a Dual-View System (Photometrics). Scale bar: 2 $\mu$ m.

## Bibliography

- Abe, A., Saeki, K., Yasunaga, T., and Wakabayashi, T. (2000). Acetylation at the N-terminus of actin strengthens weak interaction between actin and myosin. *Biochemical and biophysical research communications* 268, 14-19.
- Akella, J.S., Wloga, D., Kim, J., Starostina, N.G., Lyons-Abbott, S., Morrisette, N.S., Dougan, S.T., Kipreos, E.T., and Gaertig, J. (2010). MEC-17 is an alpha-tubulin acetyltransferase. *Nature* 467, 218-222.
- Akin, O., and Mullins, R.D. (2008). Capping protein increases the rate of actin-based motility by promoting filament nucleation by the Arp2/3 complex. *Cell* 133, 841-851.
- Ali, M.Y., Kremntsova, E.B., Kennedy, G.G., Mahaffy, R., Pollard, T.D., Trybus, K.M., and Warshaw, D.M. (2007). Myosin Va maneuvers through actin intersections and diffuses along microtubules. *Proceedings of the National Academy of Sciences of the United States of America* 104, 4332-4336.
- Ali, M.Y., Lu, H., Bookwalter, C.S., Warshaw, D.M., and Trybus, K.M. (2008). Myosin V and Kinesin act as tethers to enhance each others' processivity. *Proceedings of the National Academy of Sciences of the United States of America* 105, 4691-4696.
- Allan, V., and Vale, R. (1994). Movement of membrane tubules along microtubules in vitro: evidence for specialised sites of motor attachment. *Journal of cell science* 107 ( Pt 7), 1885-1897.
- Allen, R.D., Metzuzals, J., Tasaki, I., Brady, S.T., and Gilbert, S.P. (1982). Fast axonal transport in squid giant axon. *Science* 218, 1127-1129.
- Altman, D., Goswami, D., Hasson, T., Spudich, J.A., and Mayor, S. (2007). Precise positioning of myosin VI on endocytic vesicles in vivo. *PLoS biology* 5, e210.
- Alushin, G., and Nogales, E. (2011). Visualizing kinetochore architecture. *Curr Opin Struct Biol* 21, 661-669.
- Ananthanarayanan, V., Schattat, M., Vogel, S.K., Krull, A., Pavin, N., and Tolic-Norrelykke, I.M. (2013). Dynein Motion Switches from Diffusive to Directed upon Cortical Anchoring. *Cell* 153, 1526-1536.
- Aniento, F., Emans, N., Griffiths, G., and Gruenberg, J. (1993). Cytoplasmic dynein-dependent vesicular transport from early to late endosomes. *The Journal of cell biology* 123, 1373-1387.
- Araki, K., and Nagata, K. (2012). Protein folding and quality control in the ER. *Cold Spring Harbor perspectives in biology* 4, a015438.
- Aschenbrenner, L., Lee, T., and Hasson, T. (2003). Myo6 facilitates the translocation of endocytic vesicles from cell peripheries. *Molecular biology of the cell* 14, 2728-2743.
- Aschenbrenner, L., Naccache, S.N., and Hasson, T. (2004). Uncoated endocytic vesicles require the unconventional myosin, Myo6, for rapid transport through actin barriers. *Molecular biology of the cell* 15, 2253-2263.
- Ashkin, A., Schutze, K., Dziedzic, J.M., Euteneuer, U., and Schliwa, M. (1990). Force generation of organelle transport measured in vivo by an infrared laser trap. *Nature* 348, 346-348.
- Baker, J.E., Kremntsova, E.B., Kennedy, G.G., Armstrong, A., Trybus, K.M., and Warshaw, D.M. (2004). Myosin V processivity: multiple kinetic pathways for head-to-

head coordination. *Proceedings of the National Academy of Sciences of the United States of America* *101*, 5542-5546.

Balint, S., Verdeny Vilanova, I., Sandoval Alvarez, A., and Lakadamyali, M. (2013). Correlative live-cell and superresolution microscopy reveals cargo transport dynamics at microtubule intersections. *Proceedings of the National Academy of Sciences of the United States of America* *110*, 3375-3380.

Bananis, E., Murray, J.W., Stockert, R.J., Satir, P., and Wolkoff, A.W. (2003). Regulation of early endocytic vesicle motility and fission in a reconstituted system. *Journal of cell science* *116*, 2749-2761.

Barlan, K., Lu, W., and Gelfand, V.I. (2013). The microtubule-binding protein ensconsin is an essential cofactor of kinesin-1. *Current biology : CB* *23*, 317-322.

Beeg, J., Klumpp, S., Dimova, R., Gracia, R.S., Unger, E., and Lipowsky, R. (2008). Transport of beads by several kinesin motors. *Biophysical journal* *94*, 532-541.

Berg, H.C. (1993). *Random walks in biology*, Expanded edn (Princeton, N.J.: Princeton University Press).

Berg, J.S., Powell, B.C., and Cheney, R.E. (2001). A millennial myosin census. *Molecular biology of the cell* *12*, 780-794.

Berridge, M.J. (2002). The endoplasmic reticulum: a multifunctional signaling organelle. *Cell calcium* *32*, 235-249.

Bicek, A.D., Tuzel, E., Demtchouk, A., Uppalapati, M., Hancock, W.O., Kroll, D.M., and Odde, D.J. (2009). Anterograde microtubule transport drives microtubule bending in LLC-PK1 epithelial cells. *Molecular biology of the cell* *20*, 2943-2953.

Blatner, N.R., Wilson, M.I., Lei, C., Hong, W., Murray, D., Williams, R.L., and Cho, W. (2007). The structural basis of novel endosome anchoring activity of KIF16B kinesin. *The EMBO journal* *26*, 3709-3719.

Blehm, B.H., Schroer, T.A., Trybus, K.M., Chemla, Y.R., and Selvin, P.R. (2013). In vivo optical trapping indicates kinesin's stall force is reduced by dynein during intracellular transport. *Proceedings of the National Academy of Sciences of the United States of America* *110*, 3381-3386.

Bloemink, M.J., and Geeves, M.A. (2011). Shaking the myosin family tree: biochemical kinetics defines four types of myosin motor. *Seminars in cell & developmental biology* *22*, 961-967.

Borisy, G.G., and Svitkina, T.M. (2000). Actin machinery: pushing the envelope. *Current opinion in cell biology* *12*, 104-112.

Bouzigues, C., and Dahan, M. (2007). Transient directed motions of GABA(A) receptors in growth cones detected by a speed correlation index. *Biophysical journal* *92*, 654-660.

Brady, S.T., Lasek, R.J., and Allen, R.D. (1982). Fast axonal transport in extruded axoplasm from squid giant axon. *Science* *218*, 1129-1131.

Brawley, C.M., and Rock, R.S. (2009). Unconventional myosin traffic in cells reveals a selective actin cytoskeleton. *Proceedings of the National Academy of Sciences of the United States of America* *106*, 9685-9690.

Brinkley, B.R. (1985). Microtubule organizing centers. *Annual review of cell biology* *1*, 145-172.

Buss, F., and Kendrick-Jones, J. (2011). Multifunctional myosin VI has a multitude of cargoes. *Proceedings of the National Academy of Sciences of the United States of America* *108*, 5927-5928.

Cai, D., McEwen, D.P., Martens, J.R., Meyhofer, E., and Verhey, K.J. (2009). Single molecule imaging reveals differences in microtubule track selection between Kinesin motors. *PLoS biology* *7*, e1000216.

Capraro, B.R., Yoon, Y., Cho, W., and Baumgart, T. (2010). Curvature sensing by the epsin N-terminal homology domain measured on cylindrical lipid membrane tethers. *Journal of the American Chemical Society* *132*, 1200-1201.

Carter, A.P., Cho, C., Jin, L., and Vale, R.D. (2011). Crystal structure of the dynein motor domain. *Science* *331*, 1159-1165.

Case, R.B., Rice, S., Hart, C.L., Ly, B., and Vale, R.D. (2000). Role of the kinesin neck linker and catalytic core in microtubule-based motility. *Current biology : CB* *10*, 157-160.

Caviston, J.P., and Holzbaur, E.L. (2009). Huntingtin as an essential integrator of intracellular vesicular trafficking. *Trends in cell biology* *19*, 147-155.

Caviston, J.P., Ross, J.L., Antony, S.M., Tokito, M., and Holzbaur, E.L. (2007). Huntingtin facilitates dynein/dynactin-mediated vesicle transport. *Proceedings of the National Academy of Sciences of the United States of America* *104*, 10045-10050.

Caviston, J.P., Zajac, A.L., Tokito, M., and Holzbaur, E.L. (2011). Huntingtin coordinates the dynein-mediated dynamic positioning of endosomes and lysosomes. *Molecular biology of the cell* *22*, 478-492.

Chang, L., Barlan, K., Chou, Y.H., Grin, B., Lakonishok, M., Serpinskaya, A.S., Shumaker, D.K., Herrmann, H., Gelfand, V.I., and Goldman, R.D. (2009). The dynamic properties of intermediate filaments during organelle transport. *Journal of cell science* *122*, 2914-2923.

Chen, Y., Wang, Y., Zhang, J., Deng, Y., Jiang, L., Song, E., Wu, X.S., Hammer, J.A., Xu, T., and Lippincott-Schwartz, J. (2012). Rab10 and myosin-Va mediate insulin-stimulated GLUT4 storage vesicle translocation in adipocytes. *The Journal of cell biology* *198*, 545-560.

Christoforidis, S., Miaczynska, M., Ashman, K., Wilm, M., Zhao, L., Yip, S.C., Waterfield, M.D., Backer, J.M., and Zerial, M. (1999). Phosphatidylinositol-3-OH kinases are Rab5 effectors. *Nature cell biology* *1*, 249-252.

Citri, A., and Yarden, Y. (2006). EGF-ERBB signalling: towards the systems level. *Nature reviews. Molecular cell biology* *7*, 505-516.

Clarke, M., and Spudich, J.A. (1974). Biochemical and structural studies of actomyosin-like proteins from non-muscle cells. Isolation and characterization of myosin from amoebae of *Dictyostelium discoideum*. *Journal of molecular biology* *86*, 209-222.

Clayton, J.E., Sammons, M.R., Stark, B.C., Hodges, A.R., and Lord, M. (2010). Differential regulation of unconventional fission yeast myosins via the actin track. *Current biology : CB* *20*, 1423-1431.

Clemen, A.E., Vilfan, M., Jaud, J., Zhang, J., Barmann, M., and Rief, M. (2005). Force-dependent stepping kinetics of myosin-V. *Biophysical journal* *88*, 4402-4410.

Codling, E.A., Plank, M.J., and Benhamou, S. (2008). Random walk models in biology. *Journal of the Royal Society, Interface / the Royal Society* 5, 813-834.

Cohen, S. (1962). Isolation of a mouse submaxillary gland protein accelerating incisor eruption and eyelid opening in the new-born animal. *The Journal of biological chemistry* 237, 1555-1562.

Cohen, S., and Carpenter, G. (1975). Human epidermal growth factor: isolation and chemical and biological properties. *Proceedings of the National Academy of Sciences of the United States of America* 72, 1317-1321.

Cohen, S., Carpenter, G., and King, L., Jr. (1980). Epidermal growth factor-receptor-protein kinase interactions. Co-purification of receptor and epidermal growth factor-enhanced phosphorylation activity. *The Journal of biological chemistry* 255, 4834-4842.

Cole, D.G., Chinn, S.W., Wedaman, K.P., Hall, K., Vuong, T., and Scholey, J.M. (1993). Novel heterotrimeric kinesin-related protein purified from sea urchin eggs. *Nature* 366, 268-270.

Collins, A., Warrington, A., Taylor, K.A., and Svitkina, T. (2011). Structural organization of the actin cytoskeleton at sites of clathrin-mediated endocytosis. *Current biology : CB* 21, 1167-1175.

Corti, B. (1774). *Osservazione Microscopiche sulla Tremella e sulla Circolazione del Fluido in Una Planto Acquaguola* (Lucca, Italy: Giuseppe Rocchi).

Courty, S., Luccardini, C., Bellaiche, Y., Cappello, G., and Dahan, M. (2006). Tracking individual kinesin motors in living cells using single quantum-dot imaging. *Nano letters* 6, 1491-1495.

Coy, D.L., Hancock, W.O., Wagenbach, M., and Howard, J. (1999). Kinesin's tail domain is an inhibitory regulator of the motor domain. *Nature cell biology* 1, 288-292.

Cullen, P.J., and Korswagen, H.C. (2012). Sorting nexins provide diversity for retromer-dependent trafficking events. *Nature cell biology* 14, 29-37.

De La Cruz, E.M., Ostap, E.M., and Sweeney, H.L. (2001). Kinetic mechanism and regulation of myosin VI. *The Journal of biological chemistry* 276, 32373-32381.

De La Cruz, E.M., Wells, A.L., Rosenfeld, S.S., Ostap, E.M., and Sweeney, H.L. (1999). The kinetic mechanism of myosin V. *Proceedings of the National Academy of Sciences of the United States of America* 96, 13726-13731.

Deacon, S.W., Nascimento, A., Serpinskaya, A.S., and Gelfand, V.I. (2005). Regulation of bidirectional melanosome transport by organelle bound MAP kinase. *Current biology : CB* 15, 459-463.

DeWitt, M.A., Chang, A.Y., Combs, P.A., and Yildiz, A. (2012). Cytoplasmic dynein moves through uncoordinated stepping of the AAA+ ring domains. *Science* 335, 221-225.

Dhomen, N.S., Mariadason, J., Tebbutt, N., and Scott, A.M. (2012). Therapeutic targeting of the epidermal growth factor receptor in human cancer. *Critical reviews in oncogenesis* 17, 31-50.

Di Paolo, G., and De Camilli, P. (2006). Phosphoinositides in cell regulation and membrane dynamics. *Nature* 443, 651-657.

- Dimitrov, A., Quesnoit, M., Moutel, S., Cantaloube, I., Pous, C., and Perez, F. (2008). Detection of GTP-tubulin conformation in vivo reveals a role for GTP remnants in microtubule rescues. *Science* 322, 1353-1356.
- Dixit, R., Ross, J.L., Goldman, Y.E., and Holzbaur, E.L. (2008). Differential regulation of dynein and kinesin motor proteins by tau. *Science* 319, 1086-1089.
- Dogterom, M., and Yurke, B. (1997). Measurement of the force-velocity relation for growing microtubules. *Science* 278, 856-860.
- Dominguez, R., and Holmes, K.C. (2011). Actin structure and function. *Annual review of biophysics* 40, 169-186.
- Dompierre, J.P., Godin, J.D., Charrin, B.C., Cordelieres, F.P., King, S.J., Humbert, S., and Saudou, F. (2007). Histone deacetylase 6 inhibition compensates for the transport deficit in Huntington's disease by increasing tubulin acetylation. *The Journal of neuroscience : the official journal of the Society for Neuroscience* 27, 3571-3583.
- Driskell, O.J., Mironov, A., Allan, V.J., and Woodman, P.G. (2007). Dynein is required for receptor sorting and the morphogenesis of early endosomes. *Nature cell biology* 9, 113-120.
- Droz, B., and Leblond, C.P. (1963). Axonal Migration of Proteins in the Central Nervous System and Peripheral Nerves as Shown by Radioautography. *The Journal of comparative neurology* 121, 325-346.
- Dunn, S., Morrison, E.E., Liverpool, T.B., Molina-Paris, C., Cross, R.A., Alonso, M.C., and Peckham, M. (2008). Differential trafficking of Kif5c on tyrosinated and detyrosinated microtubules in live cells. *Journal of cell science* 121, 1085-1095.
- Eden, E.R., Huang, F., Sorkin, A., and Futter, C.E. (2012). The role of EGF receptor ubiquitination in regulating its intracellular traffic. *Traffic* 13, 329-337.
- Eden, E.R., White, I.J., Tsapara, A., and Futter, C.E. (2010). Membrane contacts between endosomes and ER provide sites for PTP1B-epidermal growth factor receptor interaction. *Nature cell biology* 12, 267-272.
- Egan, M.J., Tan, K., and Reck-Peterson, S.L. (2012). Lis1 is an initiation factor for dynein-driven organelle transport. *The Journal of cell biology* 197, 971-982.
- Egelman, E. (2012). *Comprehensive biophysics*, 1st edn (Boston, MA: Elsevier).
- Elbaz, Y., and Schuldiner, M. (2011). Staying in touch: the molecular era of organelle contact sites. *Trends in biochemical sciences* 36, 616-623.
- Elia, N., Sougrat, R., Spurlin, T.A., Hurley, J.H., and Lippincott-Schwartz, J. (2011). Dynamics of endosomal sorting complex required for transport (ESCRT) machinery during cytokinesis and its role in abscission. *Proceedings of the National Academy of Sciences of the United States of America* 108, 4846-4851.
- English, A.R., and Voeltz, G.K. (2013). Rab10 GTPase regulates ER dynamics and morphology. *Nature cell biology* 15, 169-178.
- Erickson, R.P., Jia, Z., Gross, S.P., and Yu, C.C. (2011). How molecular motors are arranged on a cargo is important for vesicular transport. *PLoS computational biology* 7, e1002032.
- Ewers, H., Smith, A.E., Sbalzarini, I.F., Lilie, H., Koumoutsakos, P., and Helenius, A. (2005). Single-particle tracking of murine polyoma virus-like particles on live cells and

artificial membranes. *Proceedings of the National Academy of Sciences of the United States of America* *102*, 15110-15115.

Fabian Gottfert, C.A.W., Veronika Mueller, Sebastian Berning, Volker C. Cordes, Alf Honigmann, and Stefan W. Hell (2013). Coaligned Dual-Channel STED Nanoscopy and Molecular Diffusion Analysis at 20 nm Resolution. *Biophysical journal* *105*, L01-L03.

Fagone, P., and Jackowski, S. (2009). Membrane phospholipid synthesis and endoplasmic reticulum function. *Journal of lipid research* *50 Suppl*, S311-316.

Faire, K., Waterman-Storer, C.M., Gruber, D., Masson, D., Salmon, E.D., and Bulinski, J.C. (1999). E-MAP-115 (ensconsin) associates dynamically with microtubules in vivo and is not a physiological modulator of microtubule dynamics. *Journal of cell science* *112 (Pt 23)*, 4243-4255.

Ferrari, R., Manfroi, A.J., and Young, W.R. (2001). Strongly and weakly self-similar diffusion. *Physica D* *154*, 111-137.

Finer, J.T., Simmons, R.M., and Spudich, J.A. (1994). Single myosin molecule mechanics: piconewton forces and nanometre steps. *Nature* *368*, 113-119.

Firestone, A.J., Weinger, J.S., Maldonado, M., Barlan, K., Langston, L.D., O'Donnell, M., Gelfand, V.I., Kapoor, T.M., and Chen, J.K. (2012). Small-molecule inhibitors of the AAA+ ATPase motor cytoplasmic dynein. *Nature* *484*, 125-129.

Flores-Rodriguez, N., Rogers, S.S., Kenwright, D.A., Waigh, T.A., Woodman, P.G., and Allan, V.J. (2011). Roles of dynein and dynactin in early endosome dynamics revealed using automated tracking and global analysis. *PloS one* *6*, e24479.

Footer, M.J., Kerssemakers, J.W., Theriot, J.A., and Dogterom, M. (2007). Direct measurement of force generation by actin filament polymerization using an optical trap. *Proceedings of the National Academy of Sciences of the United States of America* *104*, 2181-2186.

Fourniol, F.J., Sindelar, C.V., Amigues, B., Clare, D.K., Thomas, G., Perderiset, M., Francis, F., Houdusse, A., and Moores, C.A. (2010). Template-free 13-protofilament microtubule-MAP assembly visualized at 8 Å resolution. *The Journal of cell biology* *191*, 463-470.

Friedl, P., and Wolf, K. (2010). Plasticity of cell migration: a multiscale tuning model. *The Journal of cell biology* *188*, 11-19.

Friedman, D.S., and Vale, R.D. (1999). Single-molecule analysis of kinesin motility reveals regulation by the cargo-binding tail domain. *Nature cell biology* *1*, 293-297.

Friedman, J.R., Dibenedetto, J.R., West, M., Rowland, A.A., and Voeltz, G.K. (2013). Endoplasmic reticulum-endosome contact increases as endosomes traffic and mature. *Molecular biology of the cell* *24*, 1030-1040.

Friedman, J.R., Lackner, L.L., West, M., DiBenedetto, J.R., Nunnari, J., and Voeltz, G.K. (2011). ER tubules mark sites of mitochondrial division. *Science* *334*, 358-362.

Frost, A., Perera, R., Roux, A., Spasov, K., Destaing, O., Egelman, E.H., De Camilli, P., and Unger, V.M. (2008). Structural basis of membrane invagination by F-BAR domains. *Cell* *132*, 807-817.

Fujiwara, T., Ritchie, K., Murakoshi, H., Jacobson, K., and Kusumi, A. (2002). Phospholipids undergo hop diffusion in compartmentalized cell membrane. *The Journal of cell biology* *157*, 1071-1081.

Galic, M., Jeong, S., Tsai, F.C., Joubert, L.M., Wu, Y.I., Hahn, K.M., Cui, Y., and Meyer, T. (2012). External push and internal pull forces recruit curvature-sensing N-BAR domain proteins to the plasma membrane. *Nature cell biology* *14*, 874-881.

Galkin, V.E., Orlova, A., Schroder, G.F., and Egelman, E.H. (2010). Structural polymorphism in F-actin. *Nature structural & molecular biology* *17*, 1318-1323.

Gallop, J.L., Walrant, A., Cantley, L.C., and Kirschner, M.W. (2013). Phosphoinositides and membrane curvature switch the mode of actin polymerization via selective recruitment of toca-1 and Snx9. *Proceedings of the National Academy of Sciences of the United States of America* *110*, 7193-7198.

Ganguly, S., Williams, L.S., Palacios, I.M., and Goldstein, R.E. (2012). Cytoplasmic streaming in *Drosophila* oocytes varies with kinesin activity and correlates with the microtubule cytoskeleton architecture. *Proceedings of the National Academy of Sciences of the United States of America* *109*, 15109-15114.

Gee, M.A., Heuser, J.E., and Vallee, R.B. (1997). An extended microtubule-binding structure within the dynein motor domain. *Nature* *390*, 636-639.

Gennerich, A., Carter, A.P., Reck-Peterson, S.L., and Vale, R.D. (2007). Force-induced bidirectional stepping of cytoplasmic dynein. *Cell* *131*, 952-965.

Georgatos, S.D., Pyrpassopoulou, A., and Theodoropoulos, P.A. (1997). Nuclear envelope breakdown in mammalian cells involves stepwise lamina disassembly and microtubule-drive deformation of the nuclear membrane. *Journal of cell science* *110 (Pt 17)*, 2129-2140.

Giardini, P.A., and Theriot, J.A. (2001). Effects of intermediate filaments on actin-based motility of *Listeria monocytogenes*. *Biophysical journal* *81*, 3193-3203.

Gibbons, I.R. (1963). Studies on the Protein Components of Cilia from *Tetrahymena Pyriformis*. *Proceedings of the National Academy of Sciences of the United States of America* *50*, 1002-1010.

Gill, S.R., Schroer, T.A., Szilak, I., Steuer, E.R., Sheetz, M.P., and Cleveland, D.W. (1991). Dynactin, a conserved, ubiquitously expressed component of an activator of vesicle motility mediated by cytoplasmic dynein. *The Journal of cell biology* *115*, 1639-1650.

Goldman, R.D., Cleland, M.M., Murthy, S.N., Mahammad, S., and Kuczmariski, E.R. (2012). Inroads into the structure and function of intermediate filament networks. *Journal of structural biology* *177*, 14-23.

Gong, F.C., Giddings, T.H., Meehl, J.B., Staehelin, L.A., and Galbraith, D.W. (1996). Z-membranes: artificial organelles for overexpressing recombinant integral membrane proteins. *Proceedings of the National Academy of Sciences of the United States of America* *93*, 2219-2223.

Gorvel, J.P., Chavrier, P., Zerial, M., and Gruenberg, J. (1991). rab5 controls early endosome fusion in vitro. *Cell* *64*, 915-925.

Greenberg, M.J., Lin, T., Goldman, Y.E., Shuman, H., and Ostap, E.M. (2012). Myosin IC generates power over a range of loads via a new tension-sensing mechanism. *Proceedings of the National Academy of Sciences of the United States of America* *109*, E2433-2440.

Grigoriev, I., Gouveia, S.M., van der Vaart, B., Demmers, J., Smyth, J.T., Honnappa, S., Splinter, D., Steinmetz, M.O., Putney, J.W., Jr., Hoogenraad, C.C., *et al.* (2008). STIM1 is a MT-plus-end-tracking protein involved in remodeling of the ER. *Current biology* : CB *18*, 177-182.

Grimes, M.L., Zhou, J., Beattie, E.C., Yuen, E.C., Hall, D.E., Valletta, J.S., Topp, K.S., LaVail, J.H., Bunnett, N.W., and Mobley, W.C. (1996). Endocytosis of activated TrkA: evidence that nerve growth factor induces formation of signaling endosomes. *The Journal of neuroscience : the official journal of the Society for Neuroscience* *16*, 7950-7964.

Gross, S.P. (2004). Hither and yon: a review of bi-directional microtubule-based transport. *Physical biology* *1*, R1-11.

Gruenberg, J., and Maxfield, F.R. (1995). Membrane transport in the endocytic pathway. *Current opinion in cell biology* *7*, 552-563.

Gu, Y., Sun, W., Wang, G., Jeftinija, K., Jeftinija, S., and Fang, N. (2012). Rotational dynamics of cargos at pauses during axonal transport. *Nature communications* *3*, 1030.

Gunning, P., O'Neill, G., and Hardeman, E. (2008). Tropomyosin-based regulation of the actin cytoskeleton in time and space. *Physiological reviews* *88*, 1-35.

Haglund, K., Sigismund, S., Polo, S., Szymkiewicz, I., Di Fiore, P.P., and Dikic, I. (2003). Multiple monoubiquitination of RTKs is sufficient for their endocytosis and degradation. *Nature cell biology* *5*, 461-466.

Haj, F.G., Verveer, P.J., Squire, A., Neel, B.G., and Bastiaens, P.I. (2002). Imaging sites of receptor dephosphorylation by PTP1B on the surface of the endoplasmic reticulum. *Science* *295*, 1708-1711.

Hammer, J.A., 3rd, and Sellers, J.R. (2012). Walking to work: roles for class V myosins as cargo transporters. *Nature reviews. Molecular cell biology* *13*, 13-26.

Hammond, J.W., Blasius, T.L., Soppina, V., Cai, D., and Verhey, K.J. (2010a). Autoinhibition of the kinesin-2 motor KIF17 via dual intramolecular mechanisms. *The Journal of cell biology* *189*, 1013-1025.

Hammond, J.W., Huang, C.F., Kaech, S., Jacobson, C., Banker, G., and Verhey, K.J. (2010b). Posttranslational modifications of tubulin and the polarized transport of kinesin-1 in neurons. *Molecular biology of the cell* *21*, 572-583.

Hao, Y.H., Doyle, J.M., Ramanathan, S., Gomez, T.S., Jia, D., Xu, M., Chen, Z.J., Billadeau, D.D., Rosen, M.K., and Potts, P.R. (2013). Regulation of WASH-dependent actin polymerization and protein trafficking by ubiquitination. *Cell* *152*, 1051-1064.

Harris, H. (1999). *The birth of the cell* (New Haven, Conn.: Yale University Press).

Harris, T.H., Banigan, E.J., Christian, D.A., Konradt, C., Tait Wojno, E.D., Norose, K., Wilson, E.H., John, B., Weninger, W., Luster, A.D., *et al.* (2012). Generalized Levy walks and the role of chemokines in migration of effector CD8+ T cells. *Nature* *486*, 545-548.

Hayakawa, A., Leonard, D., Murphy, S., Hayes, S., Soto, M., Fogarty, K., Standley, C., Bellve, K., Lambright, D., Mello, C., *et al.* (2006). The WD40 and FYVE domain containing protein 2 defines a class of early endosomes necessary for endocytosis. *Proceedings of the National Academy of Sciences of the United States of America* *103*, 11928-11933.

Hayakawa, K., Tatsumi, H., and Sokabe, M. (2011). Actin filaments function as a tension sensor by tension-dependent binding of cofilin to the filament. *The Journal of cell biology* *195*, 721-727.

Hendricks, A.G., Holzbaur, E.L., and Goldman, Y.E. (2012a). Force measurements on cargoes in living cells reveal collective dynamics of microtubule motors. *Proceedings of the National Academy of Sciences of the United States of America* *109*, 18447-18452.

Hendricks, A.G., Lazarus, J.E., Perlson, E., Gardner, M.K., Odde, D.J., Goldman, Y.E., and Holzbaur, E.L. (2012b). Dynein tethers and stabilizes dynamic microtubule plus ends. *Current biology* : CB *22*, 632-637.

Hendricks, A.G., Perlson, E., Ross, J.L., Schroeder, H.W., 3rd, Tokito, M., and Holzbaur, E.L. (2010). Motor coordination via a tug-of-war mechanism drives bidirectional vesicle transport. *Current biology* : CB *20*, 697-702.

Hirokawa, N. (1998). Kinesin and dynein superfamily proteins and the mechanism of organelle transport. *Science* *279*, 519-526.

Hirokawa, N., Pfister, K.K., Yorifuji, H., Wagner, M.C., Brady, S.T., and Bloom, G.S. (1989). Submolecular domains of bovine brain kinesin identified by electron microscopy and monoclonal antibody decoration. *Cell* *56*, 867-878.

Hodges, A.R., Bookwalter, C.S., Krementsova, E.B., and Trybus, K.M. (2009). A nonprocessive class V myosin drives cargo processively when a kinesin-related protein is a passenger. *Current biology* : CB *19*, 2121-2125.

Hoepfner, S., Severin, F., Cabezas, A., Habermann, B., Runge, A., Gillooly, D., Stenmark, H., and Zerial, M. (2005). Modulation of receptor recycling and degradation by the endosomal kinesin KIF16B. *Cell* *121*, 437-450.

Hokanson, D.E., Laakso, J.M., Lin, T., Sept, D., and Ostap, E.M. (2006). Myo1c binds phosphoinositides through a putative pleckstrin homology domain. *Molecular biology of the cell* *17*, 4856-4865.

Hooke, R. (1665). *Micrographia: or, Some physiological descriptions of minute bodies made by magnifying glasses. With observations and inquiries thereupon* (London,: Printed by J. Martyn and J. Allestry).

Howard, J. (2001). *Mechanics of motor proteins and the cytoskeleton* (Sunderland, Mass.: Sinauer Associates, Publishers).

Howard, J., and Spudich, J.A. (1996). Is the lever arm of myosin a molecular elastic element? *Proceedings of the National Academy of Sciences of the United States of America* *93*, 4462-4464.

Hu, Y., Chuang, J.Z., Xu, K., McGraw, T.G., and Sung, C.H. (2002). SARA, a FYVE domain protein, affects Rab5-mediated endocytosis. *Journal of cell science* *115*, 4755-4763.

Huang, F., Goh, L.K., and Sorkin, A. (2007). EGF receptor ubiquitination is not necessary for its internalization. *Proceedings of the National Academy of Sciences of the United States of America* *104*, 16904-16909.

Huang, J., Roberts, A.J., Leschziner, A.E., and Reck-Peterson, S.L. (2012). Lis1 acts as a "clutch" between the ATPase and microtubule-binding domains of the dynein motor. *Cell* *150*, 975-986.

Humphries, N.E., Weimerskirch, H., Queiroz, N., Southall, E.J., and Sims, D.W. (2012). Foraging success of biological Levy flights recorded in situ. *Proceedings of the National Academy of Sciences of the United States of America* *109*, 7169-7174.

Huxley, A.F., and Niedergerke, R. (1954). Measurement of muscle striations in stretch and contraction. *The Journal of physiology* *124*, 46-47P.

Huxley, H., and Hanson, J. (1954). Changes in the cross-striations of muscle during contraction and stretch and their structural interpretation. *Nature* *173*, 973-976.

Hyman, A.A., Chretien, D., Arnal, I., and Wade, R.H. (1995). Structural changes accompanying GTP hydrolysis in microtubules: information from a slowly hydrolyzable analogue guanylyl-(alpha,beta)-methylene-diphosphonate. *The Journal of cell biology* *128*, 117-125.

Ikegami, K., Heier, R.L., Taruishi, M., Takagi, H., Mukai, M., Shimma, S., Taira, S., Hatanaka, K., Morone, N., Yao, I., *et al.* (2007). Loss of alpha-tubulin polyglutamylation in ROSA22 mice is associated with abnormal targeting of KIF1A and modulated synaptic function. *Proceedings of the National Academy of Sciences of the United States of America* *104*, 3213-3218.

Iwasaki, T., and Wang, Y.L. (2008). Cytoplasmic force gradient in migrating adhesive cells. *Biophysical journal* *94*, L35-37.

Jacobson, C., Schnapp, B., and Banker, G.A. (2006). A change in the selective translocation of the Kinesin-1 motor domain marks the initial specification of the axon. *Neuron* *49*, 797-804.

Jain, A., Liu, R., Ramani, B., Arauz, E., Ishitsuka, Y., Rangunathan, K., Park, J., Chen, J., Xiang, Y.K., and Ha, T. (2011). Probing cellular protein complexes using single-molecule pull-down. *Nature* *473*, 484-488.

Jamison, D.K., Driver, J.W., Rogers, A.R., Constantinou, P.E., and Diehl, M.R. (2010). Two kinesins transport cargo primarily via the action of one motor: implications for intracellular transport. *Biophysical journal* *99*, 2967-2977.

Jaqaman, K., Kuwata, H., Touret, N., Collins, R., Trimble, W.S., Danuser, G., and Grinstein, S. (2011). Cytoskeletal Control of CD36 Diffusion Promotes Its Receptor and Signaling Function. *Cell* *146*, 593-606.

Jaqaman, K., Loerke, D., Mettlen, M., Kuwata, H., Grinstein, S., Schmid, S.L., and Danuser, G. (2008). Robust single-particle tracking in live-cell time-lapse sequences. *Nature methods* *5*, 695-702.

Jiang, X., Huang, F., Marusyk, A., and Sorkin, A. (2003). Grb2 regulates internalization of EGF receptors through clathrin-coated pits. *Molecular biology of the cell* *14*, 858-870.

Jing, S., Tapley, P., and Barbacid, M. (1992). Nerve growth factor mediates signal transduction through trk homodimer receptors. *Neuron* *9*, 1067-1079.

Joazeiro, C.A., Wing, S.S., Huang, H., Levenson, J.D., Hunter, T., and Liu, Y.C. (1999). The tyrosine kinase negative regulator c-Cbl as a RING-type, E2-dependent ubiquitin-protein ligase. *Science* *286*, 309-312.

Johannessen, L.E., Pedersen, N.M., Pedersen, K.W., Madshus, I.H., and Stang, E. (2006). Activation of the epidermal growth factor (EGF) receptor induces formation of EGF receptor- and Grb2-containing clathrin-coated pits. *Molecular and cellular biology* *26*, 389-401.

Kalebic, N., Sorrentino, S., Perlas, E., Bolasco, G., Martinez, C., and Heppenstall, P.A. (2013). alphaTAT1 is the major alpha-tubulin acetyltransferase in mice. *Nature communications* 4, 1962.

Kao, H.P., and Verkman, A.S. (1994). Tracking of single fluorescent particles in three dimensions: use of cylindrical optics to encode particle position. *Biophysical journal* 67, 1291-1300.

Kapitein, L.C., Schlager, M.A., van der Zwan, W.A., Wulf, P.S., Keijzer, N., and Hoogenraad, C.C. (2010). Probing intracellular motor protein activity using an inducible cargo trafficking assay. *Biophysical journal* 99, 2143-2152.

Kardon, J.R., and Vale, R.D. (2009). Regulators of the cytoplasmic dynein motor. *Nature reviews. Molecular cell biology* 10, 854-865.

Keren, K., Yam, P.T., Kinkhabwala, A., Mogilner, A., and Theriot, J.A. (2009). Intracellular fluid flow in rapidly moving cells. *Nature cell biology* 11, 1219-1224.

Kilpatrick, B.S., Eden, E.R., Schapira, A.H., Futter, C.E., and Patel, S. (2013). Direct mobilisation of lysosomal Ca<sup>2+</sup> triggers complex Ca<sup>2+</sup> signals. *Journal of cell science* 126, 60-66.

Kim, Y.J., Guzman-Hernandez, M.L., and Balla, T. (2011). A highly dynamic ER-derived phosphatidylinositol-synthesizing organelle supplies phosphoinositides to cellular membranes. *Developmental cell* 21, 813-824.

King, S.J., and Schroer, T.A. (2000). Dynactin increases the processivity of the cytoplasmic dynein motor. *Nature cell biology* 2, 20-24.

Kirschner, M.W., Honig, L.S., and Williams, R.C. (1975). Quantitative electron microscopy of microtubule assembly in vitro. *Journal of molecular biology* 99, 263-276.

Klopfenstein, D.R., Kappeler, F., and Hauri, H.P. (1998). A novel direct interaction of endoplasmic reticulum with microtubules. *The EMBO journal* 17, 6168-6177.

Kodera, N., Yamamoto, D., Ishikawa, R., and Ando, T. (2010). Video imaging of walking myosin V by high-speed atomic force microscopy. *Nature* 468, 72-76.

Komaba, S., and Coluccio, L.M. (2010). Localization of myosin 1b to actin protrusions requires phosphoinositide binding. *The Journal of biological chemistry* 285, 27686-27693.

Komada, M., McLean, D.J., Griswold, M.D., Russell, L.D., and Soriano, P. (2000). E-MAP-115, encoding a microtubule-associated protein, is a retinoic acid-inducible gene required for spermatogenesis. *Genes & development* 14, 1332-1342.

Komarova, Y., De Groot, C.O., Grigoriev, I., Gouveia, S.M., Munteanu, E.L., Schober, J.M., Honnappa, S., Buey, R.M., Hoogenraad, C.C., Dogterom, M., *et al.* (2009). Mammalian end binding proteins control persistent microtubule growth. *The Journal of cell biology* 184, 691-706.

Kon, T., Imamula, K., Roberts, A.J., Ohkura, R., Knight, P.J., Gibbons, I.R., Burgess, S.A., and Sutoh, K. (2009). Helix sliding in the stalk coiled coil of dynein couples ATPase and microtubule binding. *Nature structural & molecular biology* 16, 325-333.

Kon, T., Nishiura, M., Ohkura, R., Toyoshima, Y.Y., and Sutoh, K. (2004). Distinct functions of nucleotide-binding/hydrolysis sites in the four AAA modules of cytoplasmic dynein. *Biochemistry* 43, 11266-11274.

Korkhov, V.M., and Zuber, B. (2009). Direct observation of molecular arrays in the organized smooth endoplasmic reticulum. *BMC cell biology* *10*, 59.

Kornmann, B., Currie, E., Collins, S.R., Schuldiner, M., Nunnari, J., Weissman, J.S., and Walter, P. (2009). An ER-mitochondria tethering complex revealed by a synthetic biology screen. *Science* *325*, 477-481.

Korobova, F., Ramabhadran, V., and Higgs, H.N. (2013). An actin-dependent step in mitochondrial fission mediated by the ER-associated formin INF2. *Science* *339*, 464-467.

Koster, G., Cacciuto, A., Derenyi, I., Frenkel, D., and Dogterom, M. (2005). Force barriers for membrane tube formation. *Phys Rev Lett* *94*, 068101.

Koster, G., VanDuijn, M., Hofs, B., and Dogterom, M. (2003). Membrane tube formation from giant vesicles by dynamic association of motor proteins. *Proceedings of the National Academy of Sciences of the United States of America* *100*, 15583-15588.

Kovacs, M., Wang, F., Hu, A., Zhang, Y., and Sellers, J.R. (2003). Functional divergence of human cytoplasmic myosin II: kinetic characterization of the non-muscle IIA isoform. *The Journal of biological chemistry* *278*, 38132-38140.

Krendel, M., and Mooseker, M.S. (2005). Myosins: tails (and heads) of functional diversity. *Physiology* *20*, 239-251.

Kreutzberg, G.W. (1969). Neuronal dynamics and axonal flow. IV. Blockage of intra-axonal enzyme transport by colchicine. *Proceedings of the National Academy of Sciences of the United States of America* *62*, 722-728.

Kulic, I.M., Brown, A.E., Kim, H., Kural, C., Blehm, B., Selvin, P.R., Nelson, P.C., and Gelfand, V.I. (2008). The role of microtubule movement in bidirectional organelle transport. *Proceedings of the National Academy of Sciences of the United States of America* *105*, 10011-10016.

Kull, F.J., Sablin, E.P., Lau, R., Fletterick, R.J., and Vale, R.D. (1996). Crystal structure of the kinesin motor domain reveals a structural similarity to myosin. *Nature* *380*, 550-555.

Kunwar, A., Tripathy, S.K., Xu, J., Mattson, M.K., Anand, P., Sigua, R., Vershinin, M., McKenney, R.J., Yu, C.C., Mogilner, A., *et al.* (2011). Mechanical stochastic tug-of-war models cannot explain bidirectional lipid-droplet transport. *Proceedings of the National Academy of Sciences of the United States of America* *108*, 18960-18965.

Kunwar, A., Vershinin, M., Xu, J., and Gross, S.P. (2008). Stepping, strain gating, and an unexpected force-velocity curve for multiple-motor-based transport. *Current biology : CB* *18*, 1173-1183.

Kural, C., Kim, H., Syed, S., Goshima, G., Gelfand, V.I., and Selvin, P.R. (2005). Kinesin and dynein move a peroxisome in vivo: a tug-of-war or coordinated movement? *Science* *308*, 1469-1472.

Kural, C., Serpinskaya, A.S., Chou, Y.H., Goldman, R.D., Gelfand, V.I., and Selvin, P.R. (2007). Tracking melanosomes inside a cell to study molecular motors and their interaction. *Proceedings of the National Academy of Sciences of the United States of America* *104*, 5378-5382.

Laakso, J.M., Lewis, J.H., Shuman, H., and Ostap, E.M. (2008). Myosin I can act as a molecular force sensor. *Science* *321*, 133-136.

Laan, L., Pavin, N., Husson, J., Romet-Lemonne, G., van Duijn, M., Lopez, M.P., Vale, R.D., Julicher, F., Reck-Peterson, S.L., and Dogterom, M. (2012). Cortical dynein controls microtubule dynamics to generate pulling forces that position microtubule asters. *Cell* *148*, 502-514.

Lakadamyali, M., Rust, M.J., and Zhuang, X. (2006). Ligands for clathrin-mediated endocytosis are differentially sorted into distinct populations of early endosomes. *Cell* *124*, 997-1009.

Lam, C., Vergnolle, M.A., Thorpe, L., Woodman, P.G., and Allan, V.J. (2010). Functional interplay between LIS1, NDE1 and NDEL1 in dynein-dependent organelle positioning. *Journal of cell science* *123*, 202-212.

Lawrence, C.J., Dawe, R.K., Christie, K.R., Cleveland, D.W., Dawson, S.C., Endow, S.A., Goldstein, L.S., Goodson, H.V., Hirokawa, N., Howard, J., *et al.* (2004). A standardized kinesin nomenclature. *The Journal of cell biology* *167*, 19-22.

Leonard, D., Hayakawa, A., Lawe, D., Lambright, D., Bellve, K.D., Standley, C., Lifshitz, L.M., Fogarty, K.E., and Corvera, S. (2008). Sorting of EGF and transferrin at the plasma membrane and by cargo-specific signaling to EEA1-enriched endosomes. *Journal of cell science* *121*, 3445-3458.

Levkowitz, G., Waterman, H., Ettenberg, S.A., Katz, M., Tsygankov, A.Y., Alroy, I., Lavi, S., Iwai, K., Reiss, Y., Ciechanover, A., *et al.* (1999). Ubiquitin ligase activity and tyrosine phosphorylation underlie suppression of growth factor signaling by c-Cbl/Sli-1. *Molecular cell* *4*, 1029-1040.

Lewis, J.H., Greenberg, M.J., Laakso, J.M., Shuman, H., and Ostap, E.M. (2012). Calcium regulation of myosin-I tension sensing. *Biophysical journal* *102*, 2799-2807.

Li, J., Mao, X., Dong, L.Q., Liu, F., and Tong, L. (2007). Crystal structures of the BAR-PH and PTB domains of human APPL1. *Structure* *15*, 525-533.

Ligon, L.A., Tokito, M., Finklestein, J.M., Grossman, F.E., and Holzbaur, E.L. (2004). A direct interaction between cytoplasmic dynein and kinesin I may coordinate motor activity. *The Journal of biological chemistry* *279*, 19201-19208.

Lin, D.C., Quevedo, C., Brewer, N.E., Bell, A., Testa, J.R., Grimes, M.L., Miller, F.D., and Kaplan, D.R. (2006). APPL1 associates with TrkA and GIPC1 and is required for nerve growth factor-mediated signal transduction. *Molecular and cellular biology* *26*, 8928-8941.

Lin, T., Tang, N., and Ostap, E.M. (2005). Biochemical and motile properties of Myo1b splice isoforms. *The Journal of biological chemistry* *280*, 41562-41567.

Lippincott-Schwartz, J., Roberts, T.H., and Hirschberg, K. (2000). Secretory protein trafficking and organelle dynamics in living cells. *Annual review of cell and developmental biology* *16*, 557-589.

Liu, J., Taylor, D.W., Krementsova, E.B., Trybus, K.M., and Taylor, K.A. (2006). Three-dimensional structure of the myosin V inhibited state by cryoelectron tomography. *Nature* *442*, 208-211.

Liu, J.S., Schubert, C.R., Fu, X., Fourniol, F.J., Jaiswal, J.K., Houdusse, A., Stultz, C.M., Moores, C.A., and Walsh, C.A. (2012). Molecular basis for specific regulation of neuronal kinesin-3 motors by doublecortin family proteins. *Molecular cell* *47*, 707-721.

Liu, Y., Xu, X.H., Chen, Q., Wang, T., Deng, C.Y., Song, B.L., Du, J.L., and Luo, Z.G. (2013). Myosin Vb controls biogenesis of post-Golgi Rab10 carriers during axon development. *Nature communications* 4, 2005.

Lloyd, T.E., Machamer, J., O'Hara, K., Kim, J.H., Collins, S.E., Wong, M.Y., Sahin, B., Imlach, W., Yang, Y., Levitan, E.S., *et al.* (2012). The p150(Glued) CAP-Gly domain regulates initiation of retrograde transport at synaptic termini. *Neuron* 74, 344-360.

Lo, S.Y., Brett, C.L., Plemel, R.L., Vignali, M., Fields, S., Gonen, T., and Merz, A.J. (2012). Intrinsic tethering activity of endosomal Rab proteins. *Nature structural & molecular biology* 19, 40-47.

Loisel, T.P., Boujema, R., Pantaloni, D., and Carlier, M.F. (1999). Reconstitution of actin-based motility of *Listeria* and *Shigella* using pure proteins. *Nature* 401, 613-616.

Lomakin, A.J., Kraikivski, P., Semenova, I., Ikeda, K., Zaliapin, I., Tirnauer, J.S., Akhmanova, A., and Rodionov, V. (2011). Stimulation of the CLIP-170--dependent capture of membrane organelles by microtubules through fine tuning of microtubule assembly dynamics. *Molecular biology of the cell* 22, 4029-4037.

Lomakin, A.J., Semenova, I., Zaliapin, I., Kraikivski, P., Nadezhdina, E., Slepchenko, B.M., Akhmanova, A., and Rodionov, V. (2009). CLIP-170-dependent capture of membrane organelles by microtubules initiates minus-end directed transport. *Developmental cell* 17, 323-333.

Loubery, S., Wilhelm, C., Hurbain, I., Neveu, S., Louvard, D., and Coudrier, E. (2008). Different microtubule motors move early and late endocytic compartments. *Traffic* 9, 492-509.

Luby-Phelps, K. (2000). Cytoarchitecture and physical properties of cytoplasm: volume, viscosity, diffusion, intracellular surface area. *International review of cytology* 192, 189-221.

Lymn, R.W., and Taylor, E.W. (1971). Mechanism of adenosine triphosphate hydrolysis by actomyosin. *Biochemistry* 10, 4617-4624.

Mallik, R., Carter, B.C., Lex, S.A., King, S.J., and Gross, S.P. (2004). Cytoplasmic dynein functions as a gear in response to load. *Nature* 427, 649-652.

Mallik, R., and Gross, S.P. (2004). Molecular motors: strategies to get along. *Current biology* : CB 14, R971-982.

Mallik, R., Petrov, D., Lex, S.A., King, S.J., and Gross, S.P. (2005). Building complexity: an in vitro study of cytoplasmic dynein with in vivo implications. *Current biology* : CB 15, 2075-2085.

Mandelkow, E.M., Mandelkow, E., and Milligan, R.A. (1991). Microtubule dynamics and microtubule caps: a time-resolved cryo-electron microscopy study. *The Journal of cell biology* 114, 977-991.

Mattila, E., Pellinen, T., Nevo, J., Vuoriluoto, K., Arjonen, A., and Ivaska, J. (2005). Negative regulation of EGFR signalling through integrin- $\alpha$ 1 $\beta$ 1-mediated activation of protein tyrosine phosphatase TCPTP. *Nature cell biology* 7, 78-85.

Maurer, S.P., Fourniol, F.J., Bohner, G., Moores, C.A., and Surrey, T. (2012). EBs recognize a nucleotide-dependent structural cap at growing microtubule ends. *Cell* 149, 371-382.

Maxfield, F.R., and McGraw, T.E. (2004). Endocytic recycling. *Nature reviews. Molecular cell biology* 5, 121-132.

McCullough, J., Clague, M.J., and Urbe, S. (2004). AMSH is an endosome-associated ubiquitin isopeptidase. *The Journal of cell biology* 166, 487-492.

McGuire, J.R., Rong, J., Li, S.H., and Li, X.J. (2006). Interaction of Huntingtin-associated protein-1 with kinesin light chain: implications in intracellular trafficking in neurons. *The Journal of biological chemistry* 281, 3552-3559.

McIntosh, J.R., Volkov, V., Ataullakhanov, F.I., and Grishchuk, E.L. (2010). Tubulin depolymerization may be an ancient biological motor. *Journal of cell science* 123, 3425-3434.

McKenney, R.J., Vershinin, M., Kunwar, A., Vallee, R.B., and Gross, S.P. (2010). LIS1 and NudE induce a persistent dynein force-producing state. *Cell* 141, 304-314.

Mehta, A.D., Rock, R.S., Rief, M., Spudich, J.A., Mooseker, M.S., and Cheney, R.E. (1999). Myosin-V is a processive actin-based motor. *Nature* 400, 590-593.

Merrifield, C.J., Moss, S.E., Ballestrem, C., Imhof, B.A., Giese, G., Wunderlich, I., and Almers, W. (1999). Endocytic vesicles move at the tips of actin tails in cultured mast cells. *Nature cell biology* 1, 72-74.

Mesaki, K., Tanabe, K., Obayashi, M., Oe, N., and Takei, K. (2011). Fission of tubular endosomes triggers endosomal acidification and movement. *PloS one* 6, e19764.

Miaczynska, M., Christoforidis, S., Giner, A., Shevchenko, A., Uttenweiler-Joseph, S., Habermann, B., Wilm, M., Parton, R.G., and Zerial, M. (2004). APPL proteins link Rab5 to nuclear signal transduction via an endosomal compartment. *Cell* 116, 445-456.

Miller, K., Beardmore, J., Kanety, H., Schlessinger, J., and Hopkins, C.R. (1986). Localization of the epidermal growth factor (EGF) receptor within the endosome of EGF-stimulated epidermoid carcinoma (A431) cells. *The Journal of cell biology* 102, 500-509.

Miller, R.H., and Lasek, R.J. (1985). Cross-bridges mediate anterograde and retrograde vesicle transport along microtubules in squid axoplasm. *The Journal of cell biology* 101, 2181-2193.

Mizuno, E., Iura, T., Mukai, A., Yoshimori, T., Kitamura, N., and Komada, M. (2005). Regulation of epidermal growth factor receptor down-regulation by UBPY-mediated deubiquitination at endosomes. *Molecular biology of the cell* 16, 5163-5174.

Morgan, A.J., Davis, L.C., Wagner, S.K., Lewis, A.M., Parrington, J., Churchill, G.C., and Galione, A. (2013). Bidirectional Ca<sup>2+</sup>(+) signaling occurs between the endoplasmic reticulum and acidic organelles. *The Journal of cell biology* 200, 789-805.

Moss, T.J., Daga, A., and McNew, J.A. (2011). Fusing a lasting relationship between ER tubules. *Trends in cell biology* 21, 416-423.

Moughamian, A.J., and Holzbaur, E.L. (2012). Dynactin is required for transport initiation from the distal axon. *Neuron* 74, 331-343.

Mudrakola, H.V., Zhang, K., and Cui, B. (2009). Optically resolving individual microtubules in live axons. *Structure* 17, 1433-1441.

Mueller, V., Honigsmann, A., Ringemann, C., Medda, R., Schwarzmann, G., and Eggeling, C. (2013). FCS in STED microscopy: studying the nanoscale of lipid membrane dynamics. *Methods in enzymology* 519, 1-38.

Muller, M.J., Klumpp, S., and Lipowsky, R. (2008). Tug-of-war as a cooperative mechanism for bidirectional cargo transport by molecular motors. *Proceedings of the National Academy of Sciences of the United States of America* *105*, 4609-4614.

Muller, M.J., Klumpp, S., and Lipowsky, R. (2010). Bidirectional transport by molecular motors: enhanced processivity and response to external forces. *Biophysical journal* *98*, 2610-2618.

Mullins, R.D., Heuser, J.A., and Pollard, T.D. (1998). The interaction of Arp2/3 complex with actin: nucleation, high affinity pointed end capping, and formation of branching networks of filaments. *Proceedings of the National Academy of Sciences of the United States of America* *95*, 6181-6186.

Muthukrishnan, G., Zhang, Y., Shastry, S., and Hancock, W.O. (2009). The processivity of kinesin-2 motors suggests diminished front-head gating. *Current biology : CB* *19*, 442-447.

Nagy, S., and Rock, R.S. (2010). Structured post-IQ domain governs selectivity of myosin X for fascin-actin bundles. *The Journal of biological chemistry* *285*, 26608-26617.

Nakata, T., and Hirokawa, N. (2003). Microtubules provide directional cues for polarized axonal transport through interaction with kinesin motor head. *The Journal of cell biology* *162*, 1045-1055.

Nakata, T., Niwa, S., Okada, Y., Perez, F., and Hirokawa, N. (2011). Preferential binding of a kinesin-1 motor to GTP-tubulin-rich microtubules underlies polarized vesicle transport. *The Journal of cell biology* *194*, 245-255.

Nan, X., Sims, P.A., Chen, P., and Xie, X.S. (2005). Observation of individual microtubule motor steps in living cells with endocytosed quantum dots. *J Phys Chem B* *109*, 24220-24224.

Nan, X., Sims, P.A., and Xie, X.S. (2008). Organelle tracking in a living cell with microsecond time resolution and nanometer spatial precision. *Chemphyschem : a European journal of chemical physics and physical chemistry* *9*, 707-712.

Nekrasova, O.E., Mendez, M.G., Chernouvanenko, I.S., Tyurin-Kuzmin, P.A., Kuczumarski, E.R., Gelfand, V.I., Goldman, R.D., and Minin, A.A. (2011). Vimentin intermediate filaments modulate the motility of mitochondria. *Molecular biology of the cell* *22*, 2282-2289.

Nelson, S.R., Ali, M.Y., Trybus, K.M., and Warshaw, D.M. (2009). Random walk of processive, quantum dot-labeled myosin Va molecules within the actin cortex of COS-7 cells. *Biophysical journal* *97*, 509-518.

Neuwald, A.F., Aravind, L., Spouge, J.L., and Koonin, E.V. (1999). AAA+: A class of chaperone-like ATPases associated with the assembly, operation, and disassembly of protein complexes. *Genome research* *9*, 27-43.

Nielsen, E., Severin, F., Backer, J.M., Hyman, A.A., and Zerial, M. (1999). Rab5 regulates motility of early endosomes on microtubules. *Nature cell biology* *1*, 376-382.

Niu, Y., Zhang, C., Sun, Z., Hong, Z., Li, K., Sun, D., Yang, Y., Tian, C., Gong, W., and Liu, J.J. (2013). PtdIns(4)P regulates retromer-motor interaction to facilitate dynein-cargo dissociation at the trans-Golgi network. *Nature cell biology* *15*, 417-429.

Nunes, P., Cornut, D., Bochet, V., Hasler, U., Oh-Hora, M., Waldburger, J.M., and Demaurex, N. (2012). STIM1 juxtaposes ER to phagosomes, generating Ca<sup>2+</sup>(+) hotspots that boost phagocytosis. *Current biology* : CB 22, 1990-1997.

Odrionitz, F., and Kollmar, M. (2007). Drawing the tree of eukaryotic life based on the analysis of 2,269 manually annotated myosins from 328 species. *Genome biology* 8, R196.

Ohkuma, M., Park, S.M., Zimmer, T., Menzel, R., Vogel, F., Schunck, W.H., Ohta, A., and Takagi, M. (1995). Proliferation of intracellular membrane structures upon homologous overproduction of cytochrome P-450 in *Candida maltosa*. *Biochimica et biophysica acta* 1236, 163-169.

Okabe, K., Inada, N., Gota, C., Harada, Y., Funatsu, T., and Uchiyama, S. (2012). Intracellular temperature mapping with a fluorescent polymeric thermometer and fluorescence lifetime imaging microscopy. *Nature communications* 3, 705.

Olenych, S.G., Claxton, N.S., Ottenberg, G.K., and Davidson, M.W. (2007). The fluorescent protein color palette. *Current protocols in cell biology / editorial board, Juan S. Bonifacino ... [et al.] Chapter 21, Unit 21 25.*

Ori-McKenney, K.M., Xu, J., Gross, S.P., and Vallee, R.B. (2010). A cytoplasmic dynein tail mutation impairs motor processivity. *Nature cell biology* 12, 1228-1234.

Papp, G., Bugyi, B., Ujfalusi, Z., Barko, S., Hild, G., Somogyi, B., and Nyitrai, M. (2006). Conformational changes in actin filaments induced by formin binding to the barbed end. *Biophysical journal* 91, 2564-2572.

Park, M., Serpinskaya, A.S., Papalopulu, N., and Gelfand, V.I. (2007). Rab32 regulates melanosome transport in *Xenopus melanophores* by protein kinase a recruitment. *Current biology* : CB 17, 2030-2034.

Park, S.H., Zhu, P.P., Parker, R.L., and Blackstone, C. (2010). Hereditary spastic paraplegia proteins REEP1, spastin, and atlastin-1 coordinate microtubule interactions with the tubular ER network. *The Journal of clinical investigation* 120, 1097-1110.

Parton, R.M., Hamilton, R.S., Ball, G., Yang, L., Cullen, C.F., Lu, W., Ohkura, H., and Davis, I. (2011). A PAR-1-dependent orientation gradient of dynamic microtubules directs posterior cargo transport in the *Drosophila* oocyte. *The Journal of cell biology* 194, 121-135.

Paschal, B.M., Shpetner, H.S., and Vallee, R.B. (1987). MAP 1C is a microtubule-activated ATPase which translocates microtubules in vitro and has dynein-like properties. *The Journal of cell biology* 105, 1273-1282.

Pawson, T., and Scott, J.D. (1997). Signaling through scaffold, anchoring, and adaptor proteins. *Science* 278, 2075-2080.

Perez Bay, A.E., Schreiner, R., Mazzoni, F., Carvajal-Gonzalez, J.M., Gravotta, D., Perret, E., Lehmann Mantaras, G., Zhu, Y.S., and Rodriguez-Boulan, E.J. (2013). The kinesin KIF16B mediates apical transcytosis of transferrin receptor in AP-1B-deficient epithelia. *The EMBO journal*.

Peris, L., Wagenbach, M., Lafanechere, L., Brocard, J., Moore, A.T., Kozielski, F., Job, D., Wordeman, L., and Andrieux, A. (2009). Motor-dependent microtubule disassembly driven by tubulin tyrosination. *The Journal of cell biology* 185, 1159-1166.

Peskin, C.S., Odell, G.M., and Oster, G.F. (1993). Cellular motions and thermal fluctuations: the Brownian ratchet. *Biophysical journal* *65*, 316-324.

Pfeffer, S.R. (2007). Unsolved mysteries in membrane traffic. *Annual review of biochemistry* *76*, 629-645.

Pierobon, P., Achouri, S., Courty, S., Dunn, A.R., Spudich, J.A., Dahan, M., and Cappello, G. (2009). Velocity, processivity, and individual steps of single myosin V molecules in live cells. *Biophysical journal* *96*, 4268-4275.

Pierre, P., Scheel, J., Rickard, J.E., and Kreis, T.E. (1992). CLIP-170 links endocytic vesicles to microtubules. *Cell* *70*, 887-900.

Pollard, T.D., and Ostap, E.M. (1996). The chemical mechanism of myosin-I: implications for actin-based motility and the evolution of the myosin family of motor proteins. *Cell structure and function* *21*, 351-356.

Poteryaev, D., Datta, S., Ackema, K., Zerial, M., and Spang, A. (2010). Identification of the switch in early-to-late endosome transition. *Cell* *141*, 497-508.

Prochniewicz, E., Chin, H.F., Henn, A., Hannemann, D.E., Olivares, A.O., Thomas, D.D., and De La Cruz, E.M. (2010). Myosin isoform determines the conformational dynamics and cooperativity of actin filaments in the strongly bound actomyosin complex. *Journal of molecular biology* *396*, 501-509.

Prochniewicz, E., Janson, N., Thomas, D.D., and De la Cruz, E.M. (2005). Cofilin increases the torsional flexibility and dynamics of actin filaments. *Journal of molecular biology* *353*, 990-1000.

Prochniewicz, E., Zhang, Q., Janmey, P.A., and Thomas, D.D. (1996). Cooperativity in F-actin: binding of gelsolin at the barbed end affects structure and dynamics of the whole filament. *Journal of molecular biology* *260*, 756-766.

Profant, D.A., Roberts, C.J., Koning, A.J., and Wright, R.L. (1999). The role of the 3-hydroxy 3-methylglutaryl coenzyme A reductase cytosolic domain in karmellae biogenesis. *Molecular biology of the cell* *10*, 3409-3423.

Provance, D.W., Jr., Addison, E.J., Wood, P.R., Chen, D.Z., Silan, C.M., and Mercer, J.A. (2008). Myosin-Vb functions as a dynamic tether for peripheral endocytic compartments during transferrin trafficking. *BMC cell biology* *9*, 44.

Pruyne, D., Evangelista, M., Yang, C., Bi, E., Zigmond, S., Bretscher, A., and Boone, C. (2002). Role of formins in actin assembly: nucleation and barbed-end association. *Science* *297*, 612-615.

Purcell, T.J., Sweeney, H.L., and Spudich, J.A. (2005). A force-dependent state controls the coordination of processive myosin V. *Proceedings of the National Academy of Sciences of the United States of America* *102*, 13873-13878.

Qiu, W., Derr, N.D., Goodman, B.S., Villa, E., Wu, D., Shih, W., and Reck-Peterson, S.L. (2012). Dynein achieves processive motion using both stochastic and coordinated stepping. *Nature structural & molecular biology* *19*, 193-200.

Rai, A.K., Rai, A., Ramaiya, A.J., Jha, R., and Mallik, R. (2013). Molecular adaptations allow dynein to generate large collective forces inside cells. *Cell* *152*, 172-182.

Ramesh, P., Baroji, Y.F., Reihani, S.N., Stamou, D., Oddershede, L.B., and Bendix, P.M. (2013). FBAR syndapin 1 recognizes and stabilizes highly curved tubular membranes in a concentration dependent manner. *Scientific reports* *3*, 1565.

Raposo, G., Cordonnier, M.N., Tenza, D., Menichi, B., Durrbach, A., Louvard, D., and Coudrier, E. (1999). Association of myosin I alpha with endosomes and lysosomes in mammalian cells. *Molecular biology of the cell* *10*, 1477-1494.

Reck-Peterson, S.L., and Vale, R.D. (2004). Molecular dissection of the roles of nucleotide binding and hydrolysis in dynein's AAA domains in *Saccharomyces cerevisiae*. *Proceedings of the National Academy of Sciences of the United States of America* *101*, 1491-1495.

Reck-Peterson, S.L., Yildiz, A., Carter, A.P., Gennerich, A., Zhang, N., and Vale, R.D. (2006). Single-molecule analysis of dynein processivity and stepping behavior. *Cell* *126*, 335-348.

Reed, N.A., Cai, D., Blasius, T.L., Jih, G.T., Meyhofer, E., Gaertig, J., and Verhey, K.J. (2006). Microtubule acetylation promotes kinesin-1 binding and transport. *Current biology : CB* *16*, 2166-2172.

Renvoise, B., and Blackstone, C. (2010). Emerging themes of ER organization in the development and maintenance of axons. *Current opinion in neurobiology* *20*, 531-537.

Rhee, H.W., Zou, P., Udeshi, N.D., Martell, J.D., Mootha, V.K., Carr, S.A., and Ting, A.Y. (2013). Proteomic mapping of mitochondria in living cells via spatially restricted enzymatic tagging. *Science* *339*, 1328-1331.

Ricca, B.L., and Rock, R.S. (2010). The stepping pattern of myosin X is adapted for processive motility on bundled actin. *Biophysical journal* *99*, 1818-1826.

Rice, S., Lin, A.W., Safer, D., Hart, C.L., Naber, N., Carragher, B.O., Cain, S.M., Pechatnikova, E., Wilson-Kubalek, E.M., Whittaker, M., *et al.* (1999). A structural change in the kinesin motor protein that drives motility. *Nature* *402*, 778-784.

Ries, J. (1909). Kinematographie der Befruchtung und Zellteilung. *Archiv für mikroskopische Anatomie* *74*, 1-31.

Rink, J., Ghigo, E., Kalaidzidis, Y., and Zerial, M. (2005). Rab conversion as a mechanism of progression from early to late endosomes. *Cell* *122*, 735-749.

Rocha, N., Kuijl, C., van der Kant, R., Janssen, L., Houben, D., Janssen, H., Zwart, W., and Neefjes, J. (2009). Cholesterol sensor ORP1L contacts the ER protein VAP to control Rab7-RILP-p150 Glued and late endosome positioning. *The Journal of cell biology* *185*, 1209-1225.

Rock, R.S., Rice, S.E., Wells, A.L., Purcell, T.J., Spudich, J.A., and Sweeney, H.L. (2001). Myosin VI is a processive motor with a large step size. *Proceedings of the National Academy of Sciences of the United States of America* *98*, 13655-13659.

Rogers, S.L., Tint, I.S., Fanapour, P.C., and Gelfand, V.I. (1997). Regulated bidirectional motility of melanophore pigment granules along microtubules in vitro. *Proceedings of the National Academy of Sciences of the United States of America* *94*, 3720-3725.

Ross, J.L., Shuman, H., Holzbaur, E.L., and Goldman, Y.E. (2008). Kinesin and dynein-dynactin at intersecting microtubules: motor density affects dynein function. *Biophysical journal* *94*, 3115-3125.

Ross, J.L., Wallace, K., Shuman, H., Goldman, Y.E., and Holzbaur, E.L. (2006). Processive bidirectional motion of dynein-dynactin complexes in vitro. *Nature cell biology* *8*, 562-570.

Roux, K.J., Kim, D.I., Raida, M., and Burke, B. (2012). A promiscuous biotin ligase fusion protein identifies proximal and interacting proteins in mammalian cells. *The Journal of cell biology* *196*, 801-810.

Ruppel, K.M., and Spudich, J.A. (1996). Structure-function analysis of the motor domain of myosin. *Annual review of cell and developmental biology* *12*, 543-573.

Sagot, I., Klee, S.K., and Pellman, D. (2002). Yeast formins regulate cell polarity by controlling the assembly of actin cables. *Nature cell biology* *4*, 42-50.

Sahlender, D.A., Roberts, R.C., Arden, S.D., Spudich, G., Taylor, M.J., Luzio, J.P., Kendrick-Jones, J., and Buss, F. (2005). Optineurin links myosin VI to the Golgi complex and is involved in Golgi organization and exocytosis. *The Journal of cell biology* *169*, 285-295.

Sandig, G., Kargel, E., Menzel, R., Vogel, F., Zimmer, T., and Schunck, W.H. (1999). Regulation of endoplasmic reticulum biogenesis in response to cytochrome P450 overproduction. *Drug metabolism reviews* *31*, 393-410.

Sato, O., Li, X.D., and Ikebe, M. (2007). Myosin Va becomes a low duty ratio motor in the inhibited form. *The Journal of biological chemistry* *282*, 13228-13239.

Schenck, A., Goto-Silva, L., Collinet, C., Rhinn, M., Giner, A., Habermann, B., Brand, M., and Zerial, M. (2008). The endosomal protein Appl1 mediates Akt substrate specificity and cell survival in vertebrate development. *Cell* *133*, 486-497.

Schilstra, M.J., and Martin, S.R. (2006). An elastically tethered viscous load imposes a regular gait on the motion of myosin-V. *Simulation of the effect of transient force relaxation on a stochastic process. Journal of the Royal Society, Interface / the Royal Society* *3*, 153-165.

Schnapp, B.J., and Reese, T.S. (1989). Dynein is the motor for retrograde axonal transport of organelles. *Proceedings of the National Academy of Sciences of the United States of America* *86*, 1548-1552.

Schneider, C.A., Rasband, W.S., and Eliceiri, K.W. (2012). NIH Image to ImageJ: 25 years of image analysis. *Nature methods* *9*, 671-675.

Schroeder, H.W., 3rd, Hendricks, A.G., Ikeda, K., Shuman, H., Rodionov, V., Ikebe, M., Goldman, Y.E., and Holzbaur, E.L. (2012). Force-dependent detachment of kinesin-2 biases track switching at cytoskeletal filament intersections. *Biophysical journal* *103*, 48-58.

Schroeder, H.W., 3rd, Mitchell, C., Shuman, H., Holzbaur, E.L., and Goldman, Y.E. (2010). Motor number controls cargo switching at actin-microtubule intersections in vitro. *Current biology : CB* *20*, 687-696.

Schroer, T.A. (2004). Dynactin. *Annual review of cell and developmental biology* *20*, 759-779.

Schroer, T.A., and Sheetz, M.P. (1991). Two activators of microtubule-based vesicle transport. *The Journal of cell biology* *115*, 1309-1318.

Schroer, T.A., Steuer, E.R., and Sheetz, M.P. (1989). Cytoplasmic dynein is a minus end-directed motor for membranous organelles. *Cell* *56*, 937-946.

Schuh, M. (2011). An actin-dependent mechanism for long-range vesicle transport. *Nature cell biology* *13*, 1431-1436.

Seksek, O., and Bolard, J. (1996). Nuclear pH gradient in mammalian cells revealed by laser microspectrofluorimetry. *Journal of cell science* *109* ( Pt 1), 257-262.

Semenova, I., Burakov, A., Berardone, N., Zaliapin, I., Slepchenko, B., Svitkina, T., Kashina, A., and Rodionov, V. (2008). Actin dynamics is essential for myosin-based transport of membrane organelles. *Current biology : CB* *18*, 1581-1586.

Severin, F.F., Shanina, N.A., Kuznetsov, S.A., and Gelfand, V.I. (1991). MAP2-mediated binding of chromaffin granules to microtubules. *FEBS letters* *282*, 65-68.

Shastri, S., and Hancock, W.O. (2010). Neck linker length determines the degree of processivity in kinesin-1 and kinesin-2 motors. *Current biology : CB* *20*, 939-943.

Shaw, R.M., Fay, A.J., Puthenveedu, M.A., von Zastrow, M., Jan, Y.N., and Jan, L.Y. (2007). Microtubule plus-end-tracking proteins target gap junctions directly from the cell interior to adherens junctions. *Cell* *128*, 547-560.

Sheetz, M.P., and Spudich, J.A. (1983). Movement of myosin-coated fluorescent beads on actin cables in vitro. *Nature* *303*, 31-35.

Shibata, Y., Voeltz, G.K., and Rapoport, T.A. (2006). Rough sheets and smooth tubules. *Cell* *126*, 435-439.

Shibata, Y., Voss, C., Rist, J.M., Hu, J., Rapoport, T.A., Prinz, W.A., and Voeltz, G.K. (2008). The reticulon and DP1/Yop1p proteins form immobile oligomers in the tubular endoplasmic reticulum. *The Journal of biological chemistry* *283*, 18892-18904.

Shida, T., Cueva, J.G., Xu, Z., Goodman, M.B., and Nachury, M.V. (2010). The major alpha-tubulin K40 acetyltransferase alphaTAT1 promotes rapid ciliogenesis and efficient mechanosensation. *Proceedings of the National Academy of Sciences of the United States of America* *107*, 21517-21522.

Shimada, A., Niwa, H., Tsujita, K., Suetsugu, S., Nitta, K., Hanawa-Suetsugu, K., Akasaka, R., Nishino, Y., Toyama, M., Chen, L., *et al.* (2007). Curved EFC/F-BAR-domain dimers are joined end to end into a filament for membrane invagination in endocytosis. *Cell* *129*, 761-772.

Shimmen, T., and Yokota, E. (2004). Cytoplasmic streaming in plants. *Current opinion in cell biology* *16*, 68-72.

Shubeita, G.T., Tran, S.L., Xu, J., Vershinin, M., Cermelli, S., Cotton, S.L., Welte, M.A., and Gross, S.P. (2008). Consequences of motor copy number on the intracellular transport of kinesin-1-driven lipid droplets. *Cell* *135*, 1098-1107.

Simonsen, A., Lippe, R., Christoforidis, S., Gaullier, J.M., Brech, A., Callaghan, J., Toh, B.H., Murphy, C., Zerial, M., and Stenmark, H. (1998). EEA1 links PI(3)K function to Rab5 regulation of endosome fusion. *Nature* *394*, 494-498.

Sivaramakrishnan, S., and Spudich, J.A. (2009). Coupled myosin VI motors facilitate unidirectional movement on an F-actin network. *The Journal of cell biology* *187*, 53-60.

Sivaramakrishnan, V., Bidula, S., Campwala, H., Katikaneni, D., and Fountain, S.J. (2012). Constitutive lysosome exocytosis releases ATP and engages P2Y receptors in human monocytes. *Journal of cell science* *125*, 4567-4575.

Skau, C.T., and Kovar, D.R. (2010). Fimbrin and tropomyosin competition regulates endocytosis and cytokinesis kinetics in fission yeast. *Current biology : CB* *20*, 1415-1422.

Skjeldal, F.M., Strunze, S., Bergeland, T., Walseng, E., Gregers, T.F., and Bakke, O. (2012). The fusion of early endosomes induces molecular-motor-driven tubule formation and fission. *Journal of cell science* *125*, 1910-1919.

Smyth, J.T., Beg, A.M., Wu, S., Putney, J.W., Jr., and Rusan, N.M. (2012). Phosphoregulation of STIM1 leads to exclusion of the endoplasmic reticulum from the mitotic spindle. *Current biology : CB* *22*, 1487-1493.

Snapp, E.L., Hegde, R.S., Francolini, M., Lombardo, F., Colombo, S., Pedrazzini, E., Borgese, N., and Lippincott-Schwartz, J. (2003). Formation of stacked ER cisternae by low affinity protein interactions. *The Journal of cell biology* *163*, 257-269.

Snider, J., Lin, F., Zahedi, N., Rodionov, V., Yu, C.C., and Gross, S.P. (2004). Intracellular actin-based transport: how far you go depends on how often you switch. *Proceedings of the National Academy of Sciences of the United States of America* *101*, 13204-13209.

Sonnichsen, B., De Renzis, S., Nielsen, E., Rietdorf, J., and Zerial, M. (2000). Distinct membrane domains on endosomes in the recycling pathway visualized by multicolor imaging of Rab4, Rab5, and Rab11. *The Journal of cell biology* *149*, 901-914.

Soppina, V., Rai, A.K., Ramaiya, A.J., Barak, P., and Mallik, R. (2009). Tug-of-war between dissimilar teams of microtubule motors regulates transport and fission of endosomes. *Proceedings of the National Academy of Sciences of the United States of America* *106*, 19381-19386.

Sorkin, A., and Goh, L.K. (2008). Endocytosis and intracellular trafficking of ErbBs. *Experimental cell research* *314*, 3093-3106.

Sorkin, A., and Goh, L.K. (2009). Endocytosis and intracellular trafficking of ErbBs. *Experimental cell research* *315*, 683-696.

Sousa, L.P., Lax, I., Shen, H., Ferguson, S.M., De Camilli, P., and Schlessinger, J. (2012). Suppression of EGFR endocytosis by dynamin depletion reveals that EGFR signaling occurs primarily at the plasma membrane. *Proceedings of the National Academy of Sciences of the United States of America* *109*, 4419-4424.

Southwick, F.S., Li, W., Zhang, F.L., Zeile, W.L., and Purich, D.L. (2003). Actin-based endosome and phagosome rocketing in macrophages: Activation by the secretagogue antagonists lanthanum and zinc. *Cell motility and the cytoskeleton* *54*, 41-55.

Spudich, J.A., Kron, S.J., and Sheetz, M.P. (1985). Movement of myosin-coated beads on oriented filaments reconstituted from purified actin. *Nature* *315*, 584-586.

Stenmark, H., and Aasland, R. (1999). FYVE-finger proteins--effectors of an inositol lipid. *Journal of cell science* *112 ( Pt 23)*, 4175-4183.

Sun, Y., McKenna, J.D., Murray, J.M., Ostap, E.M., and Goldman, Y.E. (2009). Parallax: high accuracy three-dimensional single molecule tracking using split images. *Nano letters* *9*, 2676-2682.

Sun, Y., Schroeder, H.W., 3rd, Beausang, J.F., Homma, K., Ikebe, M., and Goldman, Y.E. (2007). Myosin VI walks "wiggly" on actin with large and variable tilting. *Molecular cell* *28*, 954-964.

Sung, H.H., Telley, I.A., Papadaki, P., Ephrussi, A., Surrey, T., and Rorth, P. (2008). *Drosophila* ensconsin promotes productive recruitment of Kinesin-1 to microtubules. *Developmental cell* *15*, 866-876.

Svoboda, K., Schmidt, C.F., Schnapp, B.J., and Block, S.M. (1993). Direct observation of kinesin stepping by optical trapping interferometry. *Nature* 365, 721-727.

Takei, K., Mignery, G.A., Mugnaini, E., Sudhof, T.C., and De Camilli, P. (1994). Inositol 1,4,5-trisphosphate receptor causes formation of ER cisternal stacks in transfected fibroblasts and in cerebellar Purkinje cells. *Neuron* 12, 327-342.

Tang, N., and Ostap, E.M. (2001). Motor domain-dependent localization of myo1b (myr-1). *Current biology : CB* 11, 1131-1135.

Taunton, J., Rowning, B.A., Coughlin, M.L., Wu, M., Moon, R.T., Mitchison, T.J., and Larabell, C.A. (2000). Actin-dependent propulsion of endosomes and lysosomes by recruitment of N-WASP. *The Journal of cell biology* 148, 519-530.

Terman, J.R., and Kashina, A. (2013). Post-translational modification and regulation of actin. *Current opinion in cell biology* 25, 30-38.

Theriot, J.A., Mitchison, T.J., Tilney, L.G., and Portnoy, D.A. (1992). The rate of actin-based motility of intracellular *Listeria monocytogenes* equals the rate of actin polymerization. *Nature* 357, 257-260.

Thery, M., Racine, V., Piel, M., Pepin, A., Dimitrov, A., Chen, Y., Sibarita, J.B., and Bornens, M. (2006). Anisotropy of cell adhesive microenvironment governs cell internal organization and orientation of polarity. *Proceedings of the National Academy of Sciences of the United States of America* 103, 19771-19776.

Thirumurugan, K., Sakamoto, T., Hammer, J.A., 3rd, Sellers, J.R., and Knight, P.J. (2006). The cargo-binding domain regulates structure and activity of myosin 5. *Nature* 442, 212-215.

Toba, S., Watanabe, T.M., Yamaguchi-Okimoto, L., Toyoshima, Y.Y., and Higuchi, H. (2006). Overlapping hand-over-hand mechanism of single molecular motility of cytoplasmic dynein. *Proceedings of the National Academy of Sciences of the United States of America* 103, 5741-5745.

Tojkander, S., Gateva, G., Schevzov, G., Hotulainen, P., Naumanen, P., Martin, C., Gunning, P.W., and Lappalainen, P. (2011). A molecular pathway for myosin II recruitment to stress fibers. *Current biology : CB* 21, 539-550.

Tseng, Y., Kole, T.P., and Wirtz, D. (2002). Micromechanical mapping of live cells by multiple-particle-tracking microrheology. *Biophysical journal* 83, 3162-3176.

Tumbarello, D.A., Waxse, B.J., Arden, S.D., Bright, N.A., Kendrick-Jones, J., and Buss, F. (2012). Autophagy receptors link myosin VI to autophagosomes to mediate Tom1-dependent autophagosome maturation and fusion with the lysosome. *Nature cell biology* 14, 1024-1035.

Twelvetrees, A.E., Yuen, E.Y., Arancibia-Carcamo, I.L., MacAskill, A.F., Rostaing, P., Lumb, M.J., Humbert, S., Triller, A., Saudou, F., Yan, Z., *et al.* (2010). Delivery of GABAARs to synapses is mediated by HAP1-KIF5 and disrupted by mutant huntingtin. *Neuron* 65, 53-65.

Ueno, H., Huang, X., Tanaka, Y., and Hirokawa, N. (2011). KIF16B/Rab14 molecular motor complex is critical for early embryonic development by transporting FGF receptor. *Developmental cell* 20, 60-71.

Upadhyaya, A., and Sheetz, M.P. (2004). Tension in tubulovesicular networks of Golgi and endoplasmic reticulum membranes. *Biophysical journal* 86, 2923-2928.

- Vale, R.D. (2003). The molecular motor toolbox for intracellular transport. *Cell* *112*, 467-480.
- Vale, R.D., and Hotani, H. (1988). Formation of membrane networks in vitro by kinesin-driven microtubule movement. *The Journal of cell biology* *107*, 2233-2241.
- Vale, R.D., Reese, T.S., and Sheetz, M.P. (1985a). Identification of a novel force-generating protein, kinesin, involved in microtubule-based motility. *Cell* *42*, 39-50.
- Vale, R.D., Schnapp, B.J., Mitchison, T., Steuer, E., Reese, T.S., and Sheetz, M.P. (1985b). Different axoplasmic proteins generate movement in opposite directions along microtubules in vitro. *Cell* *43*, 623-632.
- Vallee, R.B., and Tsai, J.W. (2006). The cellular roles of the lissencephaly gene LIS1, and what they tell us about brain development. *Genes & development* *20*, 1384-1393.
- Vallee, R.B., Wall, J.S., Paschal, B.M., and Shpetner, H.S. (1988). Microtubule-associated protein 1C from brain is a two-headed cytosolic dynein. *Nature* *332*, 561-563.
- van Horssen, R., Janssen, E., Peters, W., van de Pasch, L., Lindert, M.M., van Dommelen, M.M., Linssen, P.C., Hagen, T.L., Fransen, J.A., and Wieringa, B. (2009). Modulation of cell motility by spatial repositioning of enzymatic ATP/ADP exchange capacity. *The Journal of biological chemistry* *284*, 1620-1627.
- van Weering, J.R., Sessions, R.B., Traer, C.J., Kloer, D.P., Bhatia, V.K., Stamou, D., Carlsson, S.R., Hurley, J.H., and Cullen, P.J. (2012). Molecular basis for SNX-BAR-mediated assembly of distinct endosomal sorting tubules. *The EMBO journal* *31*, 4466-4480.
- Varsano, T., Dong, M.Q., Niesman, I., Gacula, H., Lou, X., Ma, T., Testa, J.R., Yates, J.R., 3rd, and Farquhar, M.G. (2006). GIPC is recruited by APPL to peripheral TrkA endosomes and regulates TrkA trafficking and signaling. *Molecular and cellular biology* *26*, 8942-8952.
- Veigel, C., Schmitz, S., Wang, F., and Sellers, J.R. (2005). Load-dependent kinetics of myosin-V can explain its high processivity. *Nature cell biology* *7*, 861-869.
- Veigel, C., Wang, F., Bartoo, M.L., Sellers, J.R., and Molloy, J.E. (2002). The gated gait of the processive molecular motor, myosin V. *Nature cell biology* *4*, 59-65.
- Vergeres, G., Yen, T.S., Aggeler, J., Lausier, J., and Waskell, L. (1993). A model system for studying membrane biogenesis. Overexpression of cytochrome b5 in yeast results in marked proliferation of the intracellular membrane. *Journal of cell science* *106 (Pt 1)*, 249-259.
- Verhey, K.J., and Hammond, J.W. (2009). Traffic control: regulation of kinesin motors. *Nature reviews. Molecular cell biology* *10*, 765-777.
- Vershinin, M., Carter, B.C., Razafsky, D.S., King, S.J., and Gross, S.P. (2007). Multiple-motor based transport and its regulation by Tau. *Proceedings of the National Academy of Sciences of the United States of America* *104*, 87-92.
- Vershinin, M., Xu, J., Razafsky, D.S., King, S.J., and Gross, S.P. (2008). Tuning microtubule-based transport through filamentous MAPs: the problem of dynein. *Traffic* *9*, 882-892.
- Vincent, C., Maridonneau-Parini, I., Le Clainche, C., Gounon, P., and Labrousse, A. (2007). Activation of p61Hck triggers WASp- and Arp2/3-dependent actin-comet tail

biogenesis and accelerates lysosomes. *The Journal of biological chemistry* 282, 19565-19574.

Vischer, K., Schnitzer, M.J., and Block, S.M. (1999). Single kinesin molecules studied with a molecular force clamp. *Nature* 400, 184-189.

Voeltz, G.K., Prinz, W.A., Shibata, Y., Rist, J.M., and Rapoport, T.A. (2006). A class of membrane proteins shaping the tubular endoplasmic reticulum. *Cell* 124, 573-586.

Volkov, V.A., Zaytsev, A.V., Gudimchuk, N., Grissom, P.M., Gintsburg, A.L., Ataulkhanov, F.I., McIntosh, J.R., and Grishchuk, E.L. (2013). Long tethers provide high-force coupling of the Dam1 ring to shortening microtubules. *Proceedings of the National Academy of Sciences of the United States of America* 110, 7708-7713.

Volkova, E.G., Abramchuk, S.S., and Sheval, E.V. (2012). The overexpression of nuclear envelope protein Lap2beta induces endoplasmic reticulum reorganisation via membrane stacking. *Biology open* 1, 802-805.

Vonderheit, A., and Helenius, A. (2005). Rab7 associates with early endosomes to mediate sorting and transport of Semliki forest virus to late endosomes. *PLoS biology* 3, e233.

Wagner, W., Brenowitz, S.D., and Hammer, J.A., 3rd (2011). Myosin-Va transports the endoplasmic reticulum into the dendritic spines of Purkinje neurons. *Nature cell biology* 13, 40-48.

Walker, M.L., Burgess, S.A., Sellers, J.R., Wang, F., Hammer, J.A., 3rd, Trinick, J., and Knight, P.J. (2000). Two-headed binding of a processive myosin to F-actin. *Nature* 405, 804-807.

Walter, W.J., Beranek, V., Fischermeier, E., and Diez, S. (2012). Tubulin acetylation alone does not affect kinesin-1 velocity and run length in vitro. *PLoS one* 7, e42218.

Wandke, C., and Kutay, U. (2013). Enclosing chromatin: reassembly of the nucleus after open mitosis. *Cell* 152, 1222-1225.

Wang, Z., Khan, S., and Sheetz, M.P. (1995). Single cytoplasmic dynein molecule movements: characterization and comparison with kinesin. *Biophysical journal* 69, 2011-2023.

Warren, R.A., Green, F.A., and Enns, C.A. (1997). Saturation of the endocytic pathway for the transferrin receptor does not affect the endocytosis of the epidermal growth factor receptor. *The Journal of biological chemistry* 272, 2116-2121.

Warshaw, D.M., Guilford, W.H., Freyzon, Y., Kremmentsova, E., Palmiter, K.A., Tyska, M.J., Baker, J.E., and Trybus, K.M. (2000). The light chain binding domain of expressed smooth muscle heavy meromyosin acts as a mechanical lever. *The Journal of biological chemistry* 275, 37167-37172.

Watanabe, R., and Riezman, H. (2004). Differential ER exit in yeast and mammalian cells. *Current opinion in cell biology* 16, 350-355.

Waterman-Storer, C.M., Gregory, J., Parsons, S.F., and Salmon, E.D. (1995). Membrane/microtubule tip attachment complexes (TACs) allow the assembly dynamics of plus ends to push and pull membranes into tubulovesicular networks in interphase *Xenopus* egg extracts. *The Journal of cell biology* 130, 1161-1169.

Waterman-Storer, C.M., and Salmon, E.D. (1998). Endoplasmic reticulum membrane tubules are distributed by microtubules in living cells using three distinct mechanisms. *Current biology* : CB 8, 798-806.

Wells, A.L., Lin, A.W., Chen, L.Q., Safer, D., Cain, S.M., Hasson, T., Carragher, B.O., Milligan, R.A., and Sweeney, H.L. (1999). Myosin VI is an actin-based motor that moves backwards. *Nature* 401, 505-508.

Wirtz, D. (2009). Particle-tracking microrheology of living cells: principles and applications. *Annual review of biophysics* 38, 301-326.

Wozniak, M.J., Bola, B., Brownhill, K., Yang, Y.C., Levakova, V., and Allan, V.J. (2009). Role of kinesin-1 and cytoplasmic dynein in endoplasmic reticulum movement in VERO cells. *Journal of cell science* 122, 1979-1989.

Wu, X.S., Rao, K., Zhang, H., Wang, F., Sellers, J.R., Matesic, L.E., Copeland, N.G., Jenkins, N.A., and Hammer, J.A., 3rd (2002). Identification of an organelle receptor for myosin-Va. *Nature cell biology* 4, 271-278.

Xu, Y., Tan, L.J., Grachtchouk, V., Voorhees, J.J., and Fisher, G.J. (2005). Receptor-type protein-tyrosine phosphatase-kappa regulates epidermal growth factor receptor function. *The Journal of biological chemistry* 280, 42694-42700.

Yamamoto, A., Masaki, R., and Tashiro, Y. (1996). Formation of crystalloid endoplasmic reticulum in COS cells upon overexpression of microsomal aldehyde dehydrogenase by cDNA transfection. *Journal of cell science* 109 ( Pt 7), 1727-1738.

Yano, H., Ninan, I., Zhang, H., Milner, T.A., Arancio, O., and Chao, M.V. (2006). BDNF-mediated neurotransmission relies upon a myosin VI motor complex. *Nature neuroscience* 9, 1009-1018.

Yeh, T.Y., Quintyne, N.J., Scipioni, B.R., Eckley, D.M., and Schroer, T.A. (2012). Dynactin's pointed-end complex is a cargo-targeting module. *Molecular biology of the cell* 23, 3827-3837.

Yi, J.Y., Ori-McKenney, K.M., McKenney, R.J., Vershinin, M., Gross, S.P., and Vallee, R.B. (2011). High-resolution imaging reveals indirect coordination of opposite motors and a role for LIS1 in high-load axonal transport. *The Journal of cell biology* 195, 193-201.

Yildiz, A., Tomishige, M., Gennerich, A., and Vale, R.D. (2008). Intramolecular strain coordinates kinesin stepping behavior along microtubules. *Cell* 134, 1030-1041.

Yoshida, N., Kinjo, M., and Tamura, M. (2001). Microenvironment of endosomal aqueous phase investigated by the mobility of microparticles using fluorescence correlation spectroscopy. *Biochemical and biophysical research communications* 280, 312-318.

Yu, C., Feng, W., Wei, Z., Miyanoiri, Y., Wen, W., Zhao, Y., and Zhang, M. (2009). Myosin VI undergoes cargo-mediated dimerization. *Cell* 138, 537-548.

Zanic, M., Widlund, P.O., Hyman, A.A., and Howard, J. (2013). Synergy between XMAP215 and EB1 increases microtubule growth rates to physiological levels. *Nature cell biology* 15, 688-693.

Zeigerer, A., Gilleron, J., Bogorad, R.L., Marsico, G., Nonaka, H., Seifert, S., Epstein-Barash, H., Kuchimanchi, S., Peng, C.G., Ruda, V.M., *et al.* (2012). Rab5 is necessary for the biogenesis of the endolysosomal system in vivo. *Nature* 485, 465-470.

Zelena, J. (1968). Bidirectional movements of mitochondria along axons of an isolated nerve segment. *Zeitschrift für Zellforschung und mikroskopische Anatomie* 92, 186-196.

Zelena, J., Lubinska, L., and Gutmann, E. (1968). Accumulation of organelles at the ends of interrupted axons. *Zeitschrift für Zellforschung und mikroskopische Anatomie* 91, 200-219.

Zerial, M., and McBride, H. (2001). Rab proteins as membrane organizers. *Nature reviews. Molecular cell biology* 2, 107-117.

Zhang, D., Vjestica, A., and Oliferenko, S. (2012). Plasma membrane tethering of the cortical ER necessitates its finely reticulated architecture. *Current biology : CB* 22, 2048-2052.

Zhang, J., Yao, X., Fischer, L., Abenza, J.F., Penalva, M.A., and Xiang, X. (2011). The p25 subunit of the dynactin complex is required for dynein-early endosome interaction. *The Journal of cell biology* 193, 1245-1255.

Zhou, H.X., Rivas, G., and Minton, A.P. (2008). Macromolecular crowding and confinement: biochemical, biophysical, and potential physiological consequences. *Annual review of biophysics* 37, 375-397.

Zhu, G., Chen, J., Liu, J., Brunzelle, J.S., Huang, B., Wakeham, N., Terzyan, S., Li, X., Rao, Z., Li, G., *et al.* (2007). Structure of the APPL1 BAR-PH domain and characterization of its interaction with Rab5. *The EMBO journal* 26, 3484-3493.

Zoncu, R., Perera, R.M., Balkin, D.M., Pirruccello, M., Toomre, D., and De Camilli, P. (2009). A phosphoinositide switch controls the maturation and signaling properties of APPL endosomes. *Cell* 136, 1110-1121.